2016

Involvement of miRNAs in the Development of Androgen Independent Prostate Cancer

Richard Ottman
University of Central Florida

INVOLVEMENT OF MICRORNAS IN THE DEVELOPMENT OF ANDROGEN INDEPENDENT PROSTATE CANCER

by

RICHARD JAMES OTTMAN
B.S. University of Central Florida, 2008
M.S. University of Central Florida, 2011

A dissertation submitted in partial fulfillment of the requirements
for the degree of Doctor of Philosophy
in the Burnett School of Biomedical Sciences
in the College of Medicine
at the University of Central Florida
Orlando, Florida

Summer Term
2016

Major Professor: Ratna Chakrabarti

ABSTRACT

Development of resistance to androgen deprivation therapy (ADT) is a major obstacle for the management of advanced prostate cancer. Therapies with androgen receptor (AR) antagonists and androgen withdrawal initially result in tumor regression but development of compensatory mechanisms including AR bypass signaling leads to tumor re-growth, independent of circulating androgens. The result is the emergence of castration resistant prostate cancer (CRPC), a highly morbid disease exhibiting aberrant expression of many protein-coding and non-coding genes. Under the umbrella of non-coding RNAs is a class of small regulatory RNAs referred to as microRNAs (miRNAs). MicroRNAs are believed to function in the maintenance of cell homeostasis but are often differentially expressed in many different types of cancer including CRPC.

In this study, the association of genome wide miRNA expression (1113 unique miRNAs) with development of resistance to ADT was determined. Androgen sensitive prostate cancer cells that progressed to ADT and AR antagonist Casodex (CDX) resistance upon androgen withdrawal and treatment with CDX were used. Validation of expression of a subset of 100 miRNAs led to identification of 43 miRNAs that are significantly altered during progression of cells to treatment resistance. A correlation of altered expression of 10 proteins targeted by some of these miRNAs in these cells was shown.

Additionally, profiles of miRNA expressions in cancerous prostate tissues were created and compared with profiles of paired adjacent uninvolved areas of prostate

tissue. Among the miRNAs identified from these analyses, a cluster of miRNAs, miR-17-92a, that is under-expressed in prostate tumors and in androgen independent prostate cancer cells was highlighted. The miR-17-92a cluster miRNAs are transcribed from a polycistronic transcription unit C13orf25 that generates six mature miRNAs: miR-17, miR-18a, miR-19a, miR-19b, miR-20a and miR-92a, and is commonly de-regulated in many cancers. In this research, the expression of miR-17-92a miRNAs was found to be reduced in cancerous prostate tissues when compared to uninvolved areas and also in aggressive prostate cancer cells. Restoration of expression of all members of miR-17-92a cluster showed decreased expression of cell cycle regulatory proteins cyclin D1 and SSH1; as well as LIMK1 and FGD4 of the RhoGTPase signaling pathway. Expression of miR-17-92a miRNAs caused decreased cell proliferation, reduced activation of AKT and MAP kinases, delayed tumorigenicity and reduced tumor growth in animals. Additionally, miR-17-92a miRNA expression inhibited EMT via reduced cell migration and expression of mesenchymal markers while elevating expression and surface localization of the epithelial marker e-cadherin. Expression of miR-17-92a miRNAs improved sensitivity of androgen dependent LNCaP104-S prostate cancer cells to the Androgen Receptor antagonist bicalutamide (CDX), AKT inhibitor MK-2206 2HCl, and docetaxel. Androgen refractory PC-3 cells also showed increased sensitivity to docetaxel, MK-2206 2HCl, and Aurora kinase inhibitor VX680 upon ectopic expression of miR-17-92a cluster miRNAs.

In conclusion, dynamic alterations in miRNA expression occur early on during

androgen deprivation therapy and androgen receptor blockade. The cumulative effect of these altered miRNA expression profiles is the temporal modulation of multiple signaling pathways promoting survival and acquisition of resistance. These early events are driving the transition to castration resistance and cannot be studied in already developed CRPC cell lines or tissues. Notably, these data demonstrate a tumor suppressor effect of miR-17-92a cluster miRNAs in prostate cancer cells and restoration of expression of these miRNAs has a therapeutic benefit for both androgen-dependent and -independent prostate cancer cells. Furthermore, these results can be used as a prognostic marker of cancers with a potential to be resistant to ADT.

ACKNOWLEDGMENTS

I would first like to acknowledge my wonderful wife and our family for their unwavering support, which gave me the strength to persevere. Next, I need to thank my mentor Dr. Ratna Chakrabarti for her guidance and trust. Finally, I would like to thank my Committee members, Dr. Alex Cole, Dr. Antonis Zervos, and Dr. Annette Khaled for their assistance and support.

TABLE OF CONTENTS

LIST OF FIGURES

LIST OF TABLES

LIST OF ABBREVIATIONS

ADT – Androgen Deprivation Therapy

AIPC – Androgen Independent Prostate Cancer

CRPC – Castration Resistant Prostate Cancer

CSFBS – charcoal stripped fetal bovine sera

AD – Androgen Dependent (requires androgen for proliferation)

AI – Androgen Independent

AS – Androgen Sensitive (responsive to DHT treatment)

AR – Androgen Receptor

CDX – Casodex (anti-androgen chemotherapeutic)

DTX – Docetaxel (anti-mitotic chemotherapeutic)

AKTi - AKT inhibitor MK-2206◦2HCl

CHAPTER ONE: INTRODUCTION

The molecular regulation of gene expression is an extremely complex and multi-tiered process crucial for the maintenance of normal cellular processes; as such, the ensuing overview is intended to only provide a framework for understanding the scale of which this dissertation is investigating.

Gene regulation arbitrarily starts at the level of chromatin structure; here epigenetic modifications control the accessibility of transcriptional complexes to specific genetic regions. When chromatin is relaxed, differing patterns of regulatory regions upstream of genes recruit transcription factors, co-regulator proteins, scaffolding proteins and RNA polymerases to govern transcription of the gene into RNA. RNA-binding proteins then work to control the stability of transcripts and patterns of splicing, altering both the concentration of templates available for translation and the complete sequence of those templates [1]. Translation of mRNAs is further controlled during initiation, elongation, termination, and recycling of ribosomes [2]. Regulatory RNAs act at this level to inhibit ribosomal function or direct degradation of the mRNA. Finally, mature proteins can be modified in many ways which can have a multitude of effects including: modifying enzyme activity, fine-tuning protein-protein interactions, and targeting proteins for degradation [3]. The total sum of these processes, and many additional factors, results in the cumulative regulation of protein functionalities and concentrations.

The development and progression of cancer is likewise a product of multilayered

mechanisms spanning time and diverse regulatory events. Unlike the tightly controlled systems of normal cells, malignancies thrive by hijacking cellular systems and manipulating these processes to promote growth and survival. Each cancer develops individually as a result of accumulated cellular insults, mutations, genetic factors, and extracellular stimuli. Despite the seemingly random series of events promoting the development of different cancers, the consequence is the convergent evolution of malignant tissues. Common to all cancers is the deregulation of gene expression seemingly at every level [4]. Furthermore, aberrant expression encompasses both protein coding and non-coding genes. This is an essential adaption and functional consequence that drives the survival and progression of cancer.

1.1 Non-Coding RNAs in Cancer

Non-coding RNAs (ncRNA) are RNA molecules that are not translated into proteins, and are divided by type. The types include transfer-RNA (tRNA), ribosomal RNA (rRNA), long non-coding RNA (lncRNA), and microRNA (miRNA) among others. Non-coding RNAs are involved in many integral cellular processes including but not limited to RNA splicing, protein synthesis, DNA replication, and regulation of gene expression [5]. Development of RNA sequencing methods has led to widespread profiling of many tissue types and disease states. Results of these experiments have shown that many ncRNAs display altered patterns of expression in cancerous tissues, and these altered expressions have phenotypic implications [6, 7]. Long non-coding RNAs and microRNAs are two classes of regulatory RNA molecules and accordingly

many members of both classes display strong conservation across species. LncRNAs and miRNAs act to fine tune the expression of specific genes or genetic loci [8]. Despite the diverse functions of ncRNAs little was known about these molecules until recently. This gap in knowledge garnered great interest, and resultant studies have uncovered a complex interconnected network of differing ncRNAs and proteins which act to regulate metastatic transformation of cancer (Figure 1).

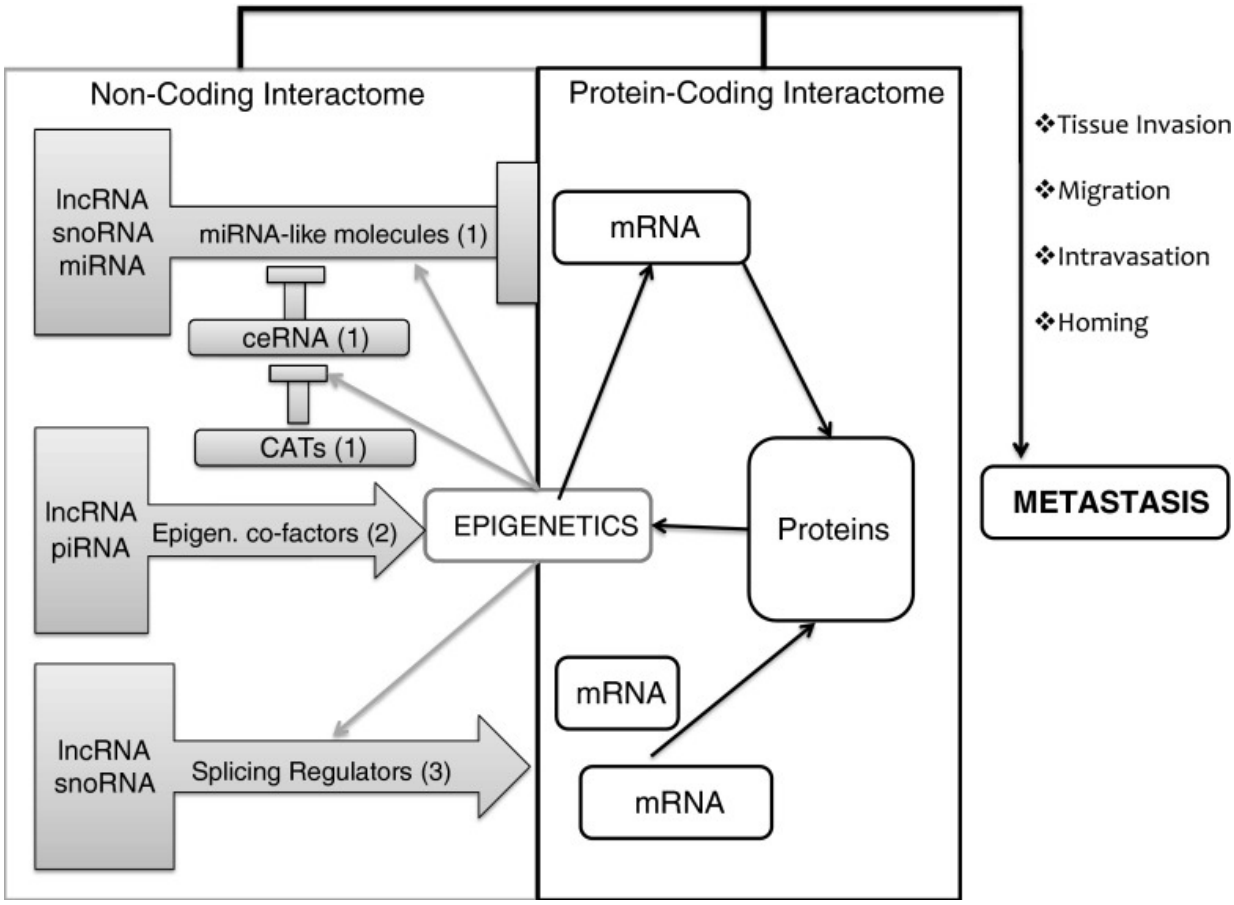

Figure 1: Depiction of ncRNA involvement in molecular networks orchestrating cancer metastasis.

The non-coding (grey boxes) and the protein-coding (white boxes) interactomes co-operate to drive each step of the metastatic cascade (e.g., tissue invasion, migration, intravasation, and homing in distant tissues). Different classes of ncRNAs can play partially overlapping functions. A summary of three main classes includes: 1 Antisense RNA inhibitors, including miRNA-like molecules, competitive endogenous RNAs (ceRNAs) and ceRNA-antisense transcripts (CATs); 2 epigenetic co-factors; 3 splicing regulators. Each component of the interactome can activate (arrows) or inhibit (rectangles) other components. Epigenetic gene regulation is depicted at the border of the two interactomes, since it can control the expression of both ncRNAs and mRNAs. Moreover, epigenetic effectors are composed of? both proteins and lncRNAs, piRNA, PIWI interacting RNA, snoRNA and small nuclear RNA.

Source: Crea F, Clermont PL. et al. (2014). “The non-coding transcriptome as a dynamic regulator of cancer metastasis”. Cancer Metas. Rev., 33(1):1-16. doi: 10.1007/s10555-013-9455-3

1.1.1 Biogenesis of microRNAs

MicroRNAs belong to a specific class of small regulatory RNAs which was first discovered in C. elegans. Mature miRNAs, 17–22 nucleotides in length, contain a specific sequence at their 5’ end which acts to repress translation through binding to the 3’UTR of the mRNAs [9].The role of small noncoding microRNAs (miRNAs) in regulation of gene expression, which is mediated by inhibition of translation or degradation of target mRNAs is an established phenomenon [9]. To date, 1881 distinct human miRNAs have been identified of which, high confidence displayed in 1357 and, each of which regulate multiple target mRNAs (www.mirbase.org Jun 2014). Genes encoding miRNAs are located heterogeneously throughout the genome. Some miRNAs are located distant from protein coding genes and are driven by their own promoters, while most are located in the introns of protein coding genes and are regularly co-expressed with the host gene. Moreover, miRNA genes can be transcribed independently or as part of a polycistronic cluster. Unique miRNA genes are generally transcribed by RNA polymerase II, producing a primary miRNA (pri-miRNA) transcript, while miRNA genes cis to ALU repeat regions have been found to be transcribed by RNA polymerase III [10] [11]. Primary-miRNA transcripts, which are generally capped at the 5’ terminus, are composed of at least one stem-loop hairpin, a terminal loop, and a single stranded flanking sequence containing a polyA-tail [12]. While still located in the nucleus, the flanking sequences of pri-miRNAs are trimmed into pre-miRNA by the microprocessor complex composed of Drosha and DGCRG8. For intron encoded miRNAs, splicing of host gene transcripts release the

“miRtrons”, producing pre-miRNAs independent of Drosha function [13]. Pre-miRNAs are then exported from the nucleus by exportin-5 and Ran-GTP. In the cytoplasm the pre-miRNA hairpin is cleaved by Dicer leaving two mature strands of the miRNA, referred to as the 5p- and 3p- strands. Although both strands are functional, it is generally accepted that the strand with the less stable base pairing at the 5′ terminus is preferentially loaded into the RNA-induced silencing complex (RISC) [14]. In this canonical theory, the miRNA* or passenger strand, is selected for degradation (Figure 2). Contrary evidence has emerged from more recent RNA-Seq data which has shown that many miRNA* strands occur at comparable levels to that of the guide strands. Whereas immunoprecipitation of Ago proteins has shown a predilection of AGO1/2 for specific 5p- and 3p- strands, deregulation during cancer may drive strand switching in RISC complexes [15].

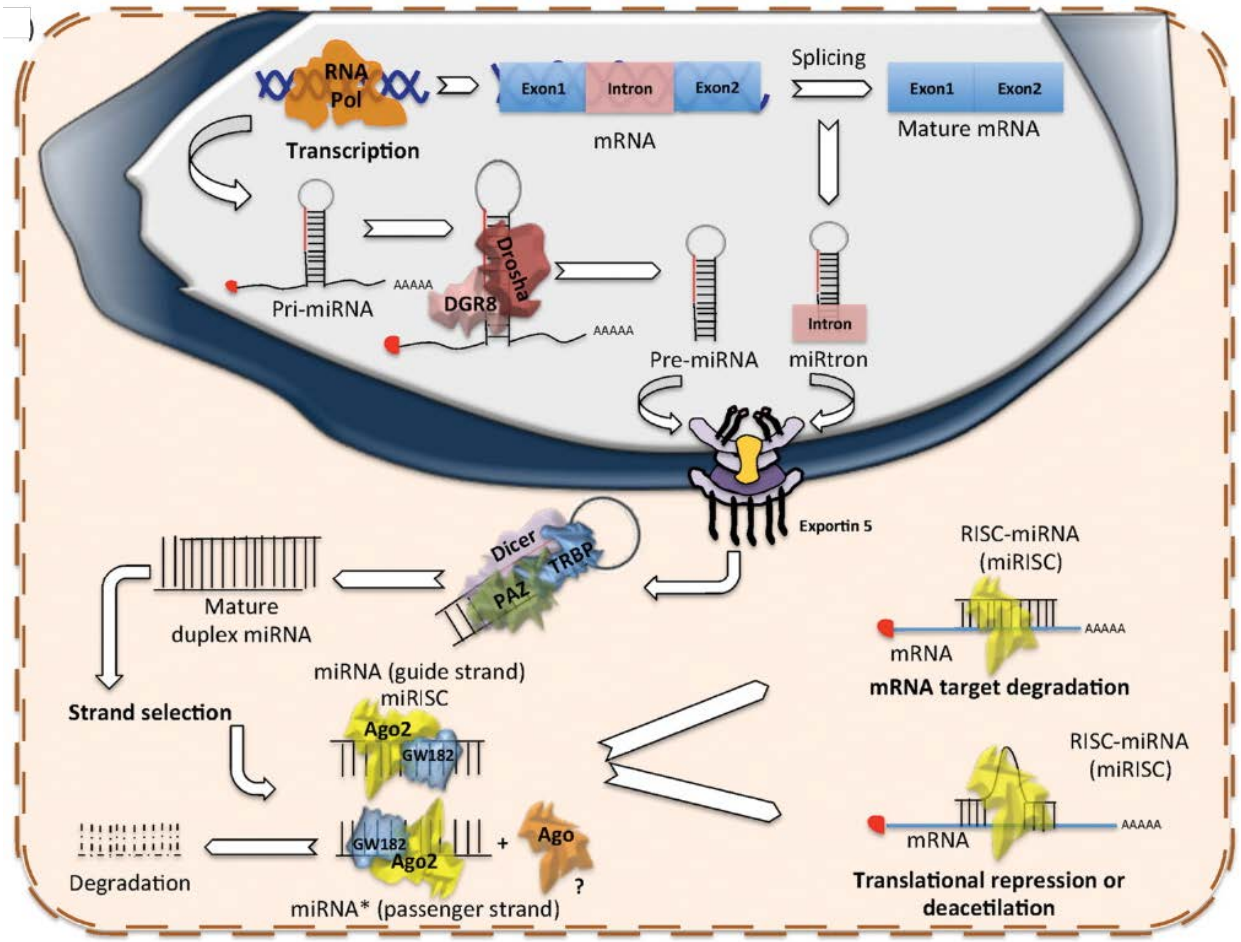

Figure 2: Biogenesis and functionality of miRNAs

MicroRNAs are transcribed and trimmed into pre-miRNAs in the nucleus before being exported into the cytoplasm. Next Dicer acts to cleave the hairpin forming the mature miRNAs which are incorporated in RISC complexes to mediate gene silencing. Source: “miRNA biogenesis: Biological impact in the development of cancer” [12]

1.1.2 Mechanisms of miRNA Gene Silencing

The primary function of miRNAs is the translational repression of target mRNAs, which is achieved through mRNA degradation, translational inhibition, or mRNA decay through recruitment to P bodies [16, 17]. The mechanism is mediated by which Argonaut protein binds the miRNA and the degree of complementarity between the miRNA seed region and the 3'UTR of the mRNA. Ago2 is the principal RISC component involved in miRNA gene silencing generally through translational inhibition. The cleavage of mRNA by Ago2 necessitates perfect complementarity of mRNA-miRNA base pairing [18] which is uncommon in vertebrates. However, this can be achieved through Ago1/3/4 [19, 20]. The extent of gene silencing is also mediated by the number of miRNA binding sites in the mRNA [21].

The effect of altered miRNA expression can vary widely in significance and transformative ability. One example in which the modulation of one miRNA can dramatically shift the gene expression is the overexpression of miR-124 in HeLa cells in which the protein expression switched to a profile mirroring that found in the brain, a tissue that expresses high levels of miR-124. Alternatively, when miR-1 is overexpressed, a miRNA highly expressed in muscle tissue, the cells express mRNA profiles consistent with that of muscle cells [22].

1.2 Prostate Cancer

1.2.1 Epidemiology of Prostate Cancer

Prostate cancer is the second most prevalent malignancy in American men, ranking just behind skin cancer. The American Cancer Society estimates that in 2016 180,890 new cases of prostate cancer will be diagnosed with an unfortunate 26,120 patients succumbing to the disease (ACS March 2016). This places prostate cancer as the second leading cause of cancer deaths in American men, behind only lung cancer. Prostate cancer normally develops in men over the age of 60 and rarely forms before age 40. Despite the fact that 1 in 7 men will develop prostate cancer in their lifetime, on average only 1 in 39 American men will die from prostate cancer. This discrepancy is a result of several factors including medical intervention, slow growth and confinement to the prostate in many cases, and later onset in age, leaving many men to die from other causes. There are risk factors which aggravate this scenario including family history, diet and obesity, STDs, and inflammation and sex hormone levels [23]. Furthermore, race and socioeconomic status are key factors contributing to the development and mortality rates of prostate cancer. African American and Caribbean men of African ancestry have the highest incidences of prostate cancer followed by Caucasians, Hispanics, and Asian men. Higher risk of prostate cancer is further linked with lower socioeconomic status [24].

Most prostate lesions develop in the form of benign prostatic hyperplasia (BPH) or prostatic intraepithelial neoplasia (PIN). BPH is largely not considered as a precursor of cancer in the prostate [25]. This is because BPH normally occurs in the transitional zone encompassing both epithelial and stromal tissues [26] [27]. The anatomy of the prostate and location of zones is displayed in Figure 3. High grade PIN, in contrast to BPH, is believed to be a precancerous condition. PIN is characterized by abnormalities of epithelial cells lining the glands and ducts in the prostate while basal cell architecture remains present. Prostate cancer more commonly develops from abnormal epithelial cells in the peripheral zone.

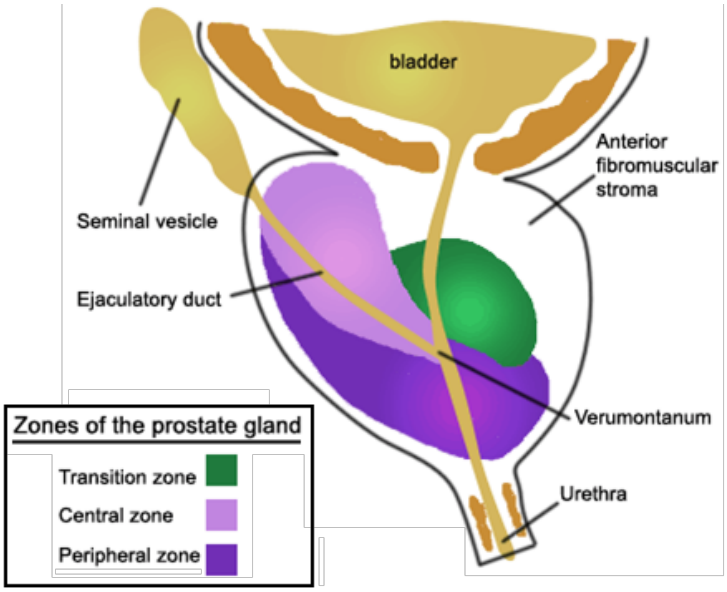

Figure 3: Anatomy of the prostate gland

The prostate gland is located below the bladder and surrounds the urethra. BPH is a common abnormality of the transitional zone (Green) while malignant lesions normally develop in the peripheral zone (Purple).

The Gleason scoring system is used to judge the progression of the tumor, early on when the tumor tissue is still well differentiated and retains many small glandular structures. As the cancer progresses, the tissue becomes less differentiated and basal cells are lost as the lesion infiltrates the surrounding stroma. Well differentiated tissue structure is assigned low values while poorly differentiated tissue structure is assigned high Gleason scores (Figure 4).

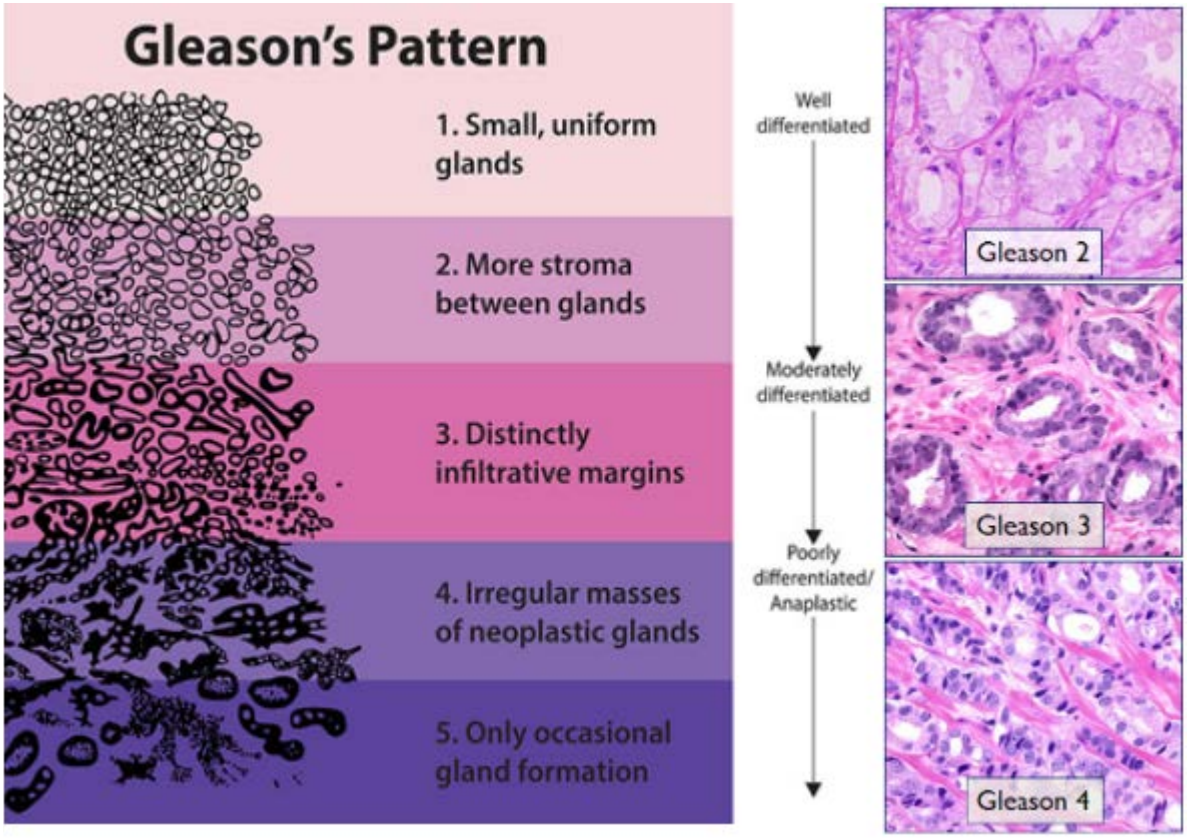

Figure 4: Gleason scoring system classification

Depiction of prostate tissue architecture in association with Gleason score.
Source: NIH SEER training modules

1.2.2 Androgen Receptor and Importance of Androgen Signaling

The Androgen Receptor (AR) is a nuclear receptor activated by androgens, a class of steroid hormones which includes 5α-dihydrotestosterone (DHT) the primary ligand of AR. In the absence of androgens, AR is primarily localized to the cytoplasm and is bound by HSPs-90/-70 where it is indirectly tethered to cytoskeletal proteins. Upon ligand binding, the heat shock proteins dissociate and AR is translocated to the nucleus. Active ARs dimerize and interact with co-regulators to drive the transcription of genes with androgen response elements in their promoter.

During prostate development the activation of AR, results in the elevated expression of transcription factors, and growth factors in prostate progenitor cells. The net effect is the increased activity of signaling pathways which promote survival, proliferation, and invasion. This drives the formation and remodeling of the immature prostate. In the adult prostate, androgen signaling is necessary for maintaining the proliferation and secretory function of luminal epithelial cells.

1.2.3 Therapeutic Strategies

Treatment options for prostate cancer depend on several basic criteria: 1) tumor stage and likelihood of progression, 2) localized or metastatic disease, and 3) risk/reward to patient. In the past, “watchful waiting” (WW), a palliative observational strategy, was commonly prescribed for patients diagnosed with low risk clinically localized prostate cancer. This was recommended because of the slow progression common in prostate cancer combined with the increased risk of surgery or radiation for elderly patients. However as of late, this strategy has come under criticism and is being replaced by “active surveillance” (AS) which is undertaken with a similar mindset but involves regular biopsies and testing for PSA levels. If the oncologist determines that immediate intervention is necessary, several options exist which are listed in Table 1.

Table 1: Therapeutic options for the management of prostate cancer

Treatment	Description
Watchful waiting	A palliative observational strategy that consists of intervening only when symptoms appear
Active surveillance	A strategy with curative intent that involves regular monitoring of PSA levels and repeat biopsies
Radiation therapy	Conventional external beam radiation therapy (EBRT) •Three-dimensional conformal radiation therapy (3D-CRT) •Intensity-modulated radiation therapy (IMRT) •Proton beam radiation therapy (PBRT) •Stereotactic body radiation therapy (SBRT)
Interstitial brachytherapy	A strategy whereby tumor tissue is specifically targeted by placing seeded radioactive material in or near the tumor
Radical prostatectomy	Open perineal •Open retropubic •Laparoscopic •Robotic-assisted laparoscopic
Cryotherapy	A strategy that uses very low temperatures to freeze and kill the tumor cells in the prostate
High-intensity focused ultrasound (HIFU)	A procedure that applies high-intensity focused ultrasound energy to locally heat and destroy tumor tissue

Source: Mottet N, et al. *Guidelines on Prostate Cancer*. Euro. Assoc. of Urology 2015

1.2.4 Androgen Independence

Androgen signaling drives the development and progression of prostate cancer. For this reason, androgen blockade is commonly used in therapeutic strategies for patients diagnosed with disseminated or locally confined advanced prostate cancer. While androgen deprivation therapy can induce significant tumor regression, the efficacy is transient. Ultimately, the treatment fails and the disease progresses to a highly malignant form referred to as androgen independent or castration resistant prostate cancer.

The development of androgen independent prostate cancer (AIPC) has been studied extensively and has revealed a diverse range of adaptive mechanisms employed by surviving tumor cells. It is generally accepted that the tumor cells initially adapt to the low androgen environment by becoming androgen hypersensitive. Through ramping up the expression of AR and its co-regulators, the cells are able to maintain basal levels of AR signaling in androgen depressed conditions. Furthermore, over active growth factor signaling pathways and expression of alternative AR isoforms or mutants can lead to ligand independent activity of AR. In the long-term androgen independent cells exhibit commonalities characterized by altered protein expression. The exact expression profiles vary between tumors, and AIPC cell lines alike, but show a trend toward increased expression and activity of proteins promoting proliferation and survival and decreased repressors of such. (↑ EGFR [28], ↑ IGFR[29], ↑ Cdks/Cylins [30], ↑ FOXA1 [31], ↓ PTEN

[32], ↓ p21 [33], etc), as well as the overhaul of metabolic pathways [34], especially those involved steroid signaling and synthesis [35, 36]. Paracrine and autocrine androgen biosynthesis is known to occur in the cells of tumor microenvironment and in the prostate cancer cells thus providing sufficient androgen levels to circumvent ADT [37, 38]. The rewiring of molecular networks observed in androgen independent prostate cancer is both an origin and a consequence of alterations in gene expression; the evolution of which is still subject to the regulatory mechanisms and molecules described earlier, including non-coding RNAs.

1.3 MicroRNAs in Cancer

1.3.1 Involvement of miRNAs in carcinogenesis

Many diseases, including cancer, are associated with abnormal transcriptomes. This dysregulation of RNA expression encompasses both protein-coding and non-coding RNAs. MicroRNAs have been found to be aberrantly expressed during the development and progression of a wide spectrum of different cancers [39, 40]. Simplistically, this leads to increased concentrations of oncogenic miRNAs with a corresponding decrease in tumor suppressive miRNAs, often from the duplication or deletion of genetic regions. In reality the oncogenic or suppressive function of a miRNA is cell type specific and mediated by the landscape of mRNAs, pseudogenes, and competitive RNAs (ceRNAs), amongst other factors [41, 42]. MicroRNA effectors may change between cancer types; however, the effects are similar: drive proliferation, inhibit apoptotic initiation, and promote a stem-like & invasive phenotype. The miR-106a-363 cluster, commonly up-regulated in cancer, targets PTEN promoting PI3K-AKT signaling and proliferation and survival [43]. Conversely, the down-regulation of the let-7 and miR-200 families, can induce epithelial to mesenchymal transition (EMT) and increase invasiveness in PCa cells [44, 45]. A summary of miRNAs altered in prostate cancer and the pathways affected is listed in Table 2.

Table 2: List of miRNAs altered in prostate cancer and the mRNA targets

MiRNA	Expression	mRNA target	Pathway
miR-21	Up	PTEN, AKT, androgen pathway	Apoptosis, mTOR pathway, A.I.
miR-24	Up	FAF1	Apoptosis
miR-32	Up	BCL2L11(Bim)	Apoptosis
miR-106b	Up	P21, E2F1	Cell Cycle/Apoptosis and Proliferation
miR-125b	Up	P53, BBC3(Puma), BAK1	Apoptosis
miR-148a	Up	CAND1	Cell Cycle
miR-221	Up	p27(kip1)	Cell Cycle and A.I.
miR-222	Up	p27(kip1)	Cell Cycle and A.I.
miR-521	Up	Cockayne syndrome protein A	DNA Repair
miR-1	Down	Exportin-6, tyrosine kinase 9	Gene Expression
miR-7	Down	ERBB-2 (EGFR, HER2)	Signal Transduction
miR-15a-16	Down	CCND1 and WNT3a	Cell Cycle Regulation, Apoptosis and Proliferation
miR-34a	Down	HuR/Bcl2/SIRT1->p53/p21/BBC3	Apoptosis and Drug-Resistance
miR-34c	Down	E2F3, bcl2, MET	Apoptosis and Proliferation
miR-107	Down	Granulin	Proliferation
miR-143	Down	MYO6, ERK5	Migration, Proliferation
miR-145	Down	MYO6, BNIP3L->AIFM1, CCNA2, TNFSF10	Migration, Apoptosis, Cell Cycle
miR-148a	Down	MSK1	Proliferation, stress response and drug resistance
miR-205	Down	IL-24 and IL-32, Cepsilon	Cell Growth and Invasion, EMT
miR-331-3P	Down	ERBB-2, CDCA5, KIF23	Signal Transduction, Cell Cycle
miR-1296	Down	MCM family	DNA Replication
Let-7a	Down	E2F2 and CCND2	Cell Cycle and Proliferation

A.I. androgen independence

Source: Catto et al. 2011. *MicroRNA in Prostate, Bladder, and Kidney Cancer: A Systematic Review*. doi:10.1016/j.eururo.2011.01.044

1.3.2 Association of miRNAs with CRPC

Castration resistant prostate cancer is a highly morbid disease and by definition is unresponsive to androgen deprivation. In spite of this clinical consequence, androgen independent cells commonly exhibit a highly active androgen receptor signaling axis important for growth and survival. The androgen receptor is known to modulate the expression of over 100 miRNAs. In prostate cancer, 22 miRNAs are well documented [46]. Sixteen miRNAs are induced by DHT (miR-594, -16, -21, -29a/b/c, -148a, -106a, -17–5p, -20a, -20b, -19b, -93, -15b, let-7g, and let-7d), and display altered expression in PCa [47]. Alternatively, miR-340, -222, -16, -100 -126*, -23b, -133a-1, and -499 are down-regulated by AR activity and show reduced expression in PCa [48]. MicroRNAs are also involved in the regulation of AR expression and activity, including miR-541, -34c, -299, -135b which directly target the 3’ UTR of AR mRNA [49]. Additionally, miR-17 can inhibit the expression of P300/CBP, a co-activator of AR, and FOXA1 which modulates AR activity [50, 51].

CHAPTER TWO: HYPOTHESIS AND SPECIFIC AIMS

MicroRNAs (miRNA) are recognized as a group of small noncoding RNAs that play a variety of roles in the regulation of biological processes mainly through repression of gene expression at the translational level. MicroRNAs have a unique expression profile that varies in a tissue and disease specific manner [52],[53]. Expression of miRNAs is often deregulated early in cancer progression, which facilitates development of aggressive and drug resistant disease [54, 55]. However, the progressive modulation of miRNA expressions has not been identified during the acquisition of resistance to anti-androgen therapy *in vitro*; moreover, a correlative analysis of miRNA expression profiles with a patient's risk of biochemical failure, which could provide a significant prognostic tool for clinicians, has never been done. We hypothesize that differential expression of miRNAs are associated with the progression of prostate cancer and with the development of androgen independence and anti-androgen (AA) drug resistance.

2.1 Aim #1. Identify miRNAs, and their protein targets, with altered expression during development of androgen independence

In this aim we will profile the expressions of 1113 miRNAs in prostate cancer cells subjected to androgen ablation and AA drug treatment and identify miRNAs displaying statistically significant changes. Using prediction algorithms, we will identify putative target genes and determine if expression of the genes was effected.

2.2 Aim #2. Identify miRNA(s) differentially expressed in tumor tissues and investigate the role the miRNA(s) play in prostate cancer development

In this aim we will profile miRNA expressions in clinical tissue, and identify deregulated miRNAs. MicroRNAs commonly deregulated in patient tumors and in androgen independent prostate cancer cells will be chosen for further investigation. Expression of these miRNAs will be manipulated in prostate cancer cells and phenotypic changes will be observed.

2.3 Aim #3. Screen and correlate expression of miRNAs in clinical specimens with different predictive outcomes

In this aim we will profile miRNA expressions from additional patient tumors. These miRNA profiles will then be correlated with the patient's risk of biochemical recurrence following surgery, identified from the patient's pathological chart information.

CHAPTER THREE: MATERIAL AND METHODS:

3.1 Cell Culture and Androgen Deprivation

LNCaP sublines LNCaP-104S and LNCaP-104R1 were a gift from Dr. Shutsung Liao (University of Chicago). LNCaP-104S cells, androgen dependent, were passaged in DMEM (Life Technologies) containing 10% Fetal Bovine Serum (Atlanta Biologicals) and 1% antibiotic/antimycotic (Life Technologies) at 37°C, 5% CO_2. LNCaP-104R1 cells, androgen independent, were maintained in DMEM containing 10% Charcoal-stripped Fetal Bovine Serum and 1% antibiotic/antimycotic (Life Technologies) at 37°C, 5% CO_2. Charcoal stripped FBS was prepared by incubating FBS with dextran(T-70) coated activated charcoal, at 45˚C for 1hr while stirring. Dextran coated charcoal was separated from serum by two rounds of centrifugation (3,000 rpm, 5 min). Serum was transferred to new conical tubes and stored at -20˚C. Because LNCaP cells do not reach 100% confluence, cells were subcultured on every second to third day. Cell dissociation process is as detailed, first, monolayer was washed with DPBS, then DPBS containing 0.05% trypsin-EDTA solution (Life Technologies) was added to culture dish for 30 seconds at room temperature. Next, trypsin-EDTA solution was aspirated and the culture dish was placed in 37°C incubator for 3 to 5 minutes. The dissociated cells were then suspended in complete growth media and split (1:3). Because LNCaP cells adhere relatively loosely to culture surfaces, caution was exercised when pipetting DPBS or media into culture

vessels containing attached cells.

The isolation of LNCaP-104S cells resistant to androgen deprivation was conducted as follows. LNCaP-104S cells were maintained in DMEM containing 10% Charcoal-Stripped Fetal Bovine Serum (CS-FBS), supplemented with or without 5 µM Casodex (Fluka). Samples of treated cells were harvested at 7, 14, and 21 days. Harvested cells were used for either RNA extraction or protein extraction. Treated cells were compared to untreated samples collected before treatment. To start treatment, $1x10^6$ LNCaP-104S cells were seeded in 100mm tissue culture dishes in DMEM containing CS-FBS and allowed to adhere for 24 hours. The media was then carefully aspirated and changed to fresh CS-FBS media, containing 10% conditioned media and supplemented with or without 5 µM Casodex (CDX). Cells were passaged every two days. Following the first week of treatment, cell proliferation had been suppressed, and during the second week of treatment many cells had undergone apoptosis. At this point, the surviving cells were dissociated and seeded at $1x10^6$ cells per 100mm dish every fourth day, to maintain sufficient cell density. Media was changed in between subculturing. During the third week of treatment, cells maintained in CS-FBS media started to recover and proliferate in a more uniform fashion, compared to cells maintained in CDX where proliferating cell populations were limited to clonal clusters. Following 21 days of treatment, all viable cells were harvested from both CS-FBS and CDX treated dishes.

PC-3 cells (ATCC) were maintained in F-12 Kaighn's Modification HAM (Sigma)

medium containing 10% Fetal Bovine Serum (Atlanta Biologicals) and 1% antibiotic/antimycotic (Life Technologies) at 37°C, 5% CO_2. When cells reached roughly 80% confluence, the monolayer was dissociated using trypsin-EDTA solution (Life Technologies). Dissociation process is as detailed, first monolayer was washed with DPBS, then DPBS containing 0.05% trypsin-EDTA solution was added to culture dish for 3 minutes at room temperature. Next, trypsin-EDTA solution was aspirated and the culture dish was placed in 37°C incubator for 3 to 5 minutes. The dissociated cells were then suspended in complete growth media and split (1:3) in complete media.

M12 cells, a metastatic subline derived from SV-40 large T antigen immortalized human prostate epithelial cells (P69), were obtained as a gift from Dr. Joy Ware (Medical College of Virginia). M12 cells were maintained in RPMI-1640 (Sigma Aldrich) containing Insulin 5µg/mL, Transferrin 5µg/mL, Selenium 5ng/mL (BD Biosciences), dexamethasone (100 nM) (Sigma), EGF (10ng/mL) (BD Biosciences), and gentamicin (0.05 mg/mL) (Life Technologies). Cells were passaged at 70-80% confluence. Dissociation process is as detailed, first monolayer was washed with DPBS, then DPBS containing 0.05% trypsin-EDTA solution was added to culture dish for 5 minutes at room temperature. Next, trypsin-EDTA solution was aspirated and the culture dish was placed in 37°C incubator for 5-10 minutes. The dissociated cells were then suspended in complete growth media and split (1:5) in complete media supplemented with 5% fetal bovine serum. After cells were attached, media was changed to serum free complete media.

3.2 Patient Selection and Procurement of Human Prostate Tissues

Prostate tissues obtained by radical prostatectomies were procured in the Cooperative Human Tissue Network (Southern division) at the University of Alabama at Birmingham (UAB) in accordance with an approved IRB protocol. Following surgery, prostate tissues were formalin-fixed and paraffin embedded (FFPE). Tissues were later analyzed by a pathologist, macro-dissected and re-embedded in paraffin. Twenty micron sections were cut from paraffin blocks and collected as curls in RNase-free micro-centrifuge tubes.

Patients were selected based on their CAPRA-S score, a prognostic tool for predicting a patient's risk of biochemical failure following radical prostatectomy. The criteria used to derive CAPRA-S scores is detailed in Table 3. The association of CAPRA-S score with a patient's probability of progression free survival is listed in Table 4. To classify patients, we designated scores 0-2 as low risk, scores 3-5 as medium risk, and scores ≥6 as high risk [56]. Applying this classification system, we obtained paired samples from 8 patients in each risk group, tumor tissue and matched uninvolved adjacent prostate tissue. The samples were stored at -80˚C until RNA was extracted.

Table 3: CAPRA-S Scoring Criteria

Variable	Level	CAPRA-S points
Pre-surgical PSA level (ng/ml)	0.00 to 6.00	0
	6.01 to 10.00	1
	10.01 to 20.00	2
	> 20.00	3
Pathologic Gleason score	≤ 3 + 3 = 6	0
	3 + 4 = 7	1
	4 + 3 = 7	2
	≥ 4 + 4 = 8	3
Surgical margin status	Negative	0
	Positive	2
Extracapsular extension	No	0
	Yes	1
Seminal vesicle invasion	No	0
	Yes	2
Lymph node invasion	No	0
	Yes	1

Source: Cooperberg MR, et al. *The CAPRA-S score: A straightforward tool for improved prediction of outcomes after radical prostatectomy*. Cancer. 2011 Nov 15;117(22):5039-46. doi: 10.1002/cncr.26169.

Table 4: Projected Patient Outcomes

CAPRA-S score	No. patients	Probability of progression-free survival (%)	
		At 3 years	At 5 years
0	1,042	96.3	94.5
1	826	95.3	91.0
2	669	89.8	83.3
3	499	80.7	72.8
4	336	74.9	70.2
5	213	63.1	42.5
6	103	49.2	25.9
7	70	50.9	26.9
8	40	26.9	12.3
9 to 12	39	7.3	0.0

Source: Cooperberg MR, et al. *The CAPRA-S score: A straightforward tool for improved prediction of outcomes after radical prostatectomy*. Cancer. 2011 Nov 15;117(22):5039-46. doi: 10.1002/cncr.26169.

3.3 RNA Extraction and cDNA Synthesis

RNA extraction from culture cells: RNA was extracted from cultured cells using the Cells-to-Cts kit from System Biosciences and processed as follows. Cultured cells were dissociated as previously described, suspended in ice cold DPBS, pelleted by centrifugation at 1,250 rpm at 4˚C for 5 minutes. Cell pellets were suspended in ice cold DPBS and counted using a hemocytometer. Cells ($1x10^6$) were then transferred to a new conical tube, pelleted, suspended in cold DPBS again, and transferred to a microcentrifuge tube. Cells were pelleted at 3,000 rpm for 5 mins. Cell pellets were finally suspended in 100 µL of ice cold Cells-to-Cts buffer, and incubated for 10 minutes at 75˚C. Samples were cooled on ice and 2 µL of DNase I was added to cell lysates, followed by a 15-minute incubation at 37˚C. Next, the added DNase was inactivated by incubating the samples at 75˚C for 5 minutes. Lysates were quickly cooled on ice, then stored at -80 ˚C or immediately used for cDNA synthesis.

RNA extraction from clinical specimens: RNA extraction from FFPE tissue sections (curls) was conducted using the RecoverAll kit from Life Technologies. RNA was isolated from 80 µm thick sections (four 20 µm curls) from tissue blocks prepared from macro-dissected FFPE tissue. First, paraffin was removed from sections by adding 100% xylene to curls placed in RNase free micro-centrifuge tubes incubated at 50˚C for 3 minutes. Next, samples were centrifuged for 2 minutes at 13,000 × g and xylene was discarded. Tissues were washed twice with 100% ethanol and allowed to air dry. Tissues were then

digested with protease and incubated at 50˚C (15 min) and 80˚C (15 min). The isolation additive/ethanol solution was added to lysates and this mixture was passed through the filter cartridge (10,000 × g for 30 s). The filter cartridge was washed once with Wash 1 and twice with Wash 2/3 solutions. DNase was added directly to the filter and the filter cartridge was incubated at room temperature for 30 minutes. The filter cartridge was then washed with Wash 1 and twice with Wash 2/3 to remove degraded DNA. Total RNA was eluted by adding 50 µL of Elution Solution directly to the filter, and incubating the filter cartridge at room temperature for 1 min. Eluted RNA was collected by centrifugation (10,000 × g for 1 min).

Synthesis of cDNA was conducted using the QuantiMir RT kit from System Biosciences. For total RNA extracted using the Cells-to-Cts kit, 5 µL of Cells-to-Cts cell lysate was directly used for cDNA synthesis. Alternatively, 100 ng of total RNA extracted using the RecoverAll kit was used for each cDNA synthesis reaction. For both RNA extracts, poly-A tail synthesis was first conducted by combining 5 µL RNA, 2 µL 5x PolyA Buffer, 1 µL 25mM MnCl2, 1.5 µL 5mM ATP, and 0.5 µL PolyA polymerase in a PCR tube then incubating at 37 ˚C for 30 min. Following polyadenylation of the RNAs the oligo dT anchor was annealed to the RNAs as follows: 0.5 µL Oligo dT adapter was added to the RNAs, and incubated at 60˚C for 5 min, then cooled to room temperature for 2 min. Final reverse transcription was accomplished at 42˚C for 60 minutes, followed by inactivation of reverse transcriptase at 95˚C for 10 minutes. QuantiMiR cDNAs were then stored at -20˚C.

3.4 Quantitative Real-Time PCR

Expression of mature microRNAs from both cultured cells and FFPE tissues was determined by quantitative real-time PCR (qRT-PCR) using the miRNome microRNA Profiling Kit (System Biosciences). The kit provides specific primers for 1,113 mature miRNAs and includes primers for 3 internal control RNAs (U6 snRNA, RNU43 snoRNA, RNU1A snRNA). MicroRNA IDs listed in the text are based on Sanger miRBase identifiers. Primers were designed to maintain uniform amplification efficiencies. qRT-PCR reaction mixtures were prepared using 2x Maxima SYBR Green/ROX qPCR Master Mix (Thermo-Fisher). The following conditions were used qPCR cycling: Stage 1: 50˚C for 2 min (1 cycle), Stage 2: 95˚C for 10 min (1 cycle), Stage 3: 95˚C for 15 sec, 60˚C for 1 min (40 two-temperature cycles). For genome wide profiling, 384-well plate (ABI) format containing 6 µL reaction volume was used for each well. For validation runs, a larger scale reaction volume, 15 µL, was used per well in a 96-well (ABI) plate format. qRT-PCR was conducted using the Applied Biosystems Inc. 7900HT thermal cycler equipped with 384-well plate module. The data was initially analyzed using the SDS 2.3 software (ABI). DNA concentrations were reported through SYBR Green fluorescence and normalized to that of the passive reference dye, ROX. Ct values calculated by the SDS 2.3 software were transferred to the miRNome analysis software (SBI) to derive ΔΔCt values. The miRNome analysis calculates the ΔCt values based of the mean of the reference genes. The individual ΔCt values are then compared across samples to generate the ΔΔCt values for

each miRNA. miRNAs that showed significant changes in expression were then subject to further analysis. The statistical analysis of the qRT-PCR data is described in detail in the follow paragraphs.

Normalization of qRT-PCR expression values was further refined using the qBasePlus software (Biogazelle). Using the Genorm functionality included with the qBasePlus software, 7 additional stably expressed miRNAs were identified. The ΔCt value for each miRNA was then re-calculated utilizing the 7 additional miRNAs plus the 3 original controls. Following normalization, the expression of the reference miRNAs was re-evaluated to ensure their stability across samples was maintained.

Fold change values were calculated next to determine the relative changes in miRNA expression as treatment of LNCaP-104S cells progressed to CDX resistance or to determine expression differences between paired uninvolved and tumor tissues. These values were generated using the qBasePlus software. After normalization, the software assigned relative expression values where mean expression of the reference genes is determined to be a value of 1. Expression of each miRNA is then assigned a relative expression value in respect to the geometric mean of the controls. The geometric means were compared using the formula: ΔCt control= $2^{-(GM\mathbf{c}-GM\mathbf{r})}$

Where GM**c** is the geo-mean of the control sample and GM**r** is the geo-mean of the reference sample. The fold change, or $\Delta\Delta$Ct, for each miRNA was then calculated using the formula: $\Delta\Delta Ct = 2^{-(Ct\mathbf{R}-Ct\mathbf{C})}*(\Delta Ct \text{ control})$

Where Ct**R**= Reference sample miRNA Ct value, and Ct**C**= Control sample miRNA Ct value.

Z-scores were calculated to rank miRNAs for use in selecting candidates for further investigation. This was accomplished by, first determining the ΔΔCt ($\mathbf{A}_i$) of all miRNAs and using these values to derive the Global mean (**g**).

$$g = \sqrt[n]{\pi_{i=1}^{n} X_i}$$

The global mean is then used to determine the global standard deviation for each comparison using the formula

$$\sigma_g = e\sqrt{\frac{\sum_{i=1}^{n}(ln\boldsymbol{A}i - ln\boldsymbol{g}))^2}{n}}$$

From which z-scores were determined using the formula.

$$z = \frac{A - g}{\sigma}$$

Additional analysis was conducted using Cluster 3.0 and heat maps were generated by Java TreeView softwares. Multiexperiment Viewer software (MEV) was used for K-means clustering, T-tests, and volcano plots.

3.5 Plasmid DNA Purification and Transfection

DNA plasmids were purchased from their respective supplier and transformed into XL-10 Gold ultra-competent cells (Stratagene). Glycerol stocks of the transformed bacterial cells were prepared and stored at -80˚C. To purify the plasmids, liquid cultures were first prepared using 3mL L/B broth, appropriate antibiotic (10 mg/mL ampicillin or 30 mg/mL kanamycin), and 20 µL of the glycerol stock. The liquid cultures were grown at for 16 hours at 37˚C while shaking at 250 rpm. The cultures were pelleted into microcentrifuge tubes and resuspended in 600 µL TE buffer. The purification of all the plasmids was conducted using the Pureyield Plasmid Miniprep System (Promega). The cells were lysed by adding 100 µL of Cell Lysis Buffer to the 600 µL bacterial suspensions. Tubes were inverted six times to ensure even mixture. The lysis buffer was then neutralized with 350 µL of Neutralization Solution, and centrifuged at maximum speed for 4 minutes. The supernatant was transferred to a new PureYield Minicolumn and centrifuged at 10,000 x g for 60 seconds. The flow through was disposed of and 250 µL of Endotoxin Removal solution was added to the column and centrifuged at 10,000 x g for 60 seconds. The column was then washed with 500 µL Column Wash solution, and centrifuged at 10,000 x g for 60 seconds. The plasmid DNA was then eluted using 40 µL of sterile TE buffer, and centrifuged at 10,000 x g for 60 seconds. Quality and concentration of the purified DNA was then assessed using a NanoDrop

spectrophotometer, additionally agarose gel electrophoresis was used to determine plasmid size and degree of supercoiling. The purified plasmids were then stored at 4˚C. The transfection of DNA plasmids was carried out using Lipofectamine 3000 transfection reagents (Life Technologies). The DNA was first diluted in OptiMem, followed by addition of the P3000 reagent. This solution was mixed and incubated for 2 minutes, during this time the Lipofectamine 3000 reagent was diluted into OptiMem in a separate tube. The diluted Lipofectamine 3000 solution was then added to the diluted DNA solution, mixed and incubated for 10 minutes at room temperature. The ratios of DNA to Lipofectamine 3000 is cell line specific. Listed in Table 5 are the cell lines specific mixtures used to transfect an individual well of a 6-well plate, containing 2 mL of complete media.

Table 5: Cell line specific transfection protocol

Cell Line	DNA/P3000 Mix	Lipofectamine Mix
PC-3	125 µL OptiMem 1.25 µg DNA 2.5 µL P3000	125 µL OptiMem 3.7 µL Lipofectamine 3000
LNCaP	125 µL OptiMem 2 µg DNA 4 µL P3000	125 µL OptiMem 5.5 µL Lipofectamine 3000

3.6 Whole Cell Protein Extraction and Immuno-Blotting

Cells were harvested by trypsinization, washed twice with ice cold DPBS. Cell pellets were thoroughly resuspended in ice cold passive lysis buffer (5mM Tris, pH 7.5, 2mM EDTA, 150mM NaCl, 1% Nonidet P- 40, 0.1% sodium deoxycholate, 5% glycerol) containing Halt Protease and Phosphatase Inhibitors Cocktail (Thermo-Fisher). The samples were placed on ice for 10 minutes, with vortexing for 20 secs at 5 and 10 minutes. The samples were then subjected to one round of freeze thawing. This was executed by flash freezing in liquid nitrogen then quickly thawing in a 37˚C water bath, and vortexing for 15 secs before placing the samples back on ice for 5 minutes. The insoluble fraction was then separated by centrifugation at 13,000 x g for 15 minutes at 4˚C. The soluble fraction was then transferred to a new tube, and the protein concentration was determined by Bradford assay. Samples were then prepared to be separated by SDS-PAGE. The samples consisted of 50 µg extracted protein diluted in Laemmli sample buffer (to a final concentration of 33mM Tris-HCl pH 6.8, 10% glycerol, 1% SDS, 355 mM b-mercaptoethanol, 0.01% bromophenol blue). Samples were separated on 10% or 12% SDS-PAGE gels, and transferred to PVDF membranes (Pall) using a wet transfer system (Bio-Rad). Membranes were transferred to trays and rocked in India ink diluted 1:1000 in TBS-T (20mM Tris base, 137mM NaCl, 0.1% Tween, pH 7.6) to stain the transferred protein bands. The membranes were then blocked for 90 minutes using 5% milk in TBS-

T or 2% BSA in TBS-T. Primary antibodies were diluted in the corresponding blocking solution and applied to the membranes using a SURF blotter (Idea Scientific), which has channels that align with the sample lanes. Membranes were incubated with primary antibodies while rocking overnight at 4˚C or for 1-3 hours at room temperature. Non-specific antibodies were removed from the membranes by rocking the membranes in blocking solution for 5 minutes per wash, 4 wash cycles. Membranes were then incubated with HRP conjugated secondary antibodies diluted in 5% milk in TBS-T. Nonspecific antibodies were removed through 4-6 15 min washes with TBS-T. Immun-Star WesternC kit (Biorad) chemiluminescent substrate solution was added to the membranes and antibody staining was visualized and quantified using ChemiDoc XRS imaging system paired with Image Lab software (Bio-Rad). Using the intensity quantification function of the Image Lab software, intensity values for individual bands were generated. Antibody of interest band values were normalized to the paired values from the loading control antibodies. These normalized values were then used to compare across samples.

Table 6: Dilutions of antibodies and incubation times

Target Antigen	Supplier	Product No.	Host	Dilution Factor	Incubation Condition
FGD4	Genetex	GTX109859	Rabbit	1:350	**o/n; 4°C**
ABHD3	Biorbyt	orb31915	Rabbit	1:100	**o/n; 4°C**
AR	US Biological	030771	Mouse	1:800	**o/n; 4°C**
PSA	Santa Cruz	sc-7638	Goat	1:350	**o/n; 4°C**
Cbl	Santa Cruz	sc-170	Rabbit	1:300	**o/n; 4°C**
TRAF6	Millipore	061110	Rabbit	1:250	**o/n; 4°C**
ZFAND1	Santa Cruz	sc-87505	Rabbit	1:100	**o/n; 4°C**
IRAK1	Santa Cruz	sc-5288	Mouse	1:250	**o/n; 4°C**
DOK4	Santa Cruz	sc-130133	Rabbi	1:150	**o/n; 4°C**
VEGF	Santa Cruz	sc-152	Goat	1:400	**o/n; 4°C**
EGFR	Santa Cruz	sc-03-G	Goat	1:500	**o/n; 4°C**
ERK1/2 (pT202/pY204	Cell Signaling	4370	Rabbit	1:800	**o/n; 4°C**
PRAS40	Cell Signaling	2691	Rabbit	1:800	**o/n; 4°C**
p-PRAS40	Cell Signaling	13175	Rabbit	1:800	
Cyclin D1	Neomarker	MS-210-	Mouse	1:100	**o/n; 4°C**
Cofilin(pS^3)	Cell Signaling	3313	Rabbit	1:100	**o/n; 4°C**
LIMK1	BD	611748	Mouse	1:100	**o/n; 4°C**
p27	Santa Cruz	sc-528	Rabbit	1:100	**o/n; 4°C**
AKT (pS473)	Cell Signaling	4060	Rabbit	1:350	**o/n; 4°C**
AKT	Transduction Labs	N/A	Rabbit	1:1000	**o/n; 4°C**
ERK1/2	Cell Signaling	4695	Rabbit	1:600	**o/n; 4°C**
E-Cadherin	Cell Signaling	3195	Rabbit	1:700	**o/n; 4°C**
Slug	Cell Signaling	9585	Rabbit	1:150	**o/n; 4°C**
Vimentin	Cell Signaling	5741	Rabbit	1:200	**o/n; 4°C**
TWIST1	Gentex	GTX60776	Rabbit	1:150	**o/n; 4°C**
TCF8/ZEB1	Cell Signaling	3396	Rabbit	1:100	**o/n; 4°C**
N-Cadherin	Cell Signaling	13116	Rabbit	1:300	**o/n; 4°C**
SSH-1	Cell Signaling	13578	Rabbit	1:1000	**o/n; 4°C**
GAPDH	Sigma	G8795	Mouse	1:1000	**1hr; RT**
α-tubulin	Sigma	T9206	Mouse	1:1000	**1hr; RT**
γ-tubulin	Sigma	T3559	Rabbit	1:500	**1hr; RT**

Table 7: Immunoblotting Secondary Antibodies

Target Antigen	Supplier	Product No.	Host	Diluion Factor	Incubation Condition
Rabbit IgG	Jackson Labs	111-035-003	Goat	1:5000	1hr; RT
Mouse IgG	Jackson Labs	115-035-003	Goat	1:10000	1hr; RT
Rat IgG	Jackson Labs	112-035-003	Goat	1:10000	1hr; RT

3.7 MTS Colorimetric Assay

The MTS assay (Promega) relies on the active conversion of soluble tetrazolium into insoluble reduced salts. With this conversion by NADPH reductase, the solution changes from a pale yellow color to red-brown, with a strong absorbance at 490 nm wavelength. Monitoring the changes in absorption at 490 nm allows for the relative quantification of viable cells in each sample well. Cells were passaged the day prior to seeding of 96-well assay plates, to ensure cell populations were in the log-phase of growth. Cells were dissociated with a trypsin-EDTA solution, washed in DPBS and counted using a hemocytometer. The appropriate number of cells were then transferred to a new conical tube containing enough complete media needed to fill the number of desired wells. The cell suspension was then equally divided into a pipetting basin. Equal volumes of the cell suspension were then distributed to each well using a multi-channel pipettor. The plate was then incubated overnight and the following steps are specific to the described experiments.

For transfection of PC-3 cells, $3x10^3$ cells were first seeded in 100 µl complete media in each well of a 96-well plate. The following day cells were transfected with either miR-17-92a expression plasmid or scrambled expression plasmid, using the cells specific protocol described previously. The media in all the wells was changed to fresh complete media, 8-12 hours post transfection. To quantify the effect of miR-17-92a on PC-3 cell proliferation, cells were incubated for 48 hours before addition of the MTS reagent. For experiments used to monitor the effect of miR-17-92a expression on drug sensitivity, treatment media was added 24 hours after transfection

3.8 Dual Luciferase 3'UTR Reporter Assay

A dual luciferase reporter assay was used to determine if the predicted mRNA targets were directly regulated by members of the miR-17-92a cluster. PC-3 cells expressing miR-17-92a or Scr RNA were seeded into 96-well plates. The following day, the cells were transfected with either control luciferase reporter plasmids or the experimental plasmids. The cells were then incubated for 48 hours to allow for the expression of luciferase. After 48 hours, luciferase activity was quantified using the Luc-Pair assay kit (Genecopoeia) or the DualGlo (Promega) in conjunction with a plate reader.

The pEZX-MT06 plasmid (Genecopoeia cat # HmiT002135-MT01) contains the first 500 nucleotides of the FGD4 3'UTR located immediately downstream of the firefly luciferase gene (FGD4-3'UTR^{WT} construct). This region contains one of the predicted

binding sites for miRs -17 and -20a. Additionally, site directed mutagenesis was employed to mutate three bases in the miR-17/20a seed region present in the cloned FGD4 3'UTR to generate the FGD4-3'UTR^{Mu} construct. Nucleotides 80-GC**ACU**UUA-90 were mutated to 80-GC**CAG**UUA-90.

The 3'UTRs of LIMK1 and SSH1 were cloned into the pMirGlo plasmid (Promega). The SSH1 3'UTR was amplified using the following primers (Forward: 5'-GTAGACAGGAGTCCCGATAAG-3', Reverse: 5'-TCACAAGAAGCACACACAC-3'). The LIMK1 3'UTR was amplified using the following primers (Forward: 5'-GTAGACCGCTTCCCCTGC-3', Reverse: 5'-CCTCCCTAAGTCATGGTCCC). Amplified 3'UTRs were ligated into pGEMT-Easy plasmids (A/T cloning vector). The 3'UTRs were then excised from pGEMT-Easy by digestion using AccI and NotI-HF (NEB), then ligated into the destination plasmid (pMirGlo), which was also digested with AccI and NotI-HF.

PC-3 cells or C4-2B cells were seeded into 96-well plates. The following day, the cells were co-transfected with miR-17-92a or Scr RNA expressing plasmids along with either control luciferase reporter plasmids or the experimental plasmids. The cells were then incubated for 48 hours to allow for the expression of luciferase. After 48 hours, luciferase activity was quantified using DualGlo (Promega) in conjunction with a plate reader.

3.9 Immunofluorescence Assay

For immunofluorescence assays of transiently transfected cells, 2 x 10^4 PC-3 cells were seeded onto poly-l-lysine coated coverslips in a 24-well dish. The next day cells were transfected as previously described with either the miR-17-92a expression plasmid or the Scr control plasmid. Cells were incubated for 48 hours following transfection before processing of coverslips.

For immunofluorescence assays of stably expressing cells, 2.5 x 10^4 cells were seeded onto poly-l-lysine coated coverslips in a 24-well dish. Coverslips were incubated for 48 hours before processing.

To process coverslips, growth media was removed from the well and coverslips were washed three times with DPBS. Cells were then fixed in 4% paraformaldehyde (Sigma Aldrich) for 10 minutes at room temperature. The coverslips were then washed twice with DPBS and permeabilization of cell membranes was achieved by incubating coverslips in DPBS containing 0.25% Tween-20 (Fisher) for 10 minutes at room temperature. Cells were then blocked in DPBS containing 10% goat serum (Sigma Aldrich), 2% BSA (Sigma Aldrich), and 0.1% Tween-20 for at least 1 hour at room temperature. Primary antibodies were diluted in DPBS containing 2% BSA, and 0.1% Tween-20, specific dilutions are listed in Table 8. Cells were incubated in primary antibody dilutions for 1 hour, then washed with blocking solution 3 times (5 minutes/wash) while rocking. Fluorescently conjugated secondary antibodies were diluted in DPBS containing

0.1% Tween-20, specific dilutions are listed in Table 9. Cells were incubated in the dark with diluted secondary antibodies for 45 minutes at room temperature. Non-specific antibodies were removed by washing with DPBS containing 0.1% Tween-20 for 3 times (5 minutes/wash) while rocking. To remove excess salts, coverslips were then washed twice (3 minutes/wash) in 100mM sodium phosphate buffer (pH 7.4). Coverslips were then removed from wells, excess buffer was wicked away using Kimwipes (Kimberly-Clark), and 20 µL of DAPI-Mount G (Southern Biotech) was applied to coverslip. Using fine tip tweezers coverslips were slowly rotated allowing the mounting media to swirl and coat coverslip. The coverslips were then inverted and held perpendicular on top of Kimwipes, allowing mounting media to absorb into wipes. This process was repeated a second time; the coverslips were then laid cell side up on clean Kimwipes for 2 minutes. The coverslips were then flipped and mounted onto slides and placed in a dark drawer for at least 12 hours. The coverslips were cleaned and sealed with clear nail polish.

Slides were imaged by confocal microscopy using a Leica SP-5 confocal microscope paired with the Leica LAS-AF software suite. The LAS-AF software was also used to quantify fluorescent intensities of individual cells.

Table 8: Immunofluorescence Primary Antibodies and Stains

Target Antigen	Supplier	Host	Dilution Factor
FGD4	Genetex	Rabbit	**1:350**
E-Cadherin	Cell Signaling	Rabbit	**1:500**
Ki67	**Cell Signaling**	**Mouse**	**1:350**
pERK1/2	Cell Signaling	Rabbit	**1:350**

Table 9: Immunofluorescence Secondary Antibodies

Antigen	Fluorophore	Company	Host	Dilution
Mouse IgG	488	Molecular Probes	Goat	**1:300**
Mouse IgG	Cy3	Jackson Immuno	Goat	**1:300**
Rabbit IgG	Cy3	Jackson Immuno	Goat	**1:300**
Mouse IgG	647	Molecular Probes	Goat	**1:300**
Rabbit IgG	647	Molecular Probes	Goat	**1:300**

3.10 Flow Cytometry

PC-3 sublines expressing miR-17-92a or Scr RNA were grown to 60-80% confluency and dissociated is DPBS containing 10 mM EDTA. Cells were collected and washed in ice-cold DPBS, and fixed in 4% paraformaldehyde for 5 mins on ice. Cells were agitated every minute to minimize clumping. After 5 mins 10 mL of cold HAM-F12K was added to fixation solution and mixed. Cells were pelleted at 1,200 x g for 5 mins at 4˚C. Cell pellets were resuspended in cold DPBS media containing 10% goat serum and counted. Cells were blocked on ice for 20 minutes and 1 x 10^5 cells were transferred to a LoBind microcentrifuge tube (Eppendorf) and pelleted. Cell pellets were then resuspended in cold DPBS containing 2% BSA. Antibodies specific for e-cadherin were added to cell suspensions to achieve a 200-fold dilution. Cells were incubated with antibodies for 1 hour while rotating. Non-specific antibodies were removed by three washes in blocking buffer. AlexaFluor488 conjugated goat anti-rabbit antibodies (Life Technologies) were diluted 1:300 in in DPBS containing 1% BSA. Cells were incubated in diluted secondary antibodies for 30 minutes while rotating. The labeled cells were washed first in DPBS then 3 times in DPBS containing 0.05% Tween-20. The labeled cells were detected using the BD Accuri Flow cytometer and analyzed with the BD CSampler Software. In addition to the experimental samples, control samples were prepared consisting of fixed but unlabeled PC-3 cells and PC-3 cells that were fixed,

blocked, and incubated with only the secondary antibodies. The control cells incubated without primary antibodies was used to establish the staining threshold. Events above this threshold were considered positive for staining.

3.11 Cell Treatments

The small molecule inhibitor MK-2206 2HCl (Selleckchem) was used to inhibit the activities of AKT1/2/3. PC-3 cells were seeded into 96-well plates and transfected the following day. Twelve hours after transfection, media was replaced with 50 µL fresh complete media. Twenty-four hours post transfection 50 µL of media containing MK-2206 was added to the 50 µL of media already present, resulting in inhibitor concentrations of 1, 5, or 10 µM. Alternatively, DMSO was diluted in the same manner and used as the vehicle control. For treatment of LNCaP-104S cells media was prepared with charcoal-stripped fetal bovine serum and without supplemented DHT. Cells were seeded in 100 µL CS-FBS containing media supplemented with 20% conditioned maintenance media. After the cells had attached, 24-30 hours, 80 µL was very slowly removed from each well. The plate was held at an angle and 100 µL of fresh CS-FBS media was very slowly pipetted onto the wall of the well. Note, this gentle pipetting method was used for all media changes. Four hours after the media was changed, the cells were transfected. The transfection media was replaced after 12 hours, and the cells were treated in a manner similar to PC-3 cells. LNCaP-104S were treated with 0.5 µM, 1 µM, or 2.5 µM concentrations of AKT inhibitor, MK-2206. DTX, CDX, VX680.

3.12 Wound Healing Assay

PC-3 sublines expressing miR-17-92a or Scr RNA were seeded into wells of 6-well plate in HAM F-12K media containing 5% fetal bovine serum. Cells were grown to confluency (24-36 hours after seeding) and wounds were created with a micropipette tip. The cells were washed twice with media, to remove debris and detached cells, before continued incubation in media containing 5% fetal bovine serum. Wound healing was observed at 14, 16, 20, and 24 hours, marks were made adjacent to each wound to permit alignment of plate for re-imaging the same wound regions. Images of the wound were taken under 10x magnification using a Nikon eclipse TE200 inverted microscope paired with Nikon elements F 2.20 software. The average width of each wound was determined using ImageJ software. small molecule

3.13 Xenograft Mouse Model

Xenograft experiments were conducted in 6-8 weeks old male NSG (NOD scid gamma, NOD-scid IL2Rgnull, NOD-scid IL2Rgammanull, NSG) mice obtained from Jackson Laboratory and maintained and treated under specific pathogen-free conditions. Stable pool of PC-3 and M-12 Cells ($2x10^6$ / mouse) suspended in 0.1% matrigel in 100µl volume were injected subcutaneously into the flank and tumor growth monitored for 60 days. Tumor growth was assessed by measurements with a caliper and volume was

calculated as 0.52 × length × width × 2 as tumor grew. Tumors were harvested, as after the specified time, tissue architecture examined by H&E staining of formalin fixed paraffin embedded sections and used for RNA extraction for qRT-PCR of the matured miR-17-92a miRNAs expressed in the tumor. Following is the detailed description of the method of harvesting of samples, Mice were euthanized and tumors were promptly excised, non-tumor tissue was trimmed, and the tumor was cut into multiple sections and washed with ice cold DPBS. Samples designated for H&E staining were added to tubes containing ice-cold formalin. Samples designated for RNA extraction were cut into smaller sections and added to tubes containing ice-cold HBSS (Hank's buffered saline solution). Samples were kept on ice until all tumors were harvested. The unfixed tumors in HBSS were then transferred to cryotubes before being flash frozen in liquid nitrogen. Xenograft experiments were performed using an animal protocol approved by the Animal Care and Use Committee of the University of Central Florida.

CHAPTER FOUR: RESULTS

4.1 MicroRNA Expression Associated with The Acquisition of Androgen Independence

The successful management of late stage metastatic prostate cancer remains a difficult task. Clinicians turn to systemic treatments, which carry the greater reductions in patient's quality of life but can treat all metastatic sites. Because androgen is required for normal growth and functioning of the prostate gland and also for development of cancer androgen deprivation therapy (ADT) has become the mainstay for advanced prostate cancer [52]. Although most patients initially respond to ADT by showing low PSA values, they eventually develop more aggressive castration resistant prostate cancer (CRPC). This has driven research into the mechanisms and biomarkers associated with androgen independence. A number of studies indicated aberrant expression of miRNAs in CRPC compared to androgen dependent (AD) prostate cancer cells [57, 58]. Several miRNAs, such as miR-21, miR-125 and miR-32 are directly regulated by androgens in cells and xenograft models [57, 59, 60]. Studies include comparative analysis between androgen sensitive (AS) and -resistant prostate cancer cells, with or without treatment of AS cells with androgens or normal vs. hormone refractory prostate cancer tissues, which only provides steady state status of miRNA and gene expression. However, none of these studies provide information on the mechanism of transition of androgen-sensitive or

dependent prostate cancer cells to antiandrogen resistant cells. In this study, we show, for the first time alteration in expression of miRNAs and their target proteins as the cells progress to antiandrogen resistance, some of which are not detectable in the established AI cell line.

4.1.1 MicroRNA Expression Profile Differentiates Between Untreated LNCaP Cells and Cells Treated with Casodex or Subjected to Androgen Withdrawal

We used genome-wide miRNA array (1113 unique primers) profiling approach to identify specific miRNAs that are involved in development of resistance to Casodex (CDX). A clonal subline of LNCaP cells LNCaP-104S (−104S) and its androgen-independent derivative LNCaP-104R1 (−104R1) were used for monitoring differential expression of miRNAs upon treatment with CDX. LNCaP-104S cells are CDX-sensitive, whereas LNCaP-104R1 cells are not despite expressing AR at a basal level higher than LNCaP-104S cells [61]. LNCaP-104S cells require DHT for maintaining their AD status but when treated with CDX for 3 weeks in CS-FBS (charcoal-stripped FBS), CDX insensitive colonies develop that are independent of androgen (CDXR). During the first week of both CS-FBS and CDX treatments, LNCaP-104S cells grew without significant cell death, however, during the second week of CDX treatment about 60% cells died and detached. From the residual 40% cells, half of the cell population remained viable during the third week of CDX treatment. CS-FBS -treated cells did not show as much cell death

during the second week of treatment and started to regrow during the third week of treatment. Cell morphology also changed as they are treated with CDX and CS-FBS (Figure 5). The cells adopted a neuroendocrine phenotype characteristic of LNCaP cells exhibiting repression of the Androgen Receptor [62]. Cells viable after third week of treatments were used for miRNA profiling experiments. Expression of AR in these cells showed gradual reduction as the treatment progresses, but the PSA expression increased, which suggests increased transcriptional activity of the residual AR in the treated cells (Figure 6).

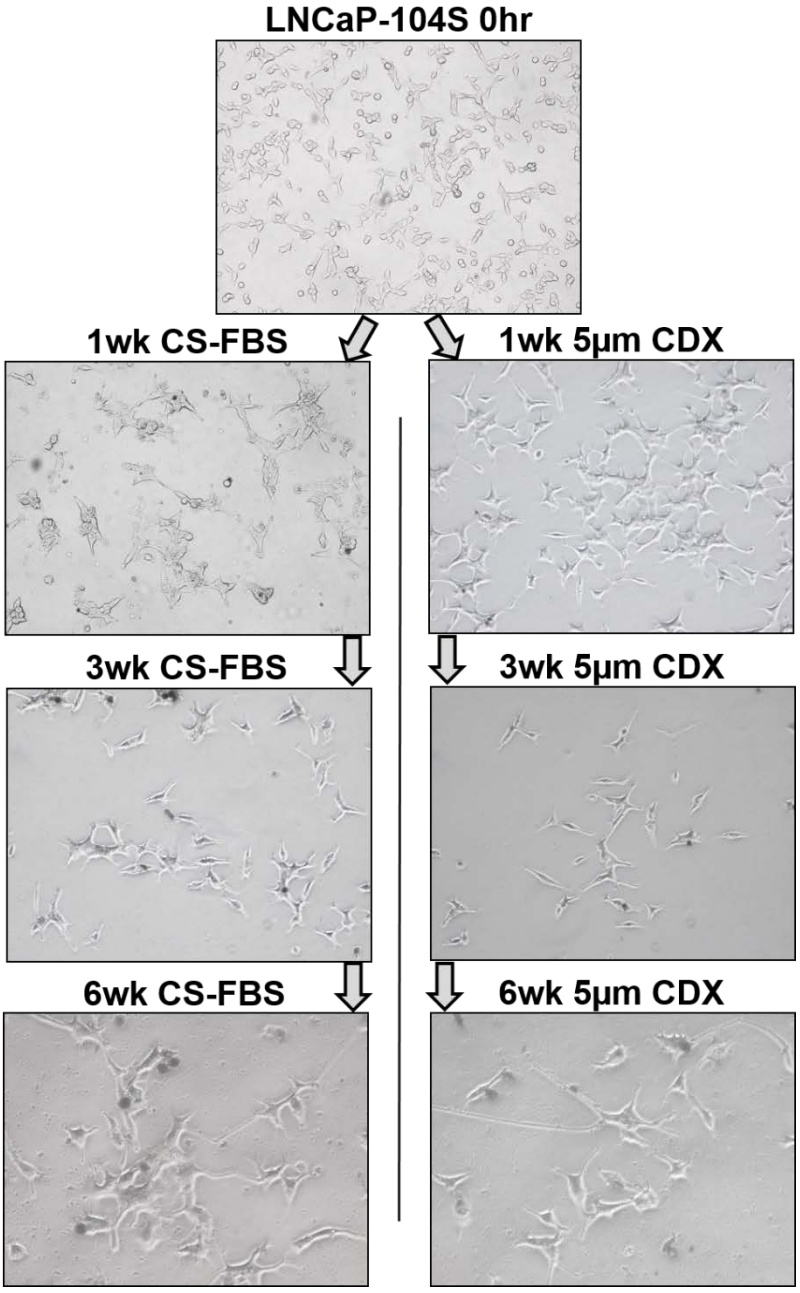

Figure 5: Altered cell morphology during ADT

Images of LNCaP-104S cells before and during androgen deprivation or androgen blockade.

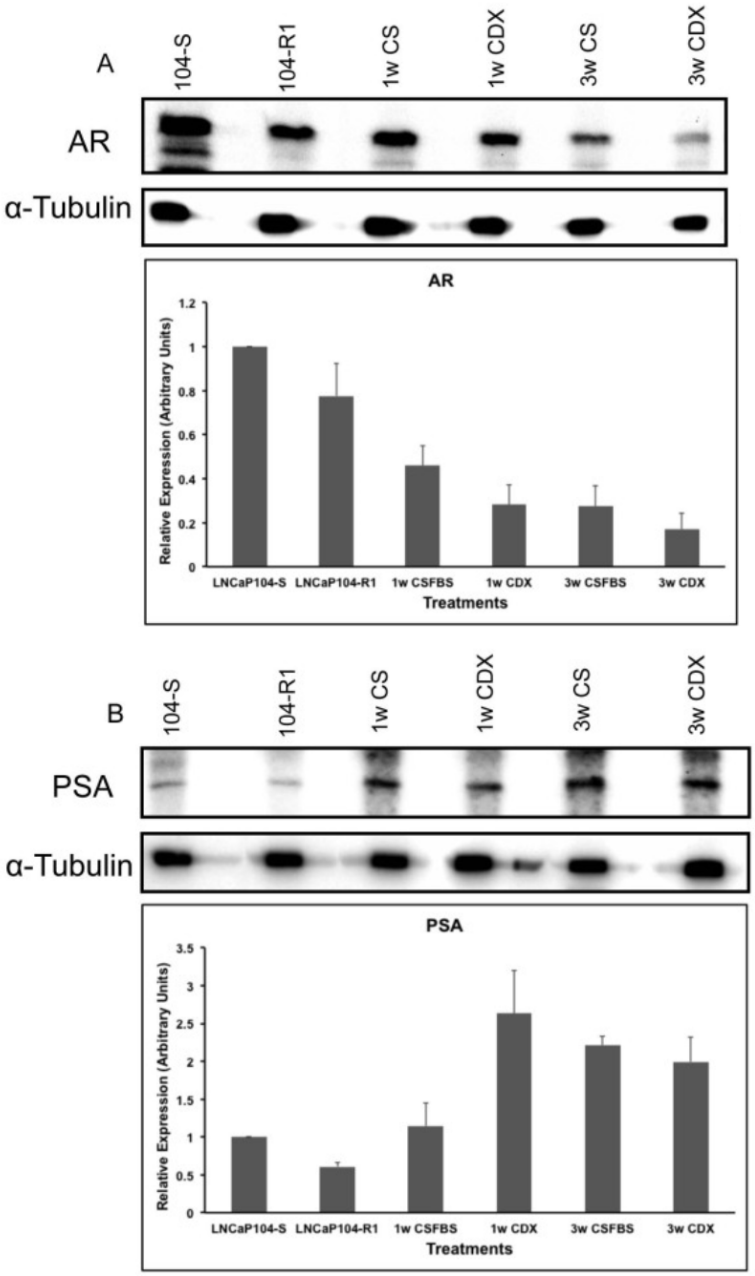

Figure 6: Expression of AR and PSA in androgen sensitive and independent cells

Immunoblots displaying expression of Androgen Receptor (A) and PSA (B) in androgen sensitive -104S cells, androgen independent -104R1, and -104S cells at 1 and 3 wks of ADT (left to right).

We compared miRNA expressions in RNA extracts from untreated and CDX treated -104S cells at 0 hr, 1wk and 3wks and untreated -104R1 cells (Table 10).

Table 10: Cell lines and treatments

		Samples		
		Cell Line	**Treatment**	**Time point**
Reference	0hr	LNCaP-104S	FBS-DHT 1nM	0 hr
	1wk CSFBS	LNCaP-104S	CSFBS	1 wk
	3wks CSFBS	LNCaP-104S	CSFBS	3 wks
	1wk CDX	LNCaP-104S	CSFBS/5μM CDX	1 wk
	3wks CDX	LNCaP-104S	CSFBS/5μM CDX	3 wks
Test/Reference	0hr	LNCaP-104R1	CSFBS	0 wks

Hierarchical clustering of the normalized and log2 transformed expression data (Additional File 1) showed 5 distinct clusters of miRNAs (Figure 7). Comparative analysis between samples from different conditions using two samples Welch t-test with Log10 transformed data and p values of 0.05 showed significant miRNAs that are differentially expressed between conditions (Figure 8:). Volcano plot (V plots) of the t-test between LNCaP-104S cells and all other samples showed 38 significant miRNAs, of which 27 miRNAs were up regulated and 11 down regulated compared to -104S (Figure 8: A). Comparison between untreated -104S and -104R1 cells showed 24 significant miRNAs, which includes 16 down regulated and 8 up regulated miRNAs in -104R1 (Figure 8: B).

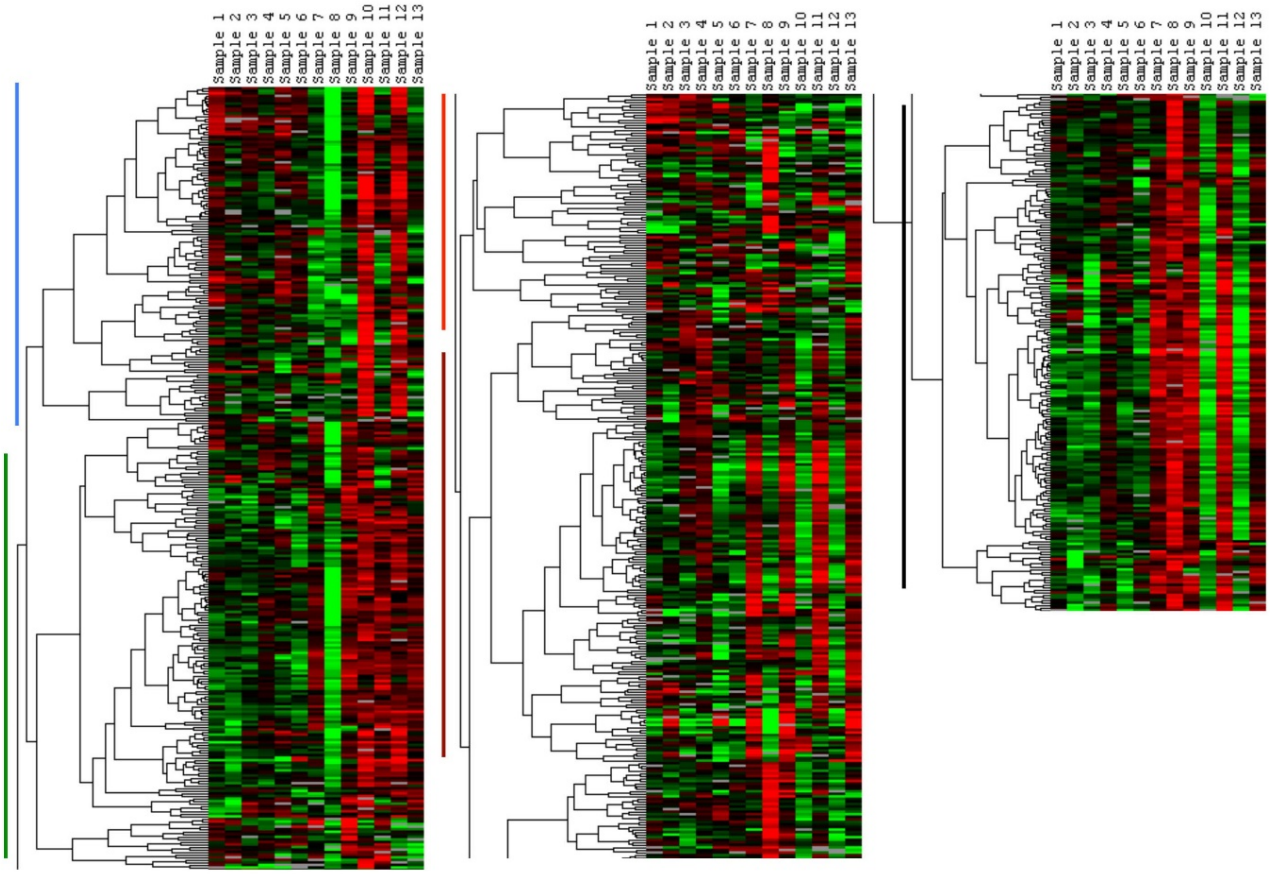

Figure 7: Hierarchical clustering of the data from genome wide miRNA profiling

Hierarchical clustering of the data from genome wide profiling of miRNAs in LNCaP Cells with or without treatment with CS-FBS and CDX. Samples 1, 2: LNCaP-104R1, Samples 3-5: LNCaP-104S1, Samples 6, 7: LNCaP-104S 1 wk CDX treated, Samples 8, 9: LNCaP-104S 1 wk CSFBS treated, Samples 10, 11: LNCaP-104S 3 wks CDX treated, Samples 112, 13: LNCaP-104S 3 wks CSFBS treated

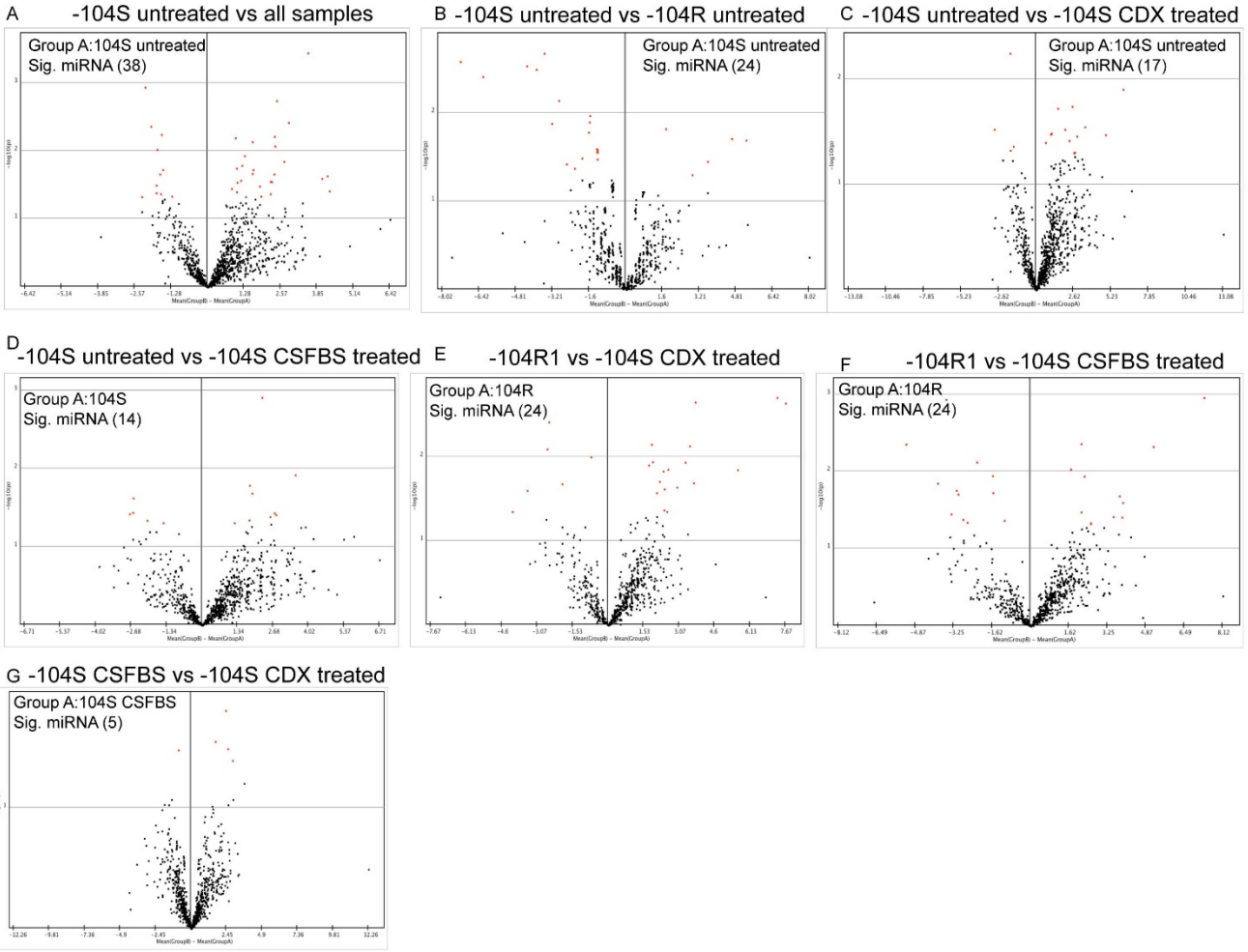

Figure 8: Volcano plots of the two samples t-tests of the normalized values of untreated and treated LNCaP cells.

Plots of the two samples t-tests of the normalized values of untreated and treated LNCaP cells as shown in Additional File 2.

Differential expression of 17 significant miRNAs was observed between untreated LNCaP-104S cells and -104S cells treated with CDX, of which 13 were up regulated and 4 were down regulated CDX treated cells (Figure 8: C). LNCaP-104S and -104S cells treated with CSFBS also showed 9 up regulated and 5 down regulated microRNAs in CSFBS treated cells (Figure 8D). Although -104R1 cells are CDX resistant there are differences in miRNA expression when -104S cells were treated with CDX (Figure 8E). T-test analysis showed 24 significant miRNAs of which 18 miRNAs were up regulated and 6 down regulated in -104R1 cells. Difference in miRNA expressions was also noted between -104S cells maintained in androgen-depleted condition and AI -104R1 cells. Twenty-four significant miRNAs were identified of which 12 were up regulated and 12 down regulated in -104R1 cells (Figure 8F). Comparison between androgen depletion and CDX treatment showed 5 significant miRNAs, 4 of which were up regulated and one down regulated in CDX treated cells (Figure 8G).

Clustering analyses using log2 transformed fold change (FC) values of four treatment conditions compared to -104S untreated cells showed two distinct clusters of up and down regulated miRNAs, which includes 307 down regulated and 197 up regulated miRNAs (Figure 9 and Additional File 3). Using Venn diagrams we identified miRNAs that were commonly or uniquely deregulated in CSFBS and CDX treated cells compared to untreated -104S cells or -104R1 (Figure 10). MicroRNAs that appeared in multiple comparisons, including miR-146a, -302c, -18a/b, -20a/b) are highlighted.

K-median clustering for the up-regulated miRNAs showed a trend of gradual increase in median FC in miRNAs in some clusters (cluster 1, 4 and 9) and a gradual decrease in some clusters (clusters 3, 7 and 8) from 1 week to 3 weeks treatments (Figure 11 and Additional File 4). In down regulated profile there is also a trend of gradual decrease in median expression of miRNAs in some clusters (clusters 1, 2, 3 and 7) (Figure 11B and Additional file 7). Of these lists, 100 miRNAs were chosen based on fold change and/or the z score ≥3.0 or ≤ -3.0 for validation using qPCR

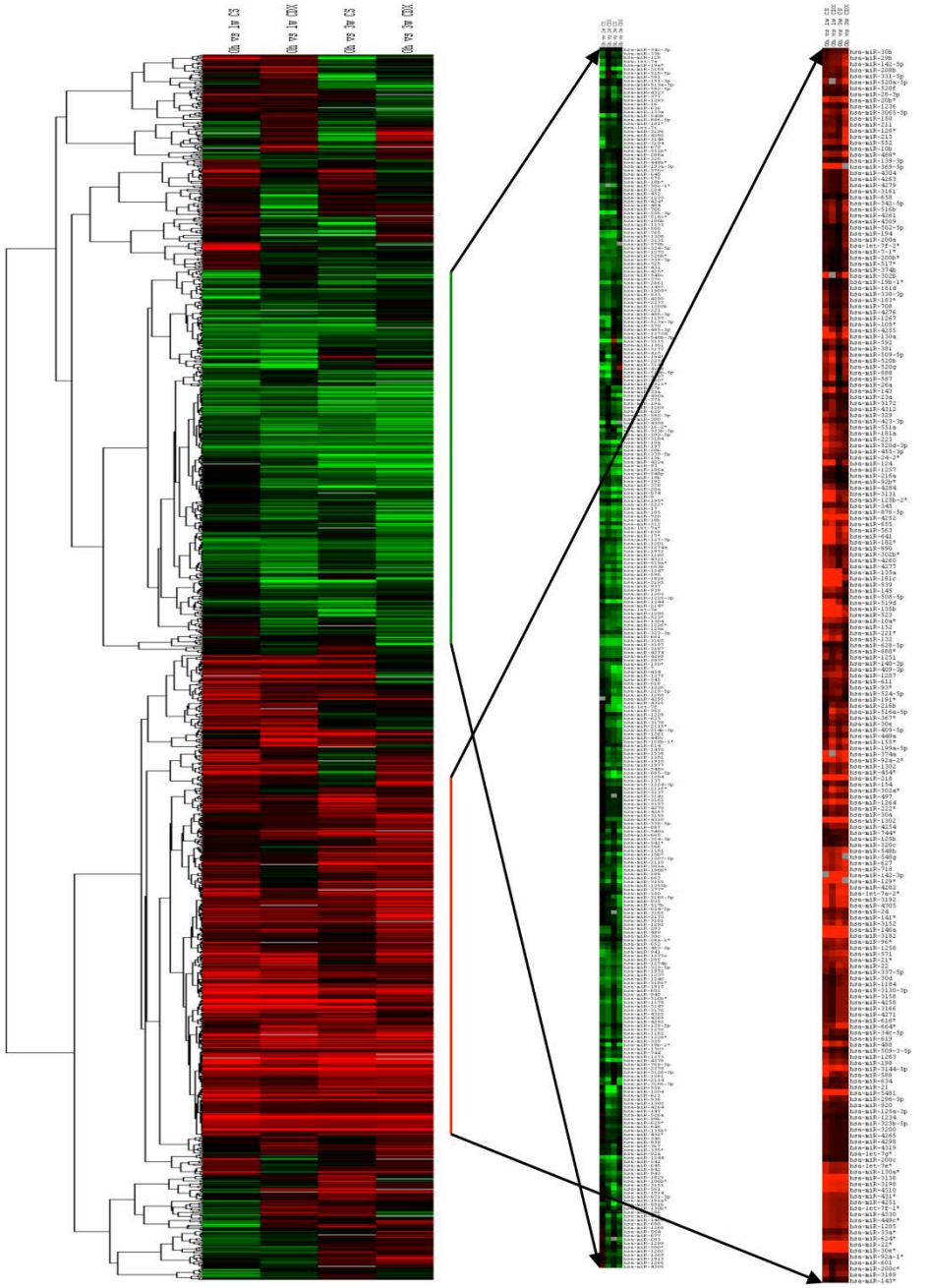

Figure 9: Cluster analysis of fold change in expression of miRNAs in different treatment conditions.

Hierarchical clustering of log_2 transformed FC expression of miRNA in four groups, 1wk CSFBS, 1wk CDX, 3wks CSFBS and 3wks CDX (Table 10). Red and Green lines showing the expression patterns of 197 up regulated and 307 down regulated miRNAs respectively (Additional File 3)

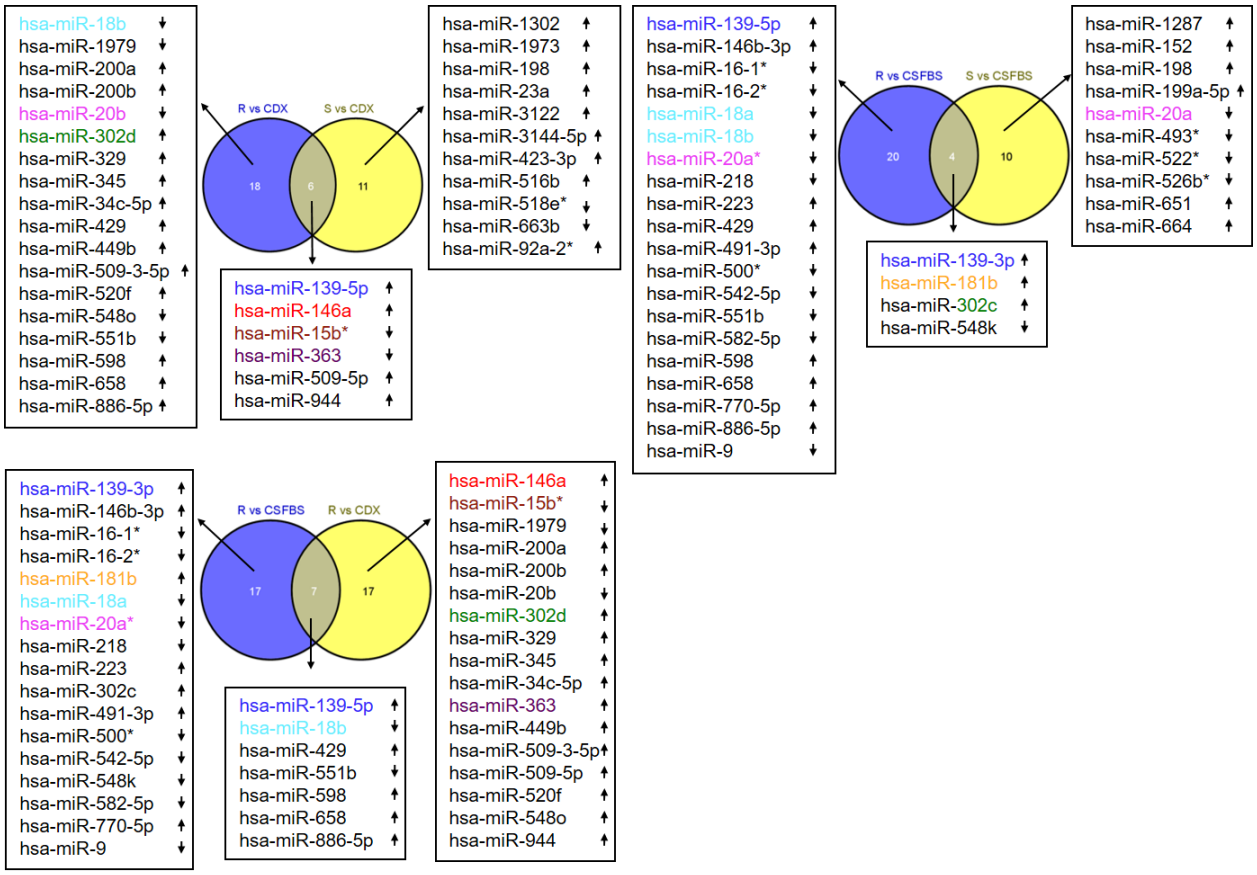

Figure 10: Analysis of commonly and uniquely regulated miRNAs across treatment conditions and LNCaP-104 sublines.

MicroRNA expressions from -104S cells at 3 weeks of treatment with CS-FBS only or CDX were compared against untreated -104R and 104S sublines. miRNAs exhibiting at least a 3-fold difference in expression from each comparison was used to construct Venn diagrams which identify common and unique alterations in miRNA expression. Colored miRNAs were identified in more than one comparison.

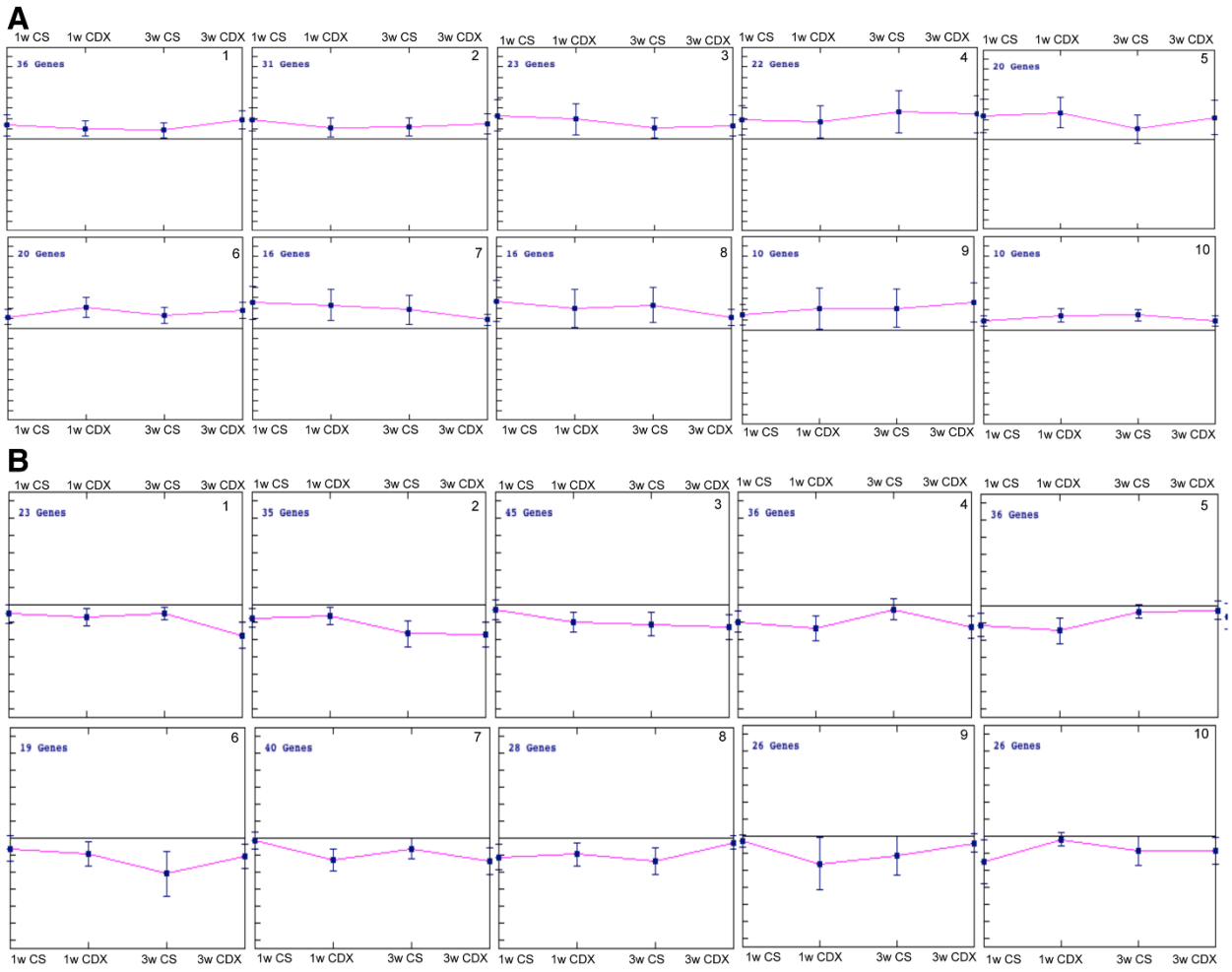

Figure 11: K-median cluster analysis for differentially expressed miRNAs at different treatment conditions and time points

A) Up regulated miRNAs separated into 10 clusters based on similar trends in expression patterns are depicted. MiRNAs in each cluster are showing a unique pattern of expression among 1wk and 3wks treatments of both CDX and CSFBS. B) Down regulated miRNAs divided into 10 clusters based on similar trends in expression are shown. MiRNAs in each cluster are showing unique patterns of expression during 1wk and 3wks treatments of CDX and CSFBS. Data shows median ± SD of expression of miRNAs in each cluster.

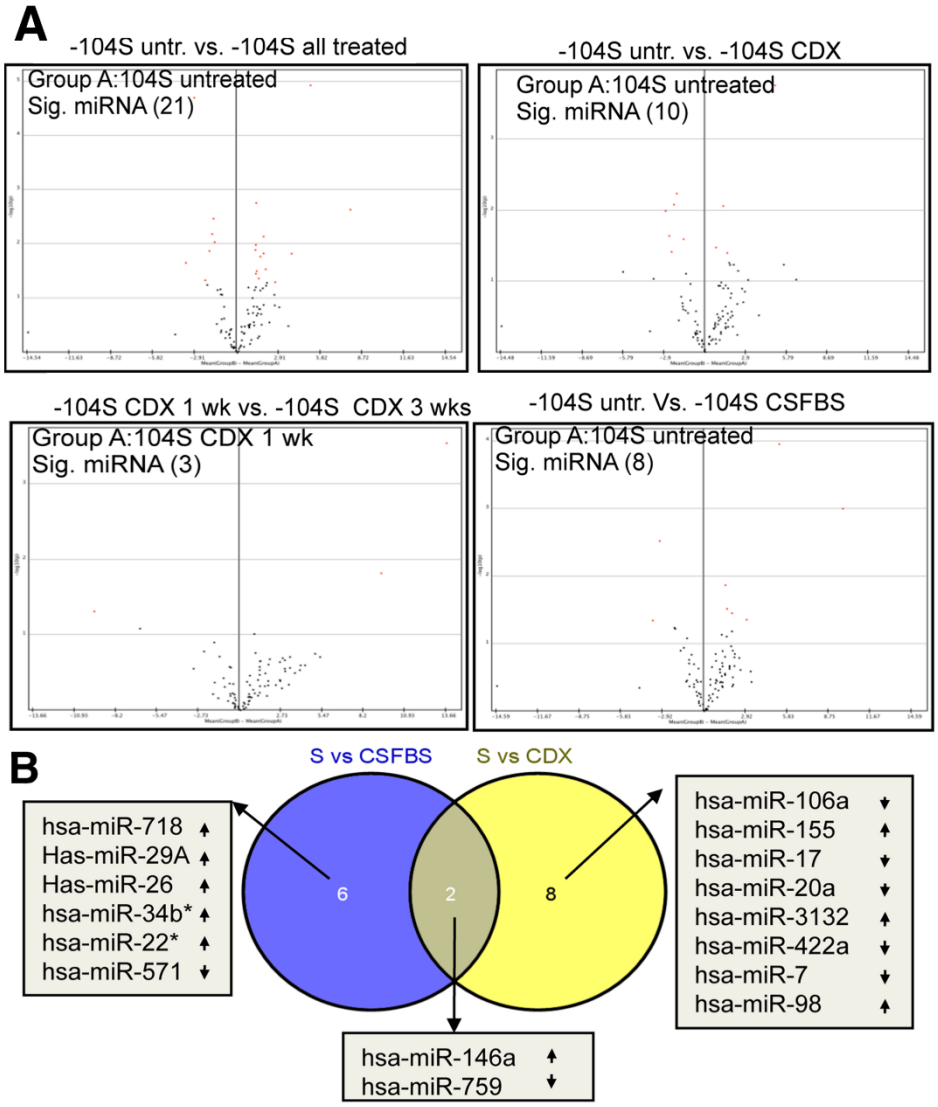

Figure 12: Comparative analysis of the expression of validated miRNAs during progression to ADT and CDX resistance.

A) Volcano plots depicting significant miRNAs identified by two sample t-test in all treatment conditions compared to untreated -104S cells (1st panel from left), in all CDX treated cells compared to untreated S cells (2nd panel from left), in 3wks CDX treated cells compared to 1wk CDX treated S cells (3rd panel from left) and in all CSFBS treated cells compared to untreated S cells (4th panel from the left). B) Venn diagram using significant miRNAs identified in two sample t-tests (volcano plots) showing common and unique miRNAs between all -104S CSFBS and -104S CDX treated cells.

Common Down-Regulated miRNAs		
All Treatments	1w CDX & 3w CDX	3w CS & 3w CDX
miR-4310	miR-518b	miR-518b
miR-518b	miR-7-2*	miR-4310
miR-759	miR-759	miR-596
miR-7	miR-4310	miR-18a
miR-596	miR-7	miR-20b*
miR-3131	miR-18a	miR-7
miR-18a	miR-596	miR-759
miR-17	miR-106a	miR-106a
miR-106a	miR-20a	miR-422a
	miR-17	miR-18b
	miR-422a	miR-20a
	miR-3131	miR-17
	miR-18b	miR-3131
	miR-1204	miR-15b
		miR-1204

Common Up-Regulated miRNAs			
All Treatments	1w CDX & 3w CDX	3w CS & 3w CDX	
miR-1197	miR-218	miR-145	miR-3192
miR-138	miR-92a-2*	miR-125b-2*	miR-184
miR-3199	miR-138	miR-493*	miR-3132
miR-20b	miR-3155	miR-3155	miR-34b*
miR-146a	miR-155	miR-3199	miR-29A
let-7f-1*	miR-4324	miR-1197	miR-22*
miR-22*	miR-1197	miR-664	miR-523
miR-19B	miR-3199	miR-548l	miR-222
miR-143	miR-20b	miR-138	miR-143
miR-145*	miR-145*	miR-302a*	miR-218
	miR-548t	miR-145*	miR-19B
	miR-19B	miR-29B	miR-20b
	miR-22*	miR-136	let-7f-1*
	miR-146a	miR-29C	miR-146a
	let-7f-1*		
	miR-143		

Figure 13: Comparative analysis of the commonly regulated miRNAs during progression to ADT and CDX resistance.

List of commonly down-regulated (Left) and up-regulated (Right) miRNAs as noted in Venn diagram in all treatment conditions, between 1wk CDX and 3wks CDX and between 3wks CDX and 3wks CSFBS cells.

4.1.2 Validated Expression of miRNAs Revealed Distinct Differences in Expression in Different Treatment Conditions

Analysis of qPCR data indicated a variable expression profile of a subset of miRNAs in LNCaP cells exposed to CDX and/or androgen withdrawal (CSFBS) for different time periods. Two sample Welch t-test with a p-value < 0.05 showed a significant change in expression of 21 miRNAs in treated samples compared to the untreated -104S cells (Figure 12A and Additional File 5). Comparison between -104S untreated and either CDX or CSFBS treated samples identified 10 and 8 significant miRNAs respectively (Figure 12A) Comparative expression analysis between CDX 1wk and CDX 3wks also revealed significant change in expression in 3 miRNAs (Figure 12A). Venn Diagram of miRNA expression profiles following CDX treatment and androgen withdrawal indicated two common miRNAs (miR-146a and miR-759) but treatment specific differential expression was observed with 8 and 6 unique miRNAs, in CDX and CSFBS treated respectively (Figure 12B). Analysis of the up-regulated miRNAs revealed 10 miRNAs that showed 2-fold or higher expressions in all treatment conditions and time points (Figure 12C). There are also 30 miRNAs that showed 2-fold or higher expression in more than one treatment conditions. In the down regulated list, 9 miRNAs showed at least 2-fold reduction in expression in all treatment conditions and 15 miRNAs with ≥2.0-fold down regulation in more than one treatment conditions (Figure 12D).

Cluster analysis of $\log_2$ transformed FC in expression of 100 miRNAs showed three

distinct clusters displaying common expression changes in 2 time points of two treatment conditions. Two clusters contained miRNAs with increased expression and one cluster containing down regulated miRNAs (Figure 14 and Additional File 6). K-median clustering of the up-regulated miRNAs showed a distinct trend of gradual increase (clusters 1 [32%], 2 [26%] and 4[11%]) and gradual decrease (cluster 3 14%) in FC expressions as the treatment progressed (Figure 15 and Additional File 7). Some of the miRNAs (21) showed across the board up regulations (Table 11). Similarly, in the list of down-regulated miRNAs a gradual decrease in expression (clusters 1 [18%] and 2 [21%]) could be noted as the treatment progressed (Figure 16) and a subset of miRNAs (22) showed down-regulation in all treatment conditions (Table 12). When compared with published expression database there are supporting reports on expression patterns of specific miRNAs in different types of cancer (Table 11 and Table 12). There are also opposing reports on expression of miRNAs, which includes, miR-106a [63], miR-15b [64], miR-17 [65], miR-18 [66], miR-205 [67], miR-20 [68], and miR-7 [69] for down regulated miRNAs; and let-7f-1 [70], miR-136a [71], miR-143 [72], miR-146a [73], miR-218 [74], miR-22 [75], miR-222 [76], miR-29a [77], miR-34b [78], and miR-493 [79] for up-regulated miRNAs.

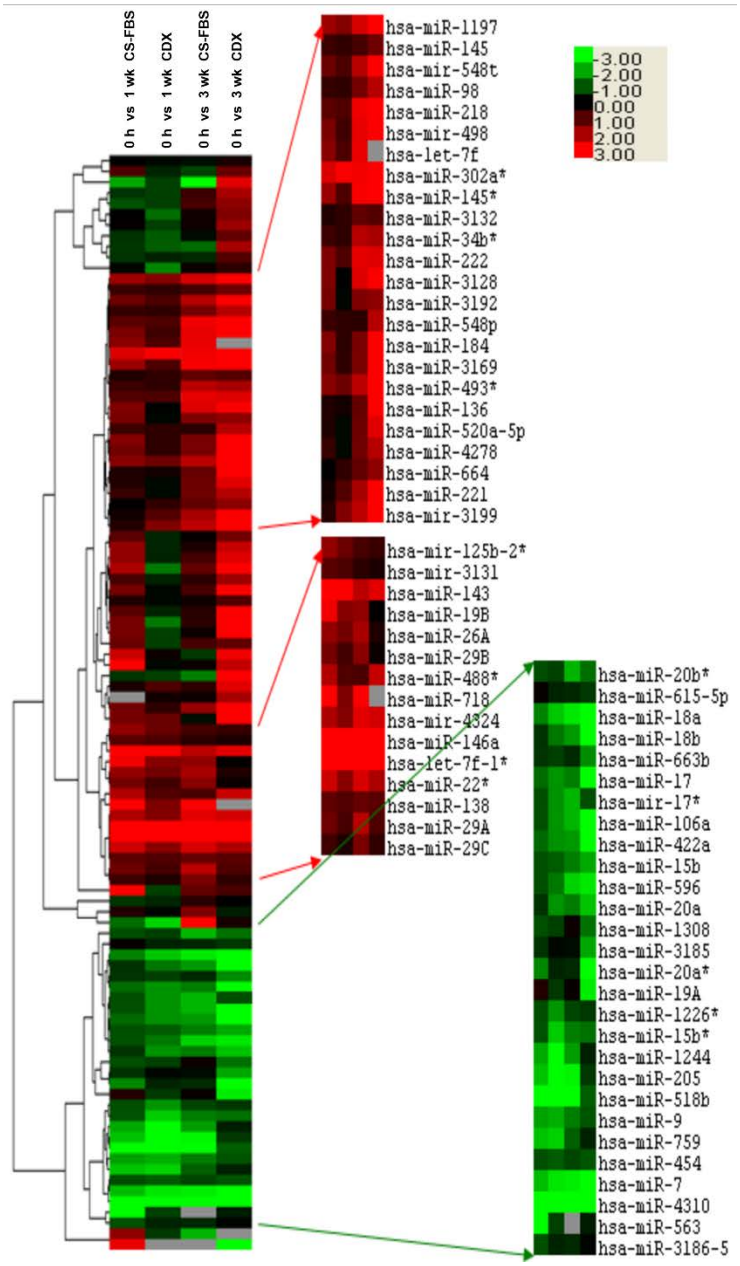

Figure 14: Cluster analysis of fold change in expression of validated miRNAs in different treatment conditions.

Hierarchical clustering of $\log_2$ transformed FC expression of miRNA in four treatment groups, 1wk CSFBS, 1wk CDX, 3wks CSFBS and 3wks CDX (Table 10). Red arrows and green arrows showing the expression patterns of 21 up regulated and 22 down regulated miRNAs (Table 11 & Table 12), respectively.

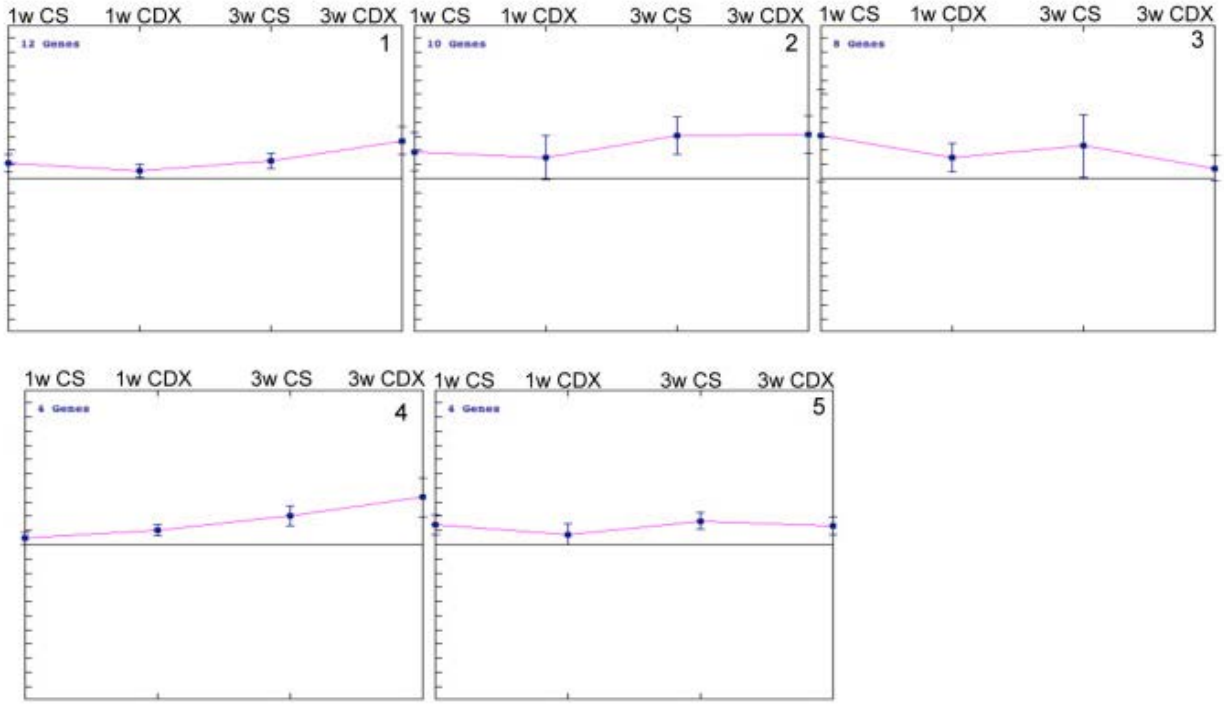

Figure 15: K-median cluster analysis of validated up-regulated miRNAs in different treatment conditions

K-median cluster analysis of the validated miRNAs in different treatment conditions Up-regulated miRNAs are divided into 5 clusters, which show unique trends of expressions. All miRNAs in each cluster show similar trends in expression in all treatment conditions and time points. Data shows median ± SD of expression of miRNAs in each cluster.

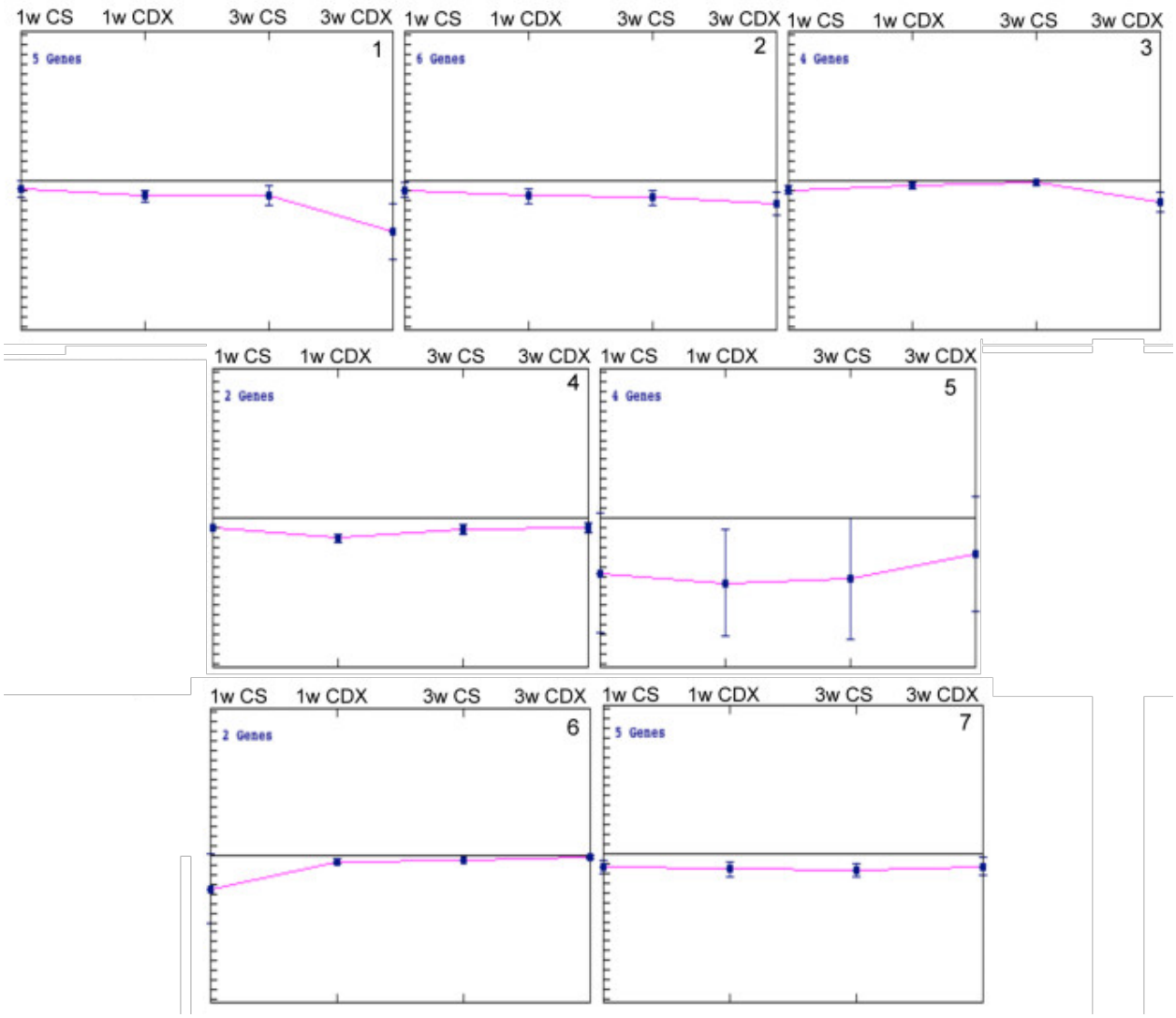

Figure 16: K-median cluster analysis of validated down-regulated miRNAs in different treatment conditions

K-median cluster analysis of the validated miRNAs in different treatment conditions. Down regulated miRNAS are divided into 7 clusters each showing unique trend of expression pattern of miRNAs. All miRNAs in each cluster is showing similar patterns of expression. Data shows median ± SD of expression of miRNAs in each cluster.

Table 11: Fold change in expression of up-regulated miRNAs in different treatment conditions and time points and its relevance with published reports

miRNA ID	1wk CSFBS Δ Change	1wk CDX ΔChange	3wks CSFBS Δ Change	3wks CDX Δ Change	Expression in Other Cancer
hsa-let-7f-1*	12.50	12.17	13.91	17.64	
hsa-miR-136	3.69	3.44	5.16	4.30	
hsa-miR-143	15.80	19.67	13.92	6.25	
hsa-miR-146a	31.44	20.83	56.46	50.68	
hsa-miR-218	4.64	2.33	18.44	11.49	
hsa-miR-22	2.39	2.43	4.58	3.10	
hsa-miR-22*	15.91	11.56	11.78	22.47	
hsa-miR-222	3.65	1.99	7.05	4.63	
hsa-miR-29A	2.09	1.58	4.60	4.24	
hsa-miR-302a*	2.97	7.73	3.87	4.48	
hsa-miR-3138	6.53	5.94	6.66	5.96	-
hsa-miR-3144-5p	11.25	4.39	4.47	8.53	
hsa-miR-3192	8.70	2.11	5.52	5.71	-
hsa-miR-3199	1.25	4.54	2.71	6.76	-
hsa-miR-34b*	3.15	2.34	6.69	8.64	
hsa-miR-493*	1.31	1.42	2.31	15.06	
hsa-miR-548h	2.12	3.76	4.06	6.72	-
hsa-miR-548l	3.94	3.11	8.66	7.40	-
hsa-miR-548p	3.88	2.44	4.64	1.55	-
hsa-miR-548t	4.89	9.65	1.26	5.46	-
hsa-miR-664	3.81	4.01	5.16	5.05	

Thickness of arrows represents number of publications available corresponding to the expression pattern

Table 12: Fold change in expression of down-regulated miRNAs in different treatment conditions and time points and its relevance with published reports

miRNA ID	1wk CSFBS Δ Change	1wk CDX Δ Change	3wks CSFBS Δ Change	3wks CDX Δ Change	Expression in Other Cancer
hsa-miR-106a	-2.37	-3.18	-5.29	-9.40	↑ ↓
hsa-miR-1244	-3.40	-8.55	-5.14	-3.38	-
hsa-miR-15b	-1.86	-2.02	-2.85	-3.33	↑ ↓
hsa-miR-15b*	-2.42	-4.65	-3.83	-9.76	↑ ↓
hsa-miR-17	-2.91	-3.37	-2.50	-24.99	↑ ↓
hsa-miR-17*	-3.15	-3.13	-5.26	-3.94	↑ ↓
hsa-miR-18a	-2.01	-4.36	-14.70	-14.13	-
hsa-miR-18b	-1.56	-2.28	-4.92	-21.36	↑ ↓
hsa-miR-205	-6.33	-12.51	-12.06	-3.89	↑ ↓
hsa-miR-205*	0.35	-1.34	-2.85	-3.23	-
hsa-miR-20a	-2.73	-3.31	-3.78	-4.12	↑ ↓
hsa-miR-20a*	-1.78	-1.25	-2.64	-18.17	-
hsa-miR-20b*	-0.64	-0.56	-7.99	-4.60	-
hsa-miR-3131	-2.35	-2.97	-3.14	-3.41	-
hsa-miR-3185	-2.95	-3.24	-4.17	-5.76	-
hsa-miR-422a	-3.15	-3.15	-4.92	-6.87	-
hsa-miR-454	-0.58	-1.89	-3.28	-3.76	↓
hsa-miR-518b	-2.64	-6.42	-5.61	-12.23	-
hsa-miR-596	-2.45	-3.94	-15.83	-12.71	-
hsa-miR-759	-13.05	-10.92	-6.17	-5.86	↓
hsa-miR-7	-3.00	-5.23	-6.76	-11.08	-
hsa-miR-9	-2.64	-4.35	-4.53	-3.55	↓

NA: Not available. *denotes the star strand, which is currently designated as -3p or -5p. Thickness of arrows represents number of publications available corresponding to the expression pattern

4.1.3 Involvement of miRNAs in Specific Cellular Processes Which Differ Between Treatment Conditions

MicroRNAs exhibiting up regulation or down regulation in all treatment conditions compared to untreated -104S cells (Table 11 and Table 12), were used for function and disease relevance to understand the possible alterations in the cellular processes as LNCaP cells progressed towards androgen withdrawal and AR antagonist resistance. We used RT-PCR FC values of the up regulated or down regulated miRNA for the analysis using IPA software (Ingenuity Systems). Based on -log (p-values) with -values <0.05, a percentage of miRNAs were assigned to certain disorder or cellular processes (Figure 17 and Figure 18). When the functional profiles of the up-regulated miRNAs were compared, there is a decrease in the percentage of miRNAs involved in cancer, dermatological disease, and hematological disease between 3wks and 1wk CDX treated cells whereas an increase in the percentage of miRNAs involved in endocrine system disease, gastrointestinal disease hepatic system disease, reproductive system disease and metabolic disease in 3wks CDX treated S cells compared to 1wk CDX treated cells (Figure 17) In cells subjected to androgen withdrawal, there are also differences in percentage of miRNAs in different cellular processes between 1wk and 3wks treatments, which show a reduction in hematological diseases, cellular development, and reproductive system disease. An increased involvement of miRNAs in a variety of cellular processes also was noted in 3wk CSFBS treated cells, which includes cell death and survival, cell movement, endocrine system disease, gastrointestinal disease,

hematological disease, hepatic system disease and metabolic disease (Figure 17).

In the list of down-regulated miRNAs, there is an increase in percentage of miRNAs involved in cell morphology, cell movement, dermatological disease, gastrointestinal disease, renal urological disease, and reproductive system disease as cells progressed from 1wk to 3wks CDX treatment. A decreased percentage of down regulated miRNAs in specific cellular processes also could be noted in these cells, which includes cellular development, endocrine system disease, hepatic system disease, tumor morphology and inflammatory response. Androgen withdrawal for 1wk to 3wks also showed changes in percentage of miRNA involvement (Figure 18). An increased percentage of down regulated miRNAs involved in cancer, cell death and survival, dermatological disease, endocrine system disease, gastrointestinal disease, metabolic disease, and tumor morphology is noted in 3wks CSFBS treated cells. 3wks androgen withdrawal also showed a decrease in miRNA percentage involved in cell growth and proliferation, cell movement, cell-cell signaling, DNA replication and repair and renal-urological disease (Figure 18).

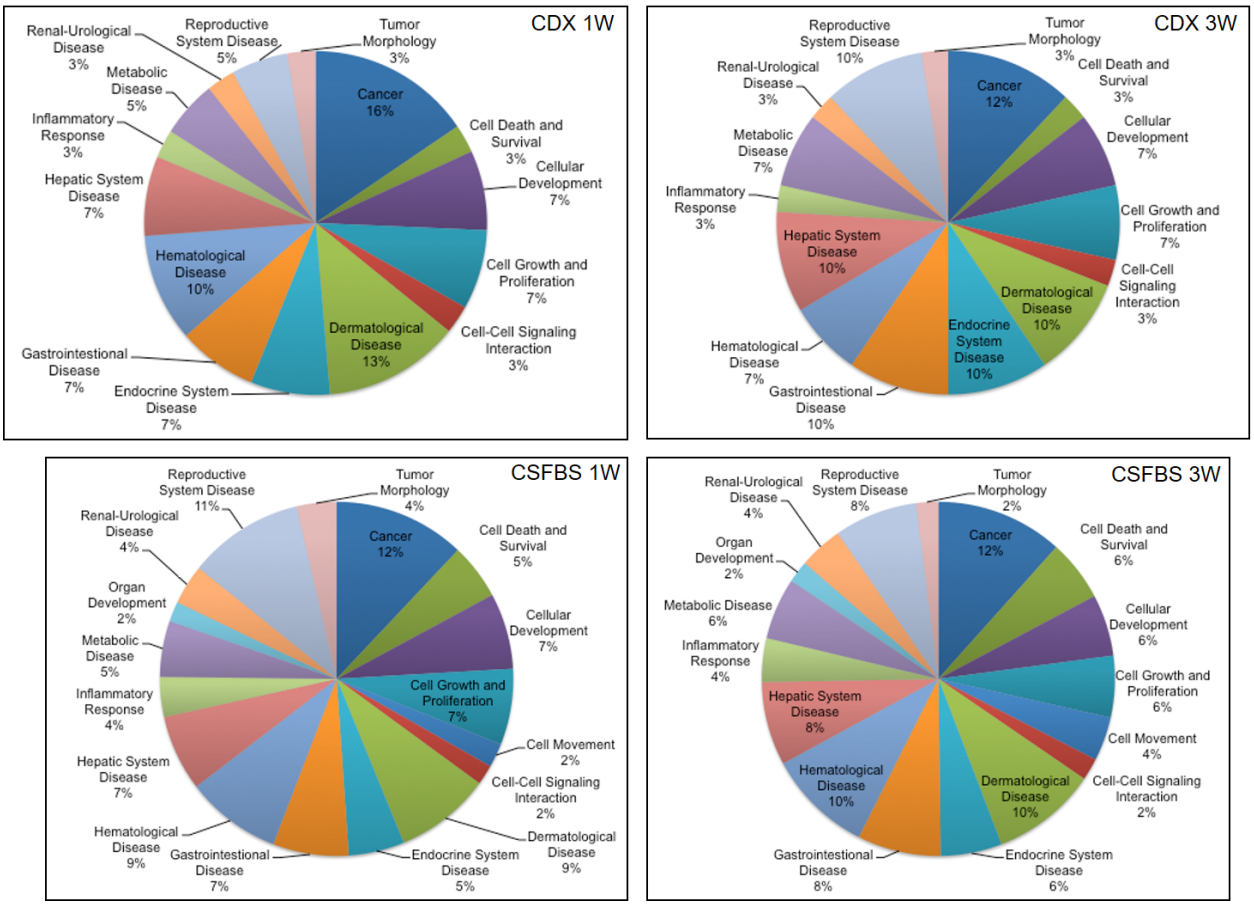

Figure 17: Correlation of ADT induced miRNAs with previously published functions

Analysis of association of deregulated miRNAs with canonical pathways and cellular processes. Pie charts showing the percentage of validated up regulated miRNAs in various cellular processes based on the published reports. Upper panel depicts the percentage of miRNAs involved in cellular processes and its changes during 1wk and 3wks treatments with CDX. Lower panel shows changes in the percentage of miRNAs involved in cellar processes during 1wk and 3wks treatments with CSFBS.

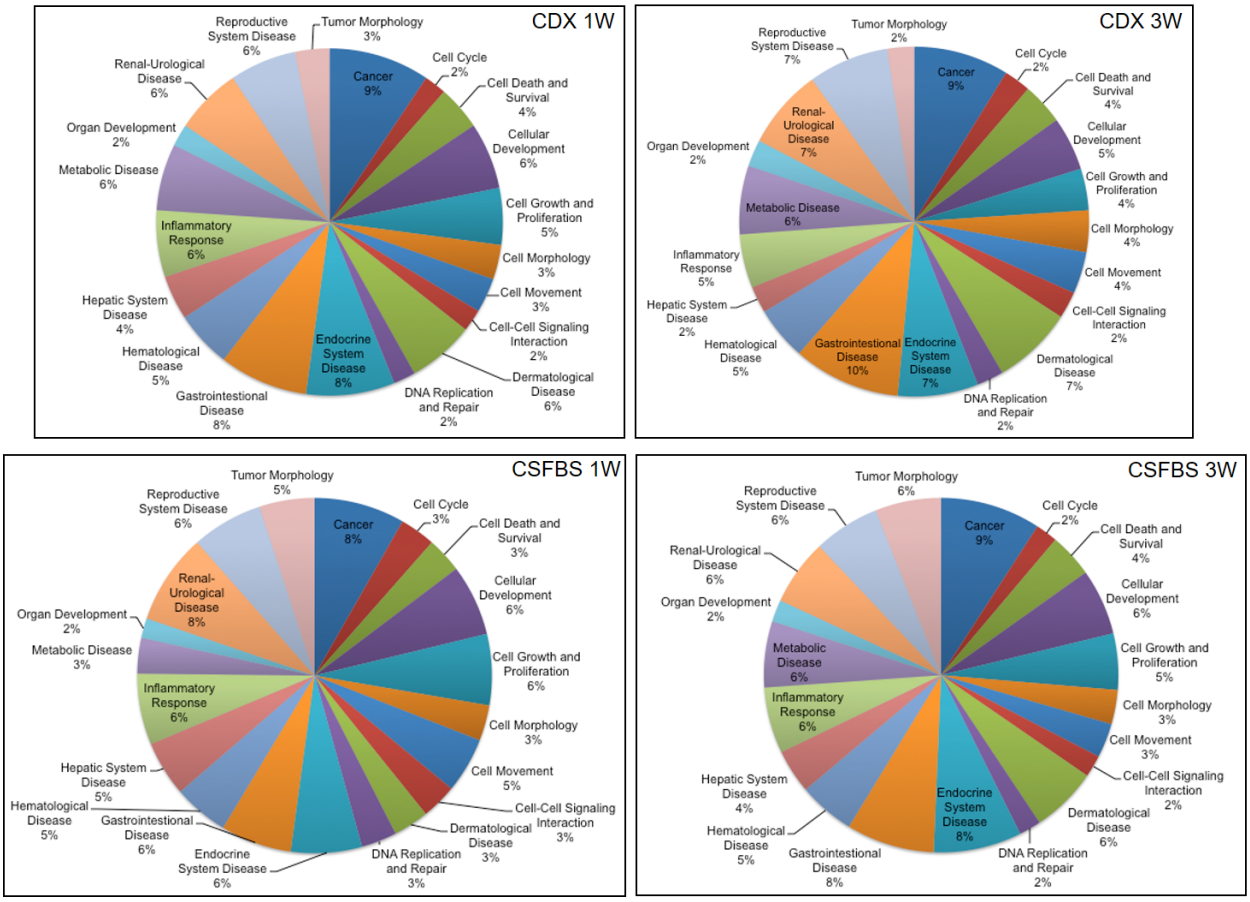

Figure 18: Correlation of ADT repressed miRNAs with previously published functions

Analysis of association of deregulated miRNAs with canonical pathways and cellular processes. Pie charts showing the percentage of validated down regulated miRNAs in various cellular processes. Upper panel illustrates the changes in the percentage of miRNAs involved in cellular processes during 1wk and 3wks treatment with CDX. Lower panel represents changes in the percentage of miRNAs involved in cellular processes during 1wk and 3wks treatments with CSFBS.

The *in silico* function analysis of the target miRNAs in different treatment conditions indicated a complex interaction of a network of miRNAs and their target proteins in these cells which rendered them adaptive to the androgen withdrawal and treatments with AR antagonists. Next, we analyzed the network of interactions among target miRNAs. We used the $\log_2$ transformed FC values of the subset of validated miRNA (Table 11 and Table 12) for analysis of the functional interrelationship among miRNAs (Figure 19). The network for up-regulated miRNAs and its putative targets in 3wks CDX showed that miR-3192 directly and miR-218 indirectly through DEAD box protein DDX20 target p53. MiR-146a also directly regulates a number of Toll-like receptors (TLR1, TLR9 and TLR10), cytokine receptors and its associated proteins (IL1R1, IL12RB2, IL1RAP) and chemokine receptors (CXCR4, CCR3) (Figure 19A). In addition, miR-146a directly targets a number of growth factors and cytokines (Figure 19A). These miR-146a targets are also shown in the up-regulated network of 3wks CSFBS, in addition to BRCA, which is a direct target of miR-146a (Figure 19E). MiR-3192 targeting of p53 is also noted in 3wks CSFBS but not of miR-218 (Figure 19E). As noted in the networks, p53 also regulates a number of miRNAs, such as, miR-29b-3p, miR-22-3p, miR-22-5p and miR-221-3p (Figure 19A and E). When the networks are overlaid with diseases, a number of miRNAs in the up-regulated list of both 3wks CDX and 3wks CSFBS showed involvement in a variety of cancers including pancreatic cancer, endocrine gland tumor, prostate cancer, ovarian tumor, mammary tumor, cervical cancer and epithelial neoplasia (Figure 19B and F). In the list of down-regulated miRNAs there is direct targeting of E2F2, E2F3, MAP3K12,

FXR1 and AR interacting nuclear protein kinase HIPK3 by miR-17-5p. MiR-16p also directly targets BCL2L2, cell death suppressor BNIP2, EGFR, RAB21 and single strand purine rich DNA binding protein PURA (Figure 19C and G) in both 3wks CDX and 3wks CSFBS treated cells. Also a number of miRNAs in the down regulated list down regulate a number of common targets, such as E2F3 is targeted by miR-1244, miR-596, miR-18a-5p, miR-16-5p and miR-17-5p. EGFR is also targeted by miR-7a-5p and miR-16-5p. Overlay of diseases on networks revealed a distinct association of miR-17-5p, with various cancers including prostate cancer, breast cancer and pancreatic cancer and endocrine gland tumors. An association of miR-16-5p with prostate cancer, pancreatic cancer, pituitary cancer and endometrial cancer also could be noted (Figure 19D and H). These networks indicate a complex interplay of microRNAs and proteins during development of resistance of LNCaP cells to androgen withdrawal and treatment with CDX.

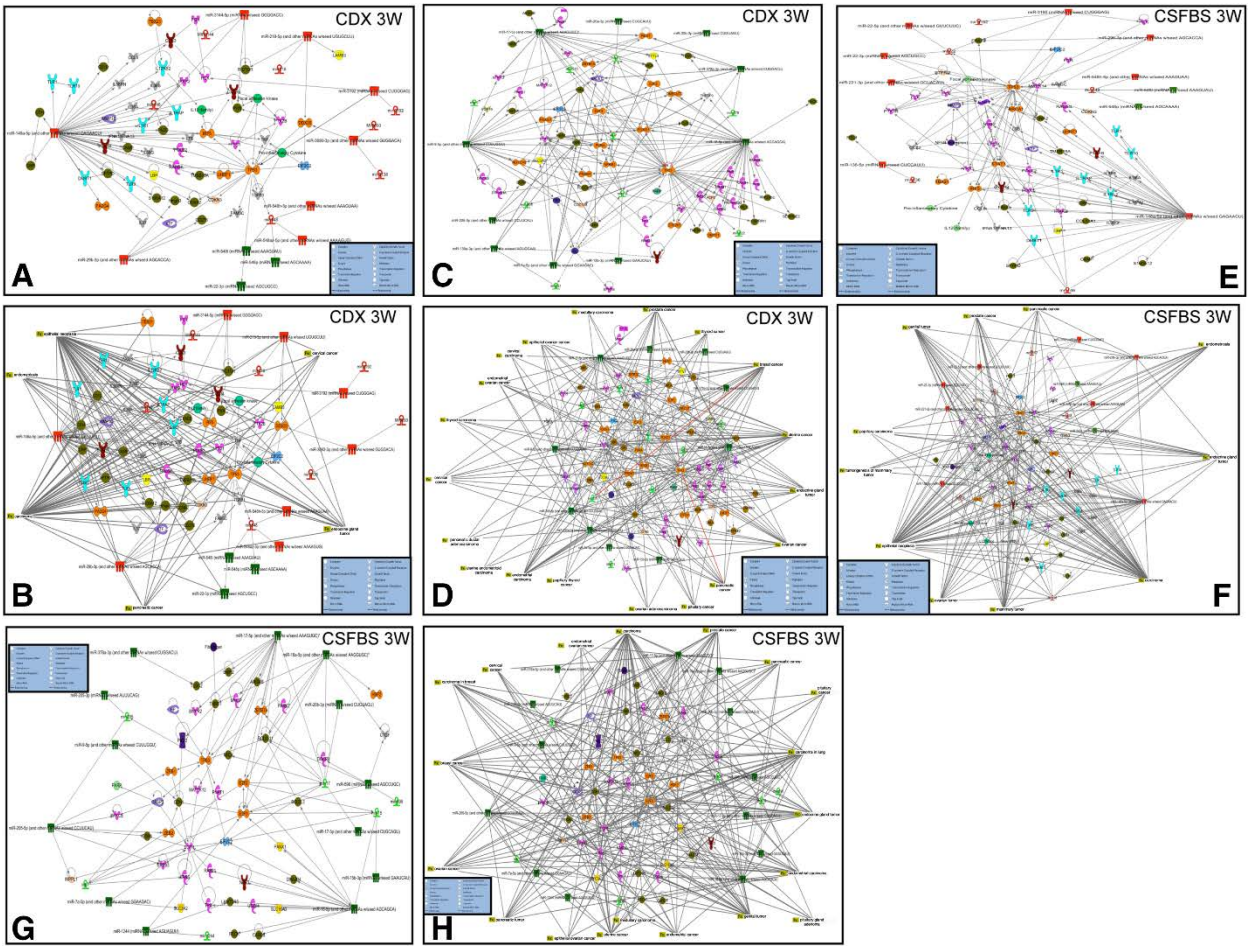

Figure 19: Analysis of miRNA-regulated network of interacting partners involved various signaling pathways.

A) Log2 transformed FC values of 21 up regulated miRNAs were imported into IPA software and a network for interacting miRNAs and their direct target proteins and proteins that target any of the up regulated miRNAs was generated for 3wks CDX treated cells. Red symbols denote miRNAs. Proteins include growth factor/cytokines, enzymes, kinases, phosphatases, peptidases, translational regulator, transcriptional regulators, and transporters. B) The network in A is overlayed with disease relationship showing association of miRNA and protein interactions with various types of cancer. C and D) Regulatory network of the log2 transformed FC values of 22 down regulated miRNAs and their target proteins in 3wks CDX treated cells (C) and overlay of disease association of the miRNA-protein regulatory network (D). Green symbols represent down regulated miRNAs. E and F) Regulatory network of log_2 transformed FC values of the up regulated miRNAs and their target proteins in cells treated with CSFBS for 3wks (E) and an overlay of disease relationship with the regulatory network in E. Red symbols represent miRNAs. G and H) Regulatory network of log_2 transformed FC values of the down regulated miRNAs and their target proteins in cells treated with CSFBS for 3wks (G) and an overlay of disease association with the regulatory network in G (H). Click here for larger image.

4.2 Identification of Genes Effected by miRNAs Deregulated in the Transition to Androgen Independence

4.2.1 Target Identification of the Subset of miRNAs Revealed Potential Activation and/or Inactivation of a Number of Proteins Involved in Different Signaling Networks

A total of 21 up regulated and 22 down regulated miRNAs in all treatment conditions were used for identification of protein targets using IPA, miRDB and TargetScan software. Venn diagram of the putative targets of up-regulated miRNAs derived from the network generated using the IPA software showed 27 proteins that are common in all treatment conditions (Figure 20). A number of which are known tumor suppressors such as BRCA1 [80], TP53 [81], RAD54L [82], IRF5 [83], DUSP2 [84], IKK1 or CHUK [85]. Other targets of up regulated miRNAs in different treatment conditions also includes proteins that inhibit tumor progression, such as DNMT3A [86], FADD [87], pTEN [88], FOXO3 [89], DDX20 [90] and PA2G4 (EBP1)[91]. There are also 41 common targets of the down-regulated miRNAs in all treatment conditions (Figure 21). Some of the targets are known oncoproteins, which includes EGFR [92], VEGFA [93], ZBTB7 (POKEMON) [94], acid phosphatase 2(ACP2) [95] and NFKB1 [96]. Additionally, proteins that are overexpressed in cancer cells are among the targets of down-regulated miRNAs in different treatment conditions, which includes Wnt3A [97], PPARα [98], UCP2 [99], CSF1 [100], and MED1 [101].

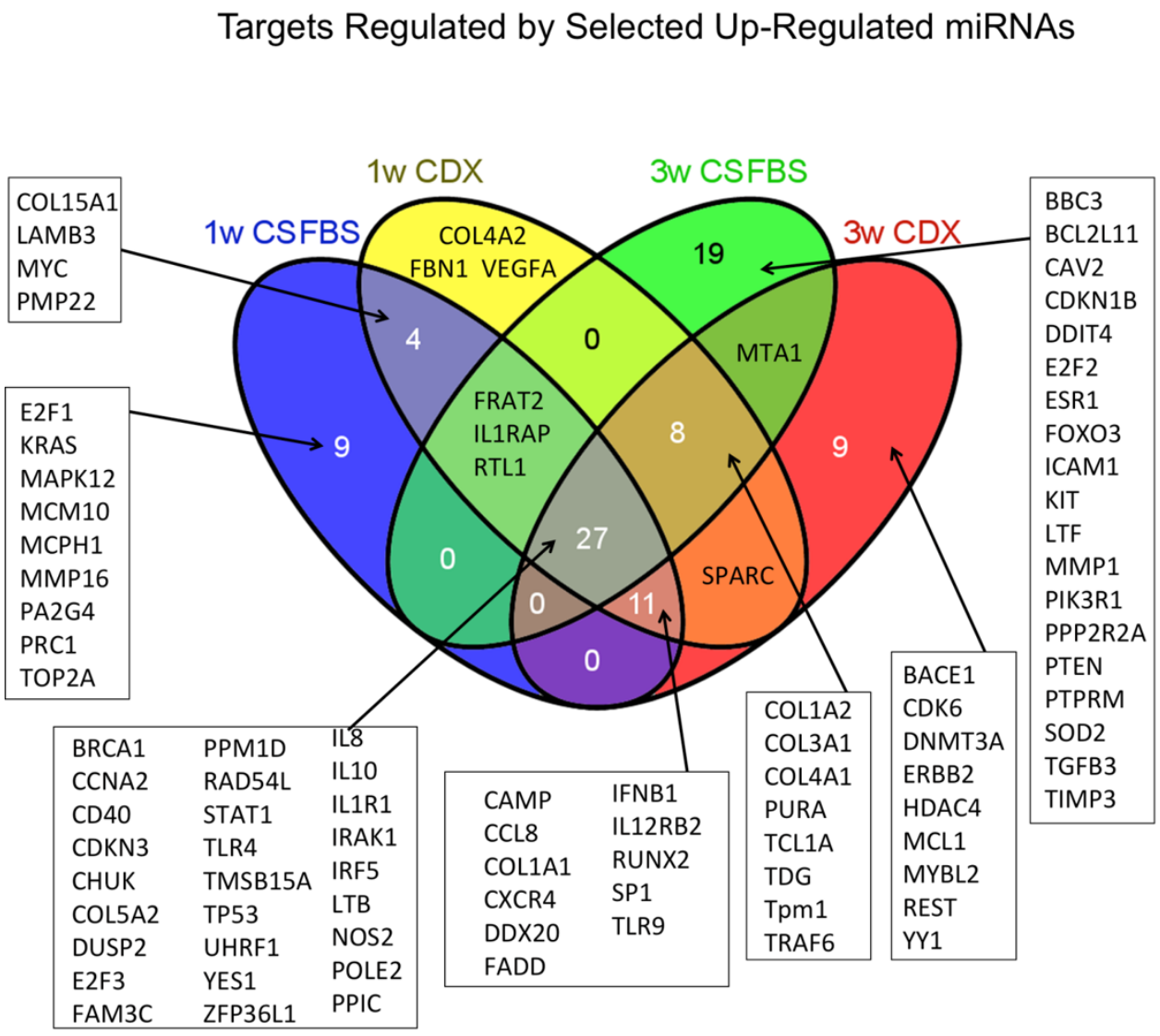

Figure 20: Analysis of treatment specific targets regulated by up-regulated miRNAs

Venn diagram showing specific targets that are potentially regulated by miRNAs that are up regulated in different treatment conditions. Putative targets were identified based on the regulatory network generated by IPA software.

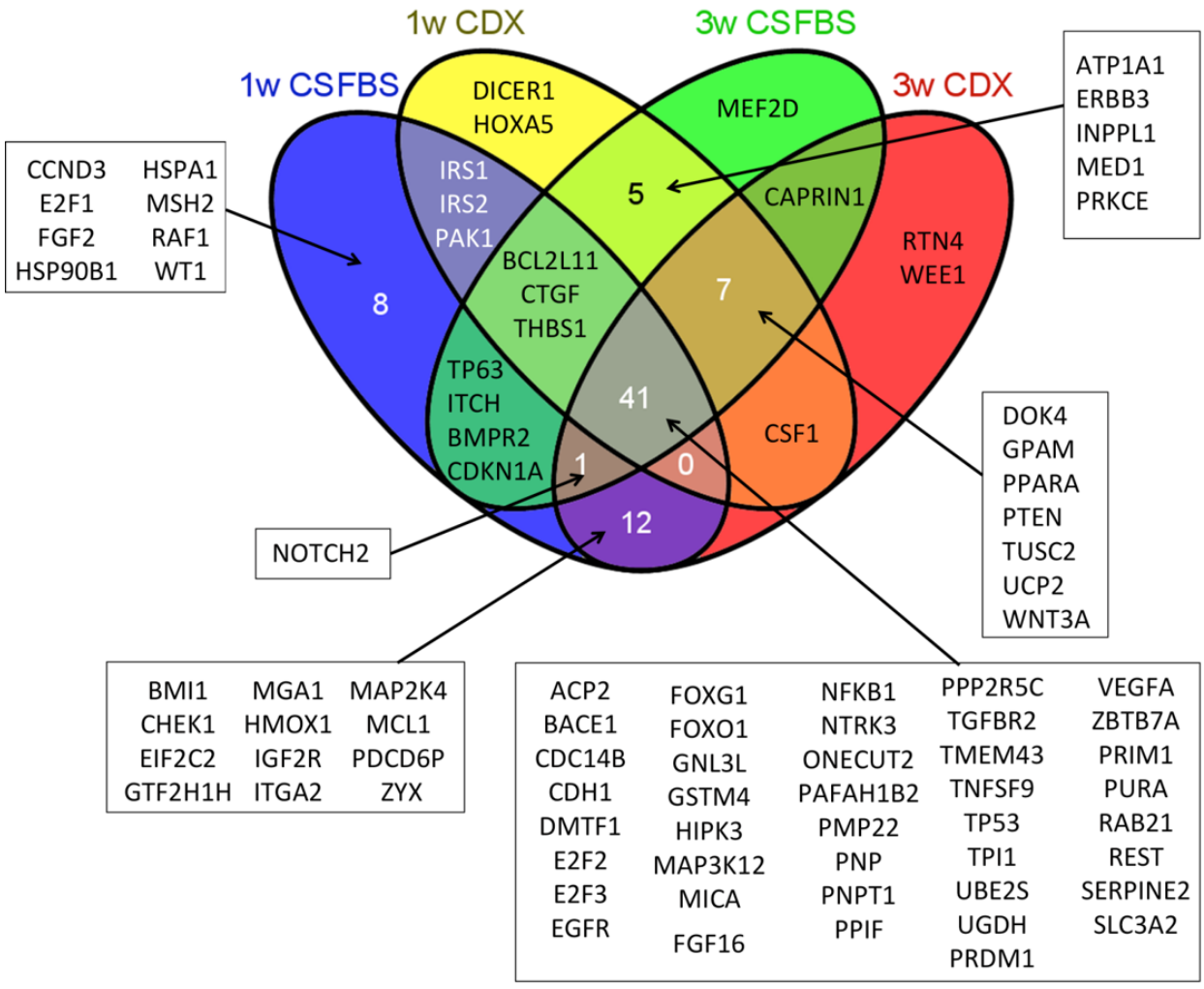

Figure 21: Analysis of treatment specific targets regulated by up-regulated miRNAs

Venn diagram depicting predicted targets regulated by the down-regulated miRNAs in different treatment conditions. Targets were identified based on the regulatory network using IPA software.

4.2.2 Targets of miRNAs Showed the Predicted Expression Profiles in LNCaP Cells Subjected to Androgen Withdrawal and CDX Treatment

Further identification of the targets of selected miRNA (Table 11 and Table 12) was conducted by miRDB and TargetScan database search and proteins that are regulated by one or multiple miRNAs from our list and received higher target scores in either or both searches are presented in (Table 13 and Table 14). The selected proteins that are regulated by the up-regulated miRNAs include TNF receptor associated factor 6 (TRAF6) [102], interleukin receptor associated kinase1 (IRAK1), BCL6 co-repressor-like 1(BCORL1) [103], Cbl [104], neuro oncological ventral antigen1 (NOVA1) [105], coiled coil domain containing 67 (CCDC67)[106], NET1 [107], ZFAND1(Acc.# NM_024699), RGS6 [108], CDKN1B (p27Kip1) [109], IGFBP5 [110], and RNASEL [111] (Table 13). The proteins that are potentially regulated by the down-regulated miRNAs include, ABHD3 [112], FGD4 [113], CCNJ [114], CHAMP1 [115], Myb [116], PIK3CD [117], VEGFA [118], SPOPL [117], RAB9B [119], EGFR [120], E2F1 [121], and DOK4 [122]. Western blot analysis confirmed the predicted expression profiles of some of the targets. Expression of Cbl, p27Kip1, TRAF6, IRAK1, and ZFAND1 were significantly and progressively down regulated in cells treated with CDX or subjected to androgen deprivation (Figure 22). Similarly, expression of FGD4, VEGFA, EGFR, DOK4 and ABHD3 were up regulated to moderate to high levels in cells treated with CDX or CSFBS (Figure 23).

Table 13: Predicted mRNA Targets of Up-Regulated miRNAs

Gene ID	Gene Description	miRNAs	miRDB (Target Score)	TargetScan (Context+Percentile)
TRAF6	TNF receptor-associated factor 6, E3 ubiquitin protein ligase	miR-146a	100	94,94,65, 50,38,19
IRAK1	Interleukin receptor associated kinase 1	miR-146a	87	98
BCORL1	BCL6 corepressor-like 1	miR-146a, miR-143, miR-548t	77,68	98,80
NOVA-1	neuro-oncological ventral antigen1	miR-146a, miR-143, miR-548l	97,93,86	97,89,87
CCDC67	coiled-coil domain containing 67	miR-22	77	99,97
Cbl	Cbl proto-oncogene, E3 ubiquitin protein ligase	miR-22, miR-222, miR-136, miR-3199, miR-1197	87,83,64,55	86,84,75, 61,43,33, 32,31
NET1	neuroepithelial cell transforming 1	miR-22, miR-222, miR-143	93,61	98
ZFAND1	zinc finger, AN1-type domain 1	miR-548h, miR-548l, has-miR-548t, miR-136	96,70	93,83,99, 52
RGS6	regulator of G-protein signaling 6	miR-222	75	91,96,12
CDKN1B	cyclin-dependent kinase inhibitor 1B (p27, Kip1)	miR-222	85	93,95
IGFBP5	insulin-like growth factor binding protein 5	miR-143	N/A	99
RNase L	ribonuclease L	miR-146a, miR-548l	74	81

Table 14: Predicted mRNA Targets of Down-Regulated miRNAs

GeneID	Gene Description	miRNAs	miRDB (TargetScore)	TargetScan (Context+Percentile)
ABHD3	abhydrolase domain containing 3	miR-1244, miR-130a, miR-205	74, > 85	84
CCNJ	cyclin J	miR-205-5p	90	98
CHAMP1/ ZNF828	chromosome alignment maintaining phosphoprotein 1	miR-7-5p, miR-378a-3p	60-96	96
MYB	v-myb myeloblastosis viral oncogene homolog (avian)	miR-15b-5p, miR-16-5p	74	96
PIK3CD	phosphoinositide-3-kinase, catalytic, delta polypeptide	miR-7-5p	94	91
VEGFA	Vascular endothelial growth factor A	miR-205, miR-15	79	97
FGD4	RhoGEF and PH domain containing 4	miR-17, miR-106a, miR-20a	100	98
SPOPL	speckle-type POZ protein-like	miR-9-3p	97	97
RAB9B	RAB9B, member RAS oncogene family	miR-15b-5p, miR-16-5p, miR-130a-3P, miR-9-5p	67-86	67-86
EGFR	Epidermal growth factor receptor	miR-7	81	93
E2F1	E2F transcription factor 1	miR-205, miR-17, miR-20b	77	80
DOK4/IRS-5	Docking protein 4	miR-205	N/A	94

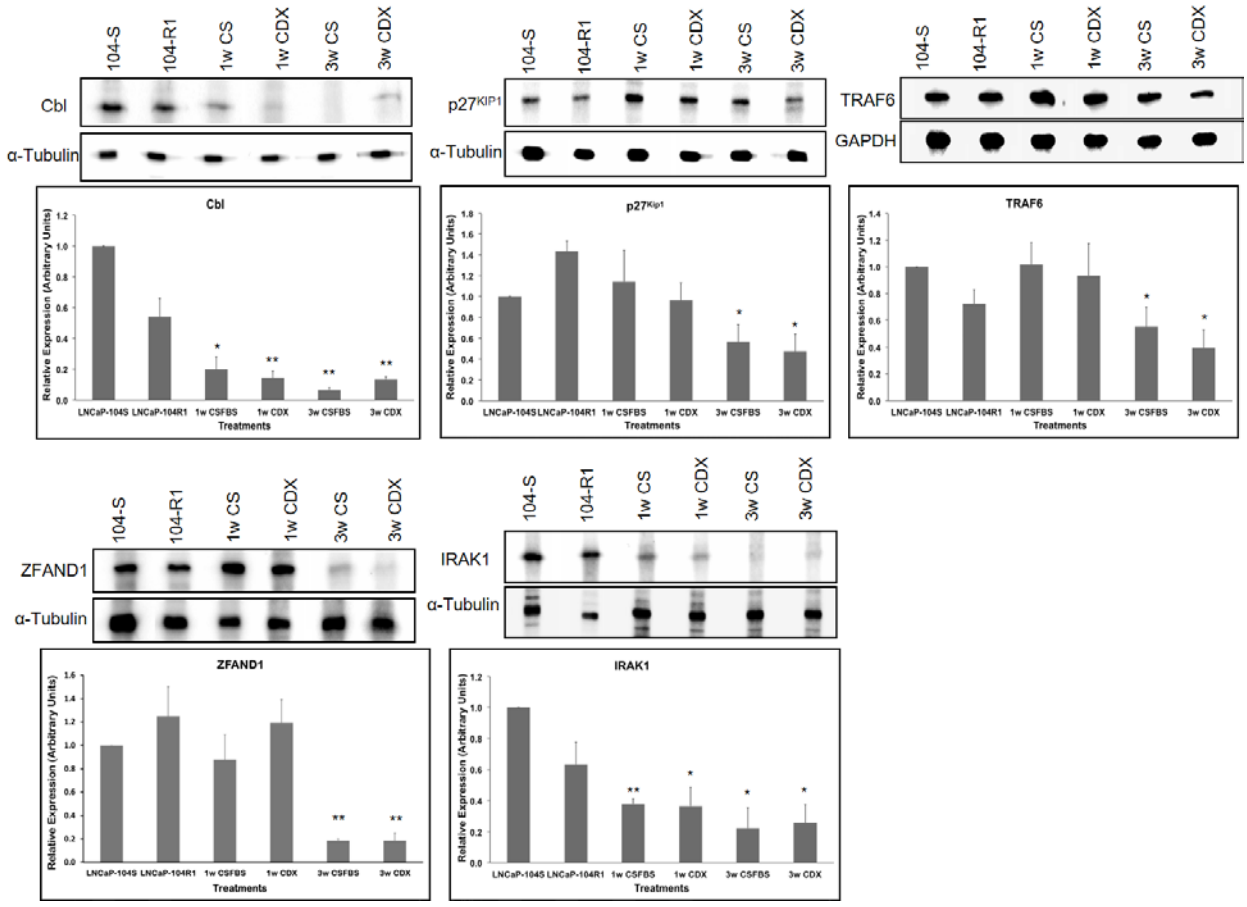

Figure 22: Comparative analysis of target protein expression in LNCaP sublines in different treatment conditions.

Western blot analysis of the target proteins identified using TargetScan and miRDB online prediction tools for a particular miRNA (shown in Table 2). Total proteins from -104S cells untreated and treated for different times, and -104R1 cells untreated were used for immunoblotting using anti-cbl (A), -p21Kip1 (B), -TRAF6 (C), -ZFAND1 (D) and –IRAK1 (E) antibodies. Upper panel shows representative images of the western blots. Bottom panel shows densitometric analysis of relation protein expression. Data shows mean ± SD of at least three independent experiments. *$p < 0.05$, **$p < 0.01$, significance was calculated between LNCaP-104S untreated vs. specified treated cells.

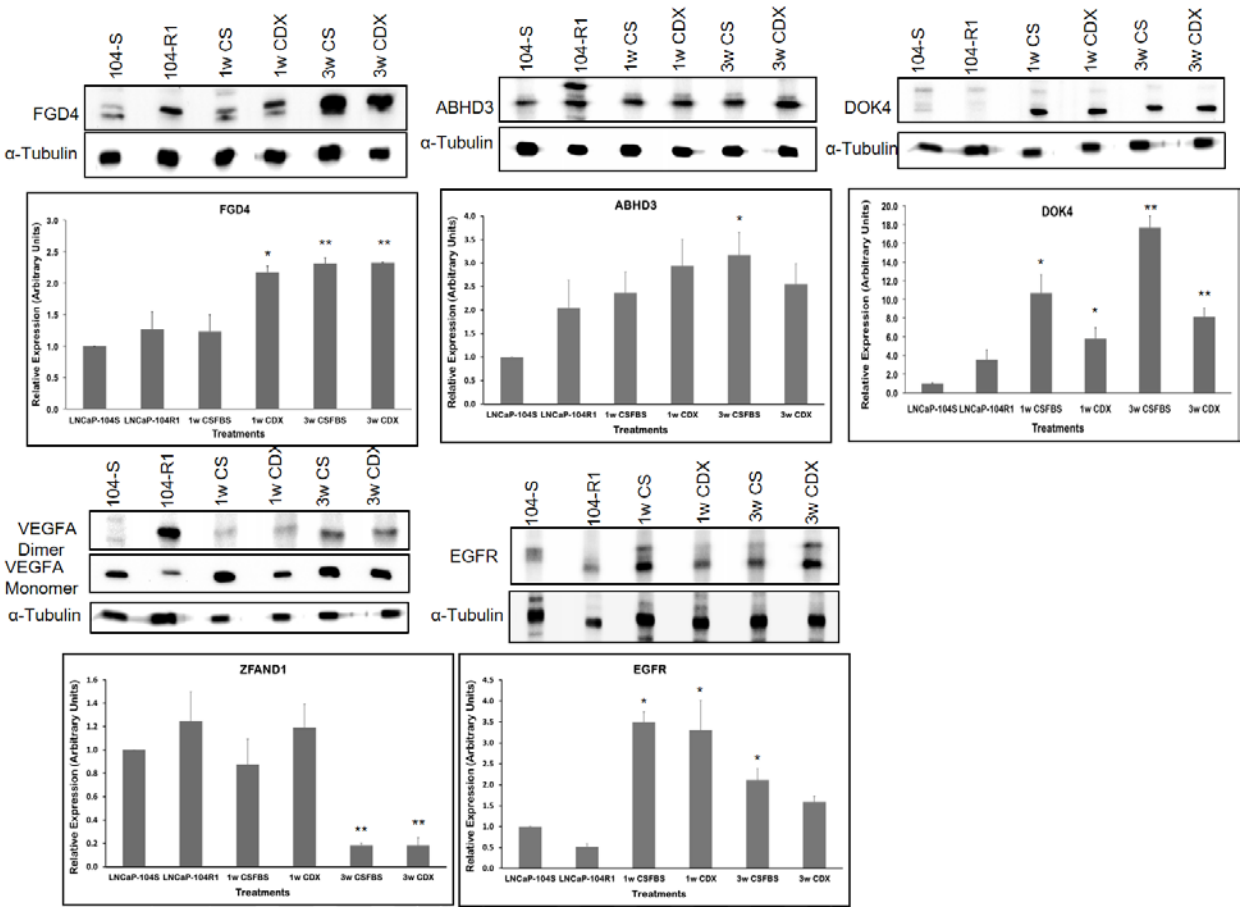

Figure 23: Comparative analysis of target protein expression in LNCaP sublines in different treatment conditions.

Western blot analysis of predicted target proteins regulated by down regulated miRNAs (shown in Table 3). Total proteins from all treated and untreated cells were used for immunoblot analysis using anti- FGD4 (A), ABHD3 (B), -DOK4 (C), VEGFA (D), and EGFR (E) antibodies. Upper panel shows representative images of the western blots. Bottom panel shows densitometric analysis of relation protein expression. Data shows mean ± SD of at least three independent experiments. *$p < 0.05$, **$p < 0.01$, significance was calculated between LNCaP-104S untreated vs. specified treated cells.:

4.3 miRNAs Deregulated in Both Androgen Independent Cells and Clinical Specimens

4.3.1 miRNA Expressions Deregulated in Human Prostate Tumors

Our studies on genome-wide profiling of miRNAs using LNCaP cell culture model showed down regulation of miR-17-92a cluster in anti-androgen resistant cells [123]. In this study, validation of expression profiles in clinical specimens also showed loss of expression of this cluster miRNAs. We used macro-dissected prostate tumor tissues and corresponding uninvolved areas to monitor expression of mature miR-17, -18a, -20a, -19a, -19b and -92a miRNAs. Patients were selected based on specific criteria including no prior treatments, Gleason Scores, pre-surgical PSA and local invasion; and based on CAPRA-S score [56] stratified into low, medium and high risk of biochemical recurrence (Table 15). Normalized fold-change (FC) expression analysis showed a distinct down regulation/loss of expression of all members of the miRNA cluster in 58-73% of the cases tested (Figure 24A). Correlative analyses of miRNA expressions, with at least a 1.5-fold change in expression, with risk assessment showed down-regulation of the cluster in 35% of low risk cases (CAPRA-S ≤ 2) and up-regulation in 19% of the cases. For patients with a higher risk (CAPRA-S ≥ 3), the percentage of patients with down-regulated miR-17-92a miRNAs showed no change at 34% (Figure 24B). However, this analysis did identify a distinct reduction in the percentage of patients with up-regulation, at only 9% for the cluster; additionally, no patients with CAPRA-S ≥3 displayed increased expression of miR-19b or miR-92a (Figure 24B). Further correlating expressions with CAPRA-S risk

showed that four, five or all miRNAs were down regulated in 67% of the cases in the high-risk and medium-risk groups (Table 16). Reduced expression of three, two or one miRNAs was noted in the rest of the 33% cases in the high or medium-risk groups. In the low risk group, four, five or all miRNAs were down regulated in 50% of the cases while loss of one, two or three miRNAs were noted in the other 50% of the cases. Analysis of endogenous expression of these miRNAs in prostate adenocarcinoma and BPH cell lines also showed reduced expression of most of the miRNAs in cancer cells compared to BPH cells (Figure 24C). This observation led to the subsequent experiments to understand the functional significance of the loss of expression of miR-17-92a cluster in phenotypic changes in prostate cancer cells.

Table 15: Patient criteria and assessment of the risk of recurrence

Patient #	PSA pre-surgery	Gleason Score	CAPRA-S score	Risk
1	14.3	3+2=5(IV)	2	low
2	5.9	3+3=6	2	low
3	4.3	3+3=6	2	low
4	8.2	3+4=7	2	low
5	7.8	3+4=7	2	low
6	8.8	3+4=7	2	low
7	6.6	3+4=7	2	low
8	3.7	3+4=7	2	low
9	23.3	3+3=6	3	medium
10	6.3	3+4=7	3	medium
11	6.2	3+4=7	3	medium
12	4.7	3+4=7	3	medium
13	5.1	3+3=6	4	medium
14	87.4	3+3=6	4	medium
15	9.8	3+4=7	4	medium
16	9.4	3+4=7	4	medium
17	8.8	3+4=7	4	medium
18	5.4	4+3=7	4	medium
19	6.5	3+4=7	5	medium
20	6.5	3+4=7	5	medium
21	4.8	3+4=7	7	high
22	14.9	3+4=7	7	high
23	13.9	4+3=7	7	high
24	5.6	4+3=7	8	high
25	51.8	4+5=9	9	high
26	51.8	4+5=9	9	high

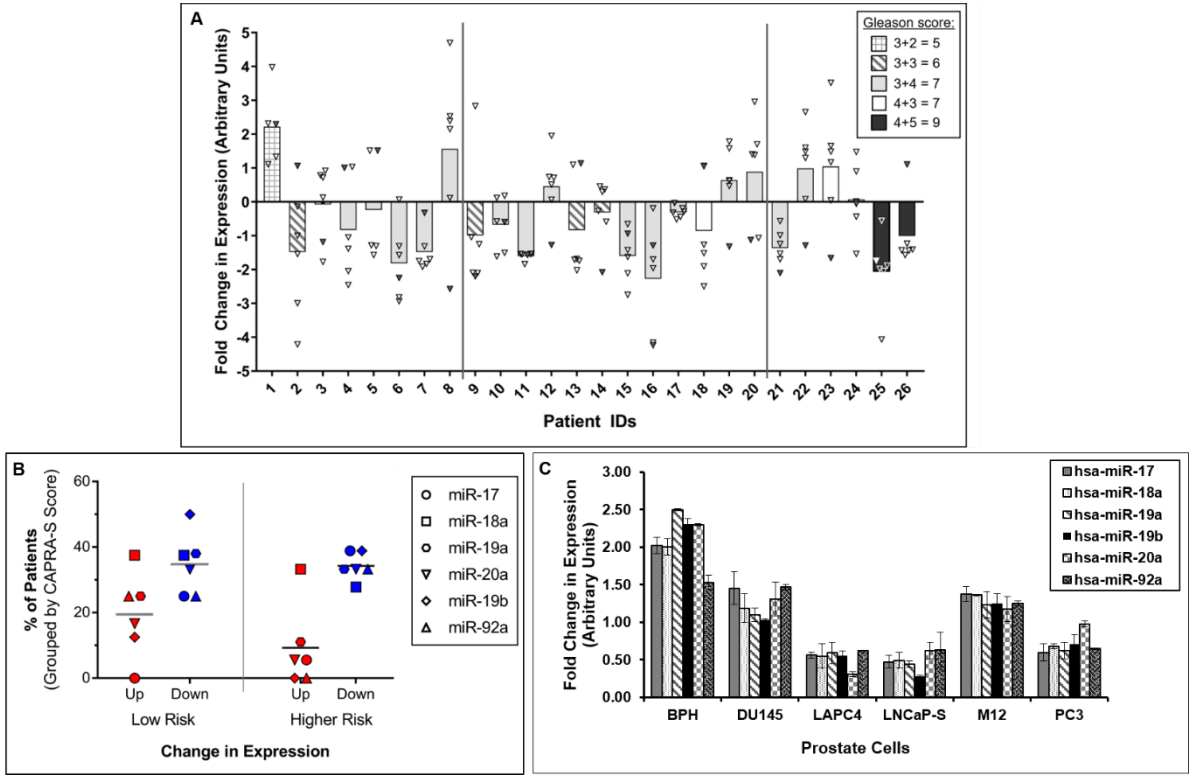

Figure 24: Expression profiles of the miR-17-92a cluster miRNAs in clinical samples and cell lines

Relative expression of miR-17, miR-18a, miR-19a, miR-20a, miR-19b, and miR-92a. Raw data have been normalized to the average of 3 reference genes (RNU43, U6 snRNA, U1 snRNA). A) Average fold change(FC) in expression of entire miR-17-92a cluster (Bars) in patient tumors compared to matched uninvolved adjacent tissues. Open triangles denote the fold change values of miR-17, miR-18a, miR-19a, miR-20a, and miR-19b. Filled triangles denote values of miR-92a. B) Dot plots displaying the percentage of patients having FC values of ≥1.5 for each miRNA. Bars identify the average value for the cluster. Red and Blue symbols indicate up- or down- regulation, respectively. Patients were separated into 2 risk groups based on CAPRA-S score (Low= ≤2, Higher= ≥3). (A and B) All values are an average of two separate analyses. C) Fold change in expression of miR-17-92a cluster miRNAs in benign and cancerous prostate cell lines. LNCaPS: LNCaP104-S cells. Data show average of three separate analyses.

Table 16: Correlative analysis of miRNA expression with risk of recurrence

Risk	All miRNAs	Five miRNAs	Four miRNAs	Three miRNAs	Two/One miRNAs
High (6)	**2**	**1** (miR-17, -18a, -20a, -19b, -19a	**1** (miR-18a, -19a, -20a and -92a)	**0**	**2** (miR-92a)
Medium (12)	**4**	**1** (miR-17, -19a, -19b, -20a, -92a)	**3** (miR-17/or-18a, -19a, -19b/or -20a/or -92a)	**1** (miR-18a, -19b, -20a)	**3** (miR-92a, and -20a)
Low (8)	**1**	**2** (miR-17, -19a, -19b, -20a, -18a/or -92a)	**1** (miR-17, -18a, -20a, -92a)	**1** (miR-19a, -17/or -18a/or -19b/or -20a)	**3** (miR-18a/ -19b/ or -92a)

4.4 Functional Relevance of miR-17-92a Cluster in Prostate Cancer

In this study, we evaluated the functional significance of miR-17-92a cluster miRNAs in prostate cancer progression and resistance to chemotherapeutic agents. Because miRNAs are integrated into positive and negative regulatory loops of gene expression, it is important to study the expression and functions of all members of miR-17-92a cluster miRNAs concurrently to mimic the in vivo environmental setting. This would help understanding the consequence of deregulation of miR-17-92a cluster as a whole. Our expression analysis data provide evidence of an association of reduced expression of miR-17-92a cluster members with higher potential of biochemical failure, as indicated by higher CAPRA-S scores, of the majority of prostate cancer patients tested. To our knowledge, this is the first report on the expression of the miR-17-92a cluster in annotated prostate cancer clinical specimens.

4.4.1 Expression of miR-17-92a Cluster Altered Cell Morphology and Reduced Expression of Actin Cytoskeleton Modulatory and Cell Cycle Regulatory Proteins

We generated sublines of PC-3 prostate cancer cells that overexpress all mature miRNAs of the miR-17-92a cluster compared to the control cells expressing scrambled (Scr) RNA upon transfection with the precursor miRNAs (Figure 26A). The extent of expression was increased between 1.3-2.5-fold, a level comparable to that was detected in BPH cells. We intended to express all miRNAs in the cluster simultaneously instead of single miRNAs to mimic the physiological condition and study the combinatorial effects.

Overexpression of all miRNAs changed the morphology of PC-3 cells from spindle shapes to a more adherent cobblestone type (Figure 25).

Expression of these miRNAs resulted in 25%-40% reduction in concentration of some of the computer algorithm based predicted target proteins FGD4, LIMK1, SSH1 and cyclin D1, which contain one or more binding site(s) of miR-17 and -20a at the 3'-UTR (Figure 27A) but no other miRNAs of the cluster. PC-3 cells were used to confirm the direct binding of miR-17 and -20a to the predicted sites of one of the targets, FGD4. Luciferase reporter assays were done upon transient co-transfection of the miR-17-92a precursor construct plus a luciferase construct containing a fragment (bases from position 80-90) of FGD4 3'-UTR, in PC-3 cells.

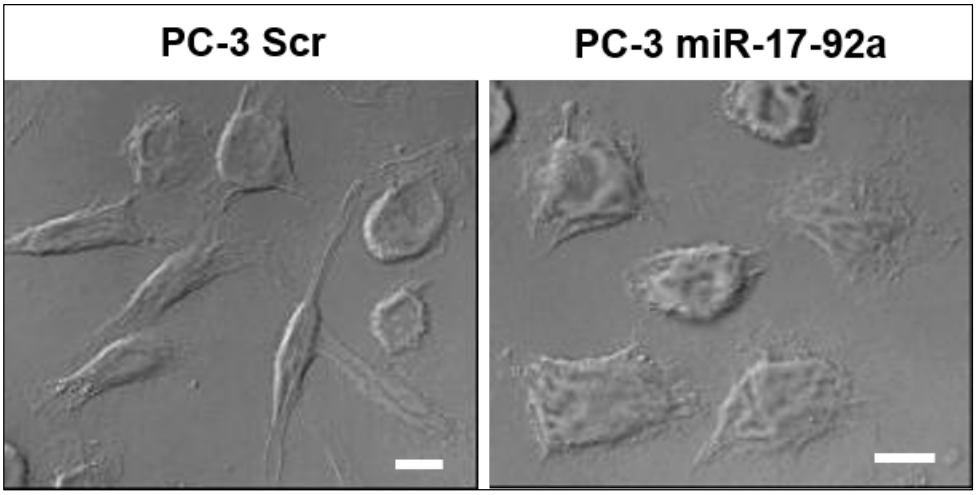

Figure 25: Altered morphology of PC-3 cells expressing miR-17-92a cluster

Differential interference contrast (DIC) images of PC-3 cells expressing Scr RNA (left) or miR-17-92a cluster miRNAs (Right). Scr RNA expressing cells retain parental PC-3 cell morphology, whereas stable expression of miR-17-92a cluster miRNAs induced a more adherent phenotype and reduced the number of spindle-like cells (Right) Scale bar: 10 µm.

Results showed 54% inhibition of translation of FGD4 mRNA, which could be rescued by mutating miR-17 and -20a binding sites at the 3'-UTR (Figure 27D). Additionally, LIMK1 and SSH1 3'UTRS resulted in a 45% and 25% reduction in luciferase activity, respectively. Taken together, these results confirmed that overexpression of miR-17-92a reduced synthesis of protein involved in activation of RhoGTPase pathway (FGD4) [124], actin cytoskeleton reorganization (LIMK1) [125, 126] and cell cycle regulation (SSH1, Cyclin D1), that are often hyper-activated or over-expressed in advanced prostate cancer [127-129]. Our results showing inhibition of expression of Cyclin D1 prompted us to study cell proliferation and activation of the signaling pathways that promote cell proliferation. Using western blots, we detected expression of phosphorylated ERK1/2, phosphorylated AKT and phosphorylated AKT substrate, PRAS40, as markers for activation of MAP Kinase and AKT pathways in whole cell lysates of PC-3 cells expressing miR-17-92a cluster miRNAs. Our analyses showed a significant reduction (35%-55%) of these proteins in cells expressing miR-17-92a miRNAs compared to control cells expressing Scr RNAs (Figure 28A and B). Furthermore, no significant changes in total protein concentrations were observed for AKT1, ERK1/2, or PRAs40 (Additional File 8). A reduced expression of p-ERK1/2 in miR-17-92a miRNAs expressing cells as detected by immunofluorescence analysis, confirmed the western blot data (Figure 29A). The percentage of cells expressing Ki-67 antigen, a cell proliferation marker [130], was also reduced significantly in transiently transfected PC-3 cells upon expression of miR-17-92a (63% vs. 83%) compared to Scr RNA expression as detected by

immunofluorescence (Figure 29A). Comparative MTS assays showed a significantly reduced (20%-30%) growth of transiently transfected LNCaP104-S and PC-3 cells upon expression of miR-17-92a miRNAs (Figure 29B).

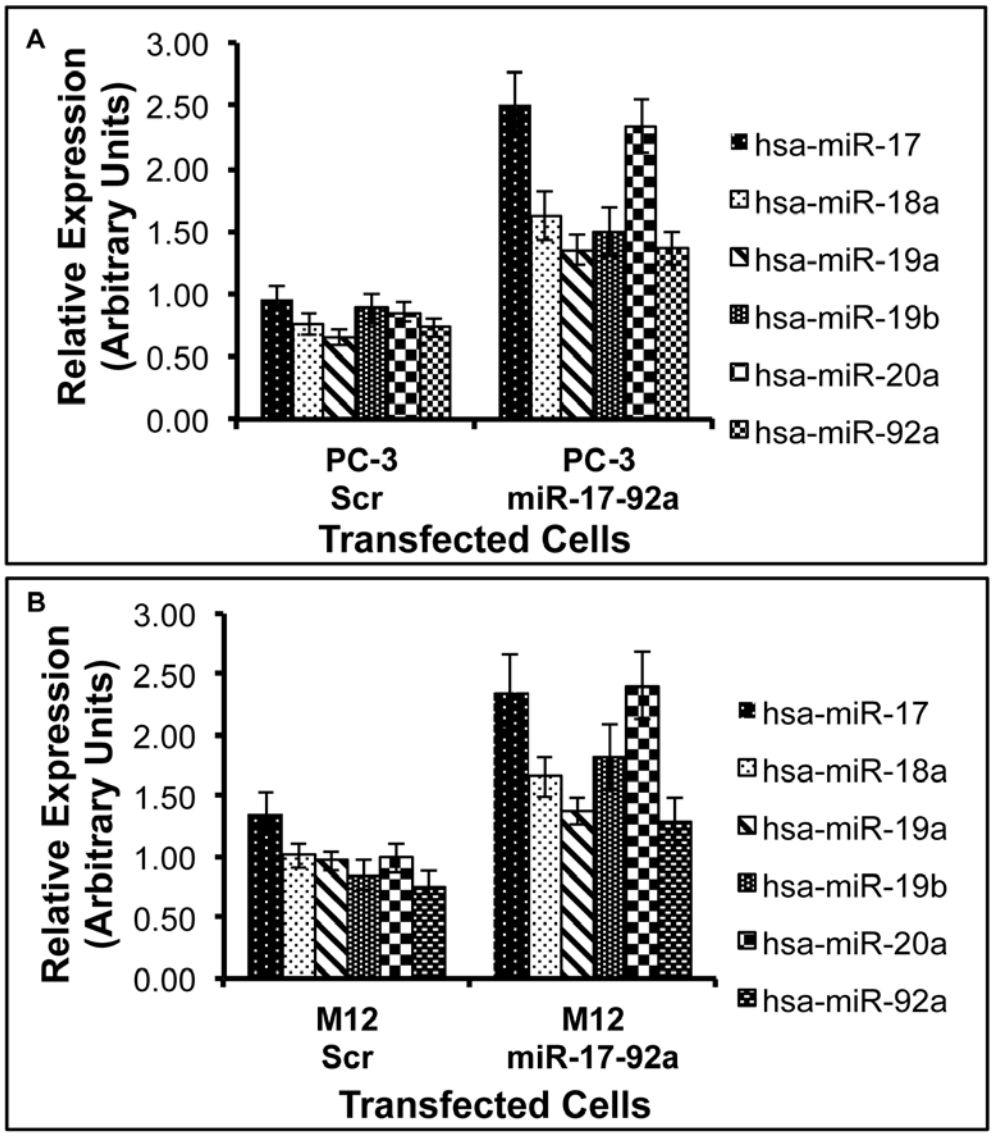

Figure 26: Expression of miR-17-92a cluster in transfected cells

Quantitative PCR analysis of the expression of the members of the miR-17-92a cluster in stably transfected PC-3 (A) and M12 (B) cells expressing miR-17-92a miRNAs of Scr RNA. Data representmean±SD of 3 or

more independent analyses.

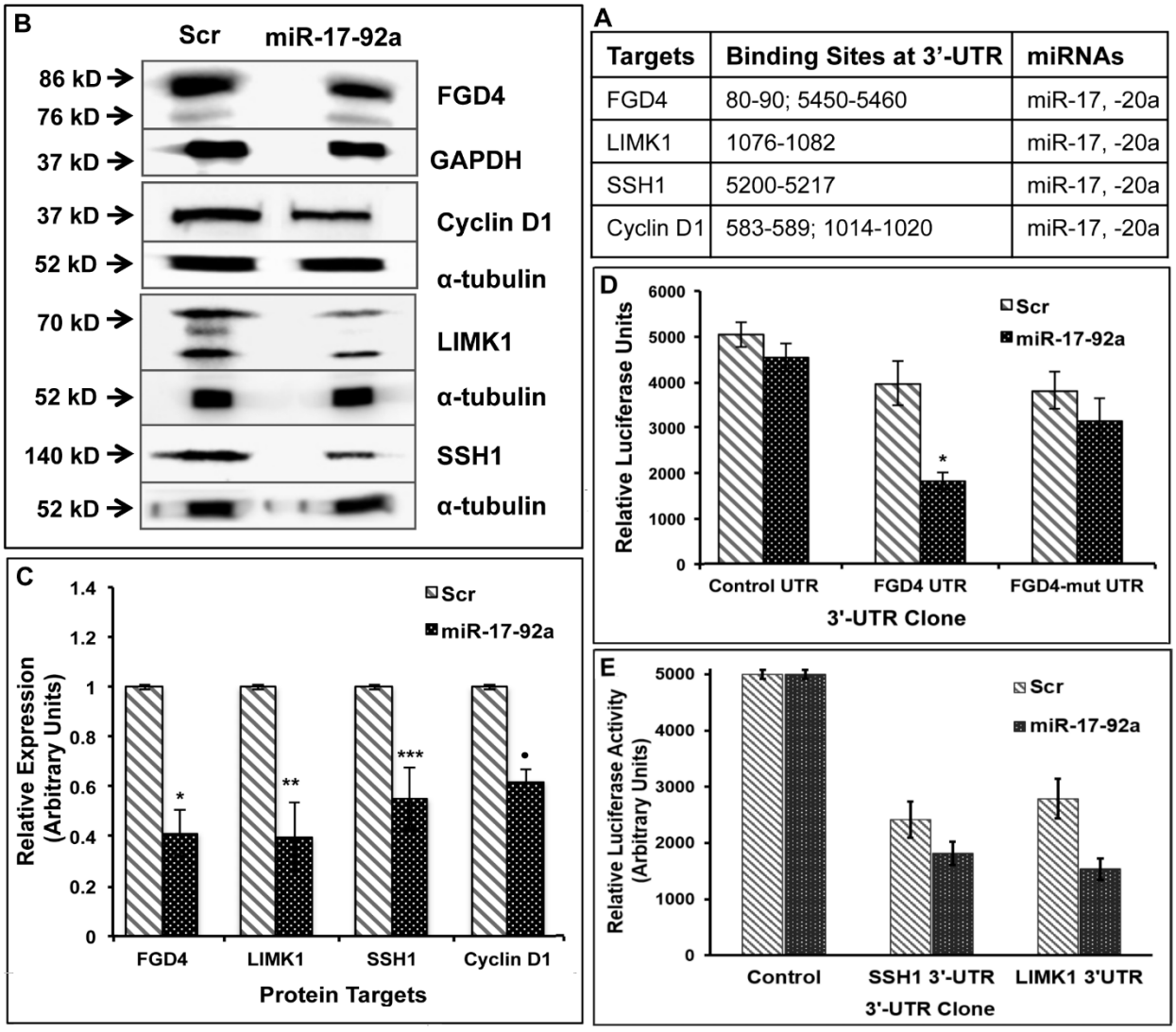

Figure 27: Expression of miR-17-92a cluster in prostate cancer cells reduced expression of the putative target genes.

A) Predicted binding sites of miR-17, and miR-20a in the 3'UTRs of the target mRNAs B) Representative images of immunoblots of FGD4, cyclin D1, LIMK1, and SSH1 in PC-3 cell lysates showing reduced expression of all of these predicted targets upon expression of miR-17-92a. GAPDH and α-tubulin were used as the loading controls. C) Densitometric analysis of protein concentrations normalized to the internal controls. Data shows mean±SD of three independent analyses. *p=0.0004, **p=0.0004; ***p=0.003 •p <0.0001. D and E) Luciferase reporter assays confirming that miR-17a and -20a directly target FGD4 (D), SSH1 and LIMK1 (E) through binding to the specified seed sequence at the 3'UTR. PC-3 cells were co-transfected with the luciferase constructs containing a nonspecific DNA sequence, a fragment of wild type 3' UTRs or a fragment of FGD4 3' UTR containing mutations at the miR-17/-20a seed sequence (D only) along with a plasmid expressing either miR-17-92a miRNAs or scrambled RNA. Data represent the mean±SD of three independent experiments. * p=0.001.

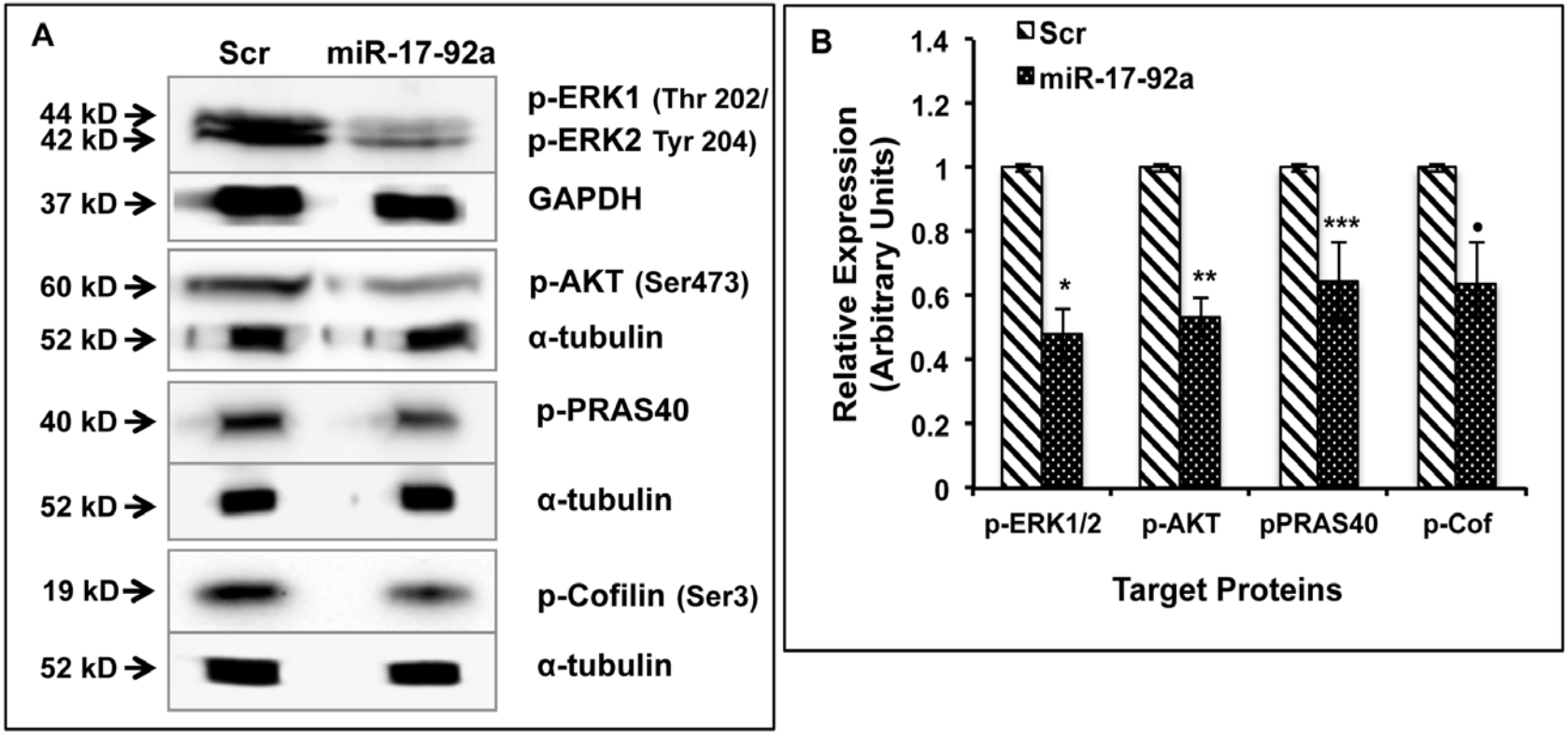

Figure 28: Expression of miR-17-92a miRNAs reduced activation of MAPK and AKT pathways.

A) Immunoblot analysis showing reduced phosphorylated ERK1/ERK2, -AKT, -PRAS40 (AKT substrate), and -Cofilin (LIMK1 substrate) in lysates from PC-3 cells stably expressing miR-17-92a cluster compared to cells expressing Scr RNAs. GAPDH or α-tubulin was used as the loading controls. B) Densitometric analysis of the phosphoprotein concentrations normalized to internal controls. Data represent mean±SD of three separate experiments. *p=0.0003, **p=0.0001, ***p=0.007, •p=0.008.

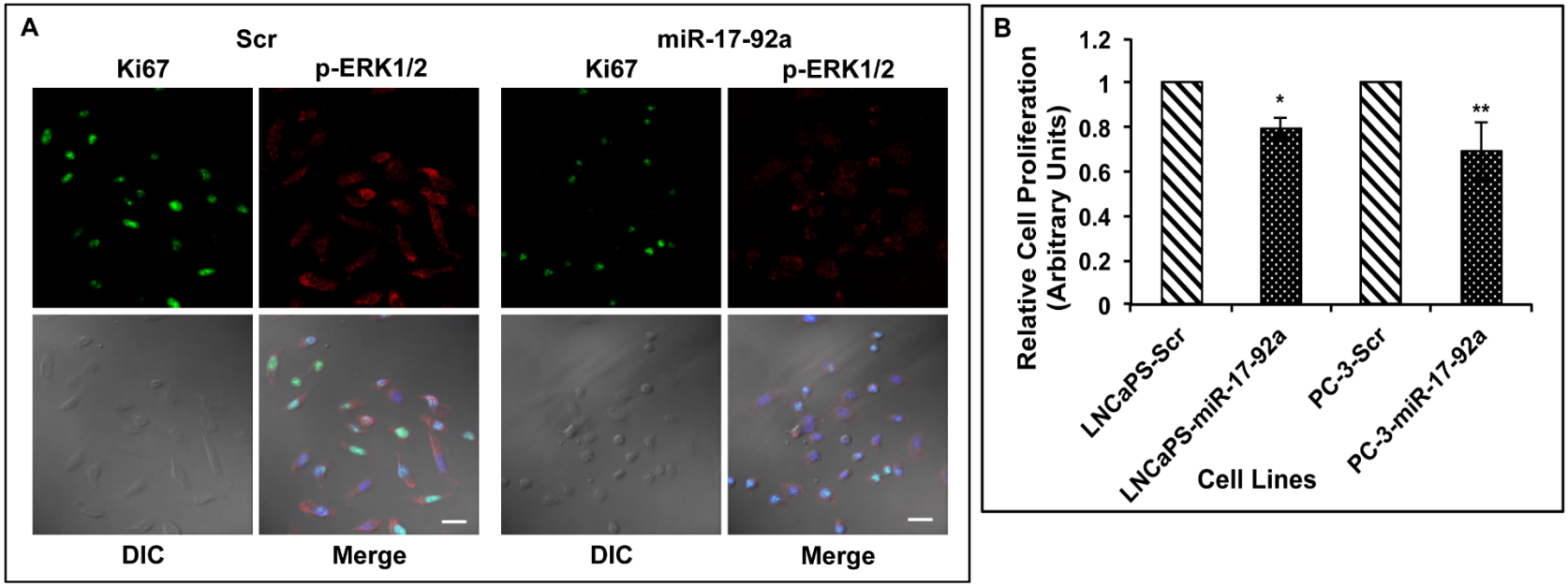

Figure 29: Expression of miR-17-92a miRNAs decreased cell proliferation.

A) Immunofluorescence analysis showing reduced expression of Ki-67 proliferation marker and phosphorylated ERK1/2 in PC-3 cells transiently expressing miR-17-92a miRNAs compared to control cells. Scale bar: 25μm. B) Cell proliferation assay showing reduced cell growth in miR-17-92a cluster miRNA expressing cells. LNCaP104-S (LNCaPS) or PC-3 cells were transiently transfected with DNA constructs for Scr RNA or miR-17-92a precursor miRNAs and cell proliferation at 72 hr were detected by MTS assays. Data represent mean±SD of six independent experiments in triplicates. *p<0.0001; **p=0.0001

4.4.2 Expression of miR-17-92a Cluster Delayed Tumorigenicity and Reduced Tumor Growth

We generated stable sublines expressing miR-17-92a miRNAs or Scr RNA of another metastatic prostate cancer cell line, M-12 (Figure 26B). Both PC-3 and M12 transfected sublines expressing miR-17-92a miRNAs or Scr RNAs were used for experiments on tumor growth in xenograft models. Cells were injected into the flanks of humanized NSG mice and tumor growth monitored for 55 days. The results showed a significant reduction in tumor volume (35%-53%) in mice injected with PC-3 and M12 cells expressing miR-17-92a cluster compared to the tumors in mice injected with cells expressing Scr RNAs (Figure 30A, B, C, D, E and F). A delayed tumorigenesis was also noted in mice injected with prostate cancer cells expressing miR-17-92a cluster (Figure 31). Quantitative RT-PCR Analysis of expression of the matured miRNAs in tumor tissues showed a sustained maintenance of the increased (>2.0 to >7.0 fold) expression of all cluster miRNAs (Figure 30G and H). In general, animals with both PC-3 and M-12 miR-17-92a tumors survived longer than animals with tumors with Scr RNA. Some of the M12-miR-17-92a tumor bearing animals were alive till 80 days post injection and showed sluggish or stunted tumor growth (data not shown)

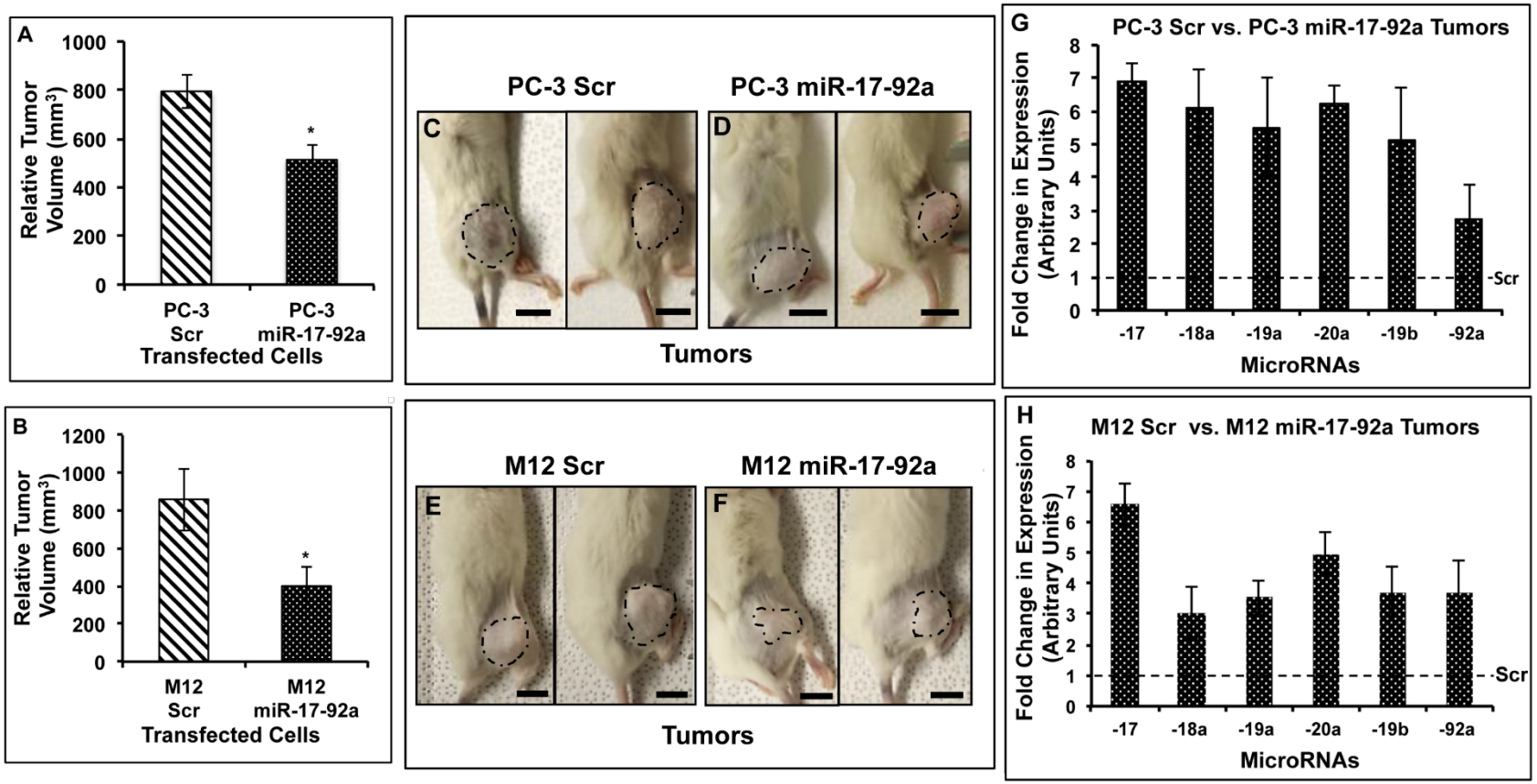

Figure 30: Expression of miR-17-92a cluster miRNAs reduced tumor growth in xenograft models.

Transfected sublines of PC-3 and M12 cells stably expressing miR-17-92a miRNAs or Scr RNAs were used to establish tumors in the flank of NSG mice. (A and B) Comparison of tumor volumes at 55 days post injection for PC-3 cells (A) or M12 cells (B). Data represent mean tumor volume±SD of 4 animals/group. *p=0.002 (A); **p=0.003 (B). (C-F) Representative images of tumors in situ developed from PC-3 cells (C and D) or M12 cells (E and F). Scale bar: 10mm. (G and H) Quantitative PCR showing sustained expression of the miR-17-92a cluster miRNAs in PC-3 and M12 tumors compared to the tumors developed from control cells expressing Scr RNAs. Data show mean expression ±SD of 4 animals/group

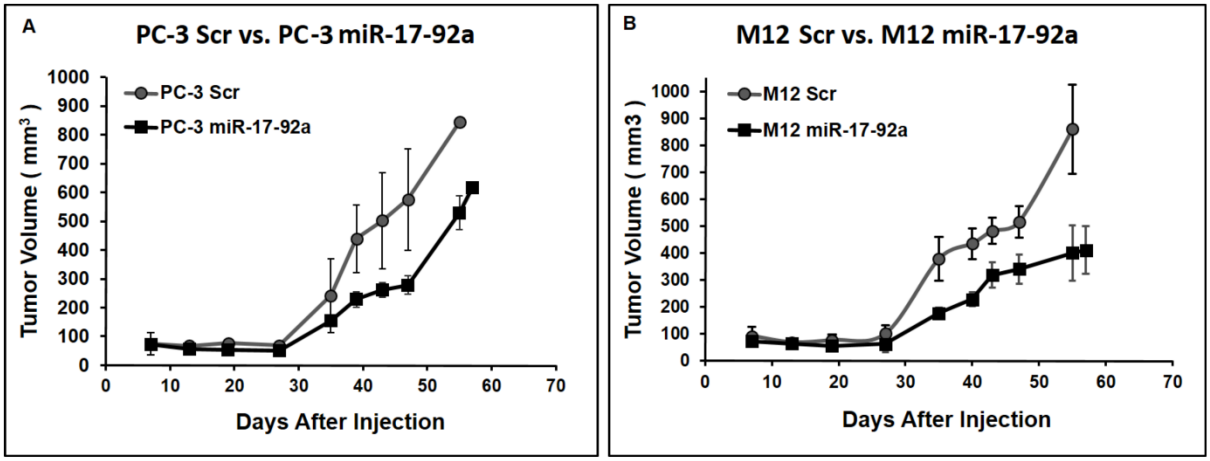

Figure 31: Progression of tumor growth in mice

Mice were injected with PC-3 or M12 cells stably expressing miR-17-92a cluster miRNAs or Scr RNA and tumor growth monitored for 55-57 days by tumor volume measurement.

4.4.3 Expression of miR-17-92a Inhibited Cell Migration and EMT

Previously, we noted a change in cell morphology upon restored expression of miR-17-92a miRNAs. To understand the contribution of miR-17-92a cluster expression to changes in cell behavior and phenotypes, we tested cell migration and expression of EMT markers such as, vimentin [131], Twist1 [132], Slug [133], TCF8/ZEB1 [134] and n-cadherin [135] in PC-3 stable sublines expressing miR-17-92a miRNAs. The bright field images and quantification of the distance traversed by the cells in scratch assays after 24h of incubation showed a significantly slower rate (25%-27%) of migration upon expression of miR-17-92a compared to the control cells expressing Scr RNAs (Figure 32A and B). This observation was supported by the immunoblot assay results showing

significantly reduced expressions of n-cadherin, vimentin, Twist1, Slug, and TCF8/ZEB1 in these cells compared to the control cells (Figure 33A and B). Conversely, increased expression (3.2-fold) and surface localization (22%) of the epithelial maker e-cadherin [136] was noted in PC-3 cells upon expression of miR-17-92a as determined by western blots (Figure 33A and B) and flow cytometric analysis (Figure 33C and D). Our results demonstrate a phenotypic conversion of the highly aggressive PC-3 cells to a more adherent type of cells with a reduced migration rate.

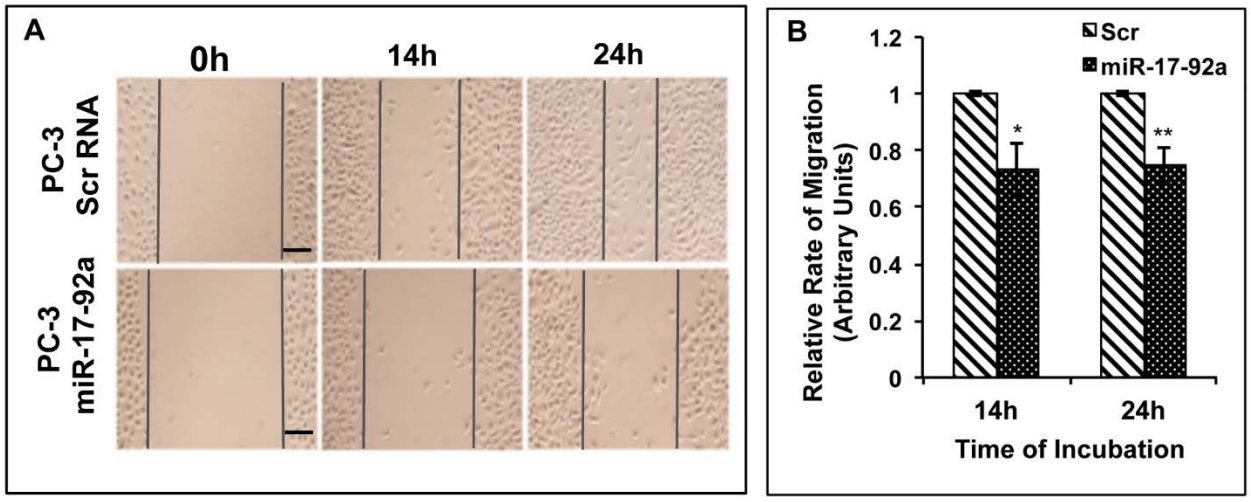

Figure 32: Expression of miR-17-92a cluster miRNAs inhibited migration

Migration was compared between PC-3 cells stably expressing miR-17-92a or scrambled RNA. (A and B) Migratory properties of cells were tested through wound healing assays at 14 and 24 hours after wound formation. The width of each wound was measured at three areas using light microscopy. Three wounds were made in each dish and the experiment was conducted in triplicate. A) Representative images of comparative migratory rates. Scale bar: 200□m. B) Relative rates of migration at 14 and 24 hours. Data represent mean±SD of three different experiments in triplicate wounds. *p=0.002; **p= 0.0004.

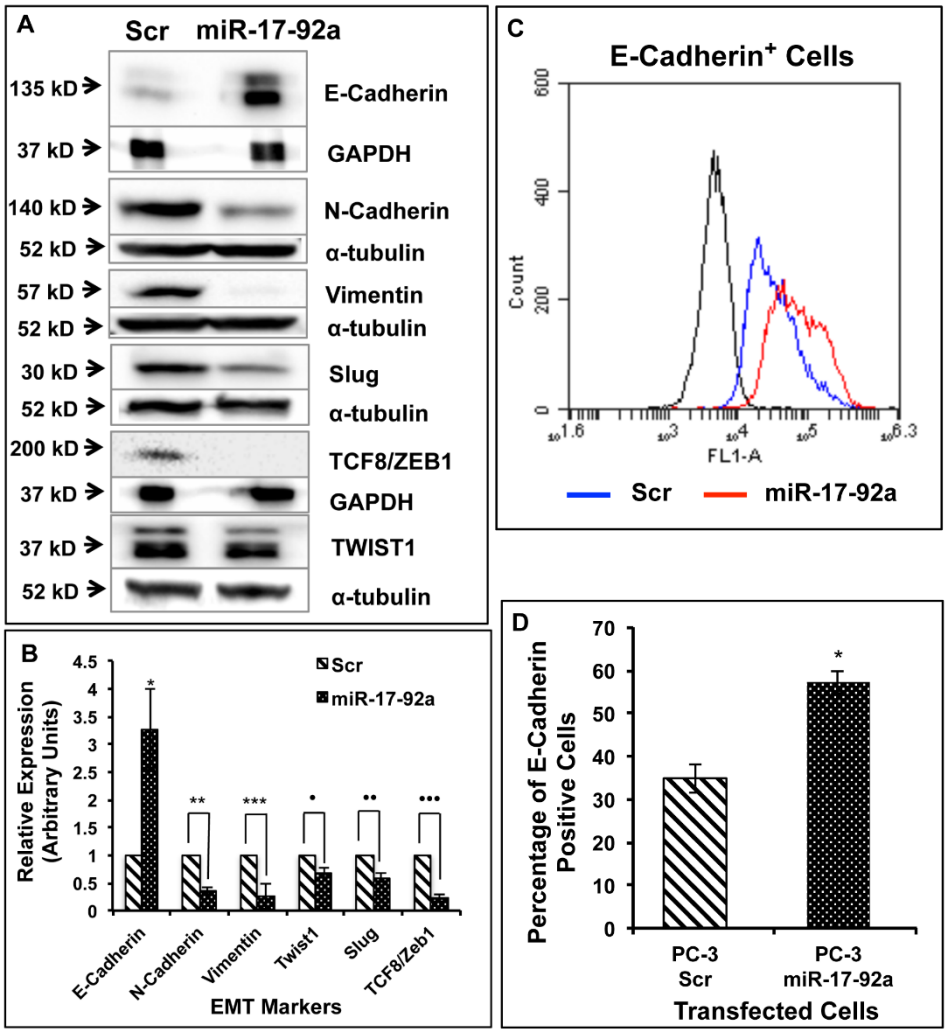

Figure 33: Expression of miR-17-92a cluster miRNAs promoted an epithelial phenotype in prostate cancer cells.

Expression of EMT markers were compared between PC-3 cells stably expressing miR-17-92a or Scr RNA. (A-D) Expression of miR-17-92a cluster in PC-3 cells promoted a switch from EMT to MET phenotype A) Representative images of the immunoblots of EMT markers. GAPDH or α-Tubulin was used as internal controls. B) Comparative analysis of EMT marker expression showing decreased expression of EMT markers but increased expression of the epithelial marker e-cadherin. Values were normalized to internal controls. Data represent mean±SD of three separate experiments. *p=0.005; **p=0.00006; ***p=0.004; •p=0.00002; ••p=0.001; •••p=0.00002. E) Overlay of a two-parameter histogram of the cell population exhibiting surface expression of e-cadherin. Result shows increased surface expression of e-cadherin in PC-3 cells expressing miR-17-92a cluster miRNAs. F) Quantification of the transfected PC-3 cells expressing e-cadherin on the cell surface as determined by flow cytometry showing a 22% increase in the cells expressing e- cadherin upon expression of miR-17-92a cluster miRNAs.

4.4.4 Expression of miR-17-92a Cluster Improved Drug Sensitivity of Androgen Dependent and Castration Resistant Prostate Cancer Cells

Our previous studies showed down-regulation of miR-17-92a cluster miRNAs in LNCaP104-S cells as they developed resistance to Casodex (CDX) [123]. Here we examined the involvement of miR-17-92a cluster in acquisition of CDX resistance of LNCaP104-S cells. We used androgen-dependent LNCaP104-S cells transiently transfected with pre miR-17-92a cluster DNA, and treated with CDX singly and in combination with the pan-AKT inhibitor (AKTi) (MK-2206 2HCl), or docetaxel (DTX). As noted earlier, expression of miR-17-92a cluster miRNAs reduced the number of viable cells upon vehicle treatment compared to the Scr RNA expressing cells (Figure 34A). Viability assays after single and combination treatments showed a synergistic effect of expression of miR-17-92a cluster and CDX treatment on the number of viable cells (Figure 34A). Treatment with DHT (10nM) showed an increased number of metabolically active cells expressing Scr RNAs whereas expression of miR-17-92a miRNAs made these cells less responsive to DHT (Figure 34A). LNCaP104-S cells expressing miR-17-92a miRNAs also showed an increased sensitivity to DTX at 1nM and 5nM concentrations compared to control cells. Combination treatments with CDX and DTX at a lower (1nM) concentration showed higher sensitivity than monotherapy (Figure 34A). Treatments with AKTi at 0.5, 1.0 and 2.5μM concentrations reduced cell viability significantly for both cell lines but to a much greater extent for cells expressing miR-17-92a (Figure 34B) compared to control cells expressing Scr RNAs. Combination treatments with CDX (10uM)

maintained the similar percentage of cell viability, which establishes a synergistic but not an additive effect of both drugs (Figure 34B).

Next we examined the effect of miR-17-92a cluster on drug sensitivity of androgen independent prostate cancer cells. Treatment of transiently transfected PC-3 cells expressing miR-17-92a cluster miRNAs or Scr RNAs with DTX and Aurora kinase inhibitor, VX680, in combination showed a significant reduction in cell viability but not when treated singly, except at a higher concentration (25nM) of DTX (Figure 34D). We tested a pan inhibitor of Aurora kinases as Aurora kinase inhibition, which causes mitotic arrest and apoptosis, has been recognized as an effective anticancer therapeutic strategy [137, 138]. Treatments with AKTi and DTX also showed a synergistic effect on reduced viability of PC-3 cells upon expression of miR-17-92a cluster miRNAs compared to control cells (Figure 34C) but not when treated singly. These observations indicate that restored expression of miR-17-92a cluster has a potential therapeutic benefit for treatment of both androgen dependent and CRPC cells.

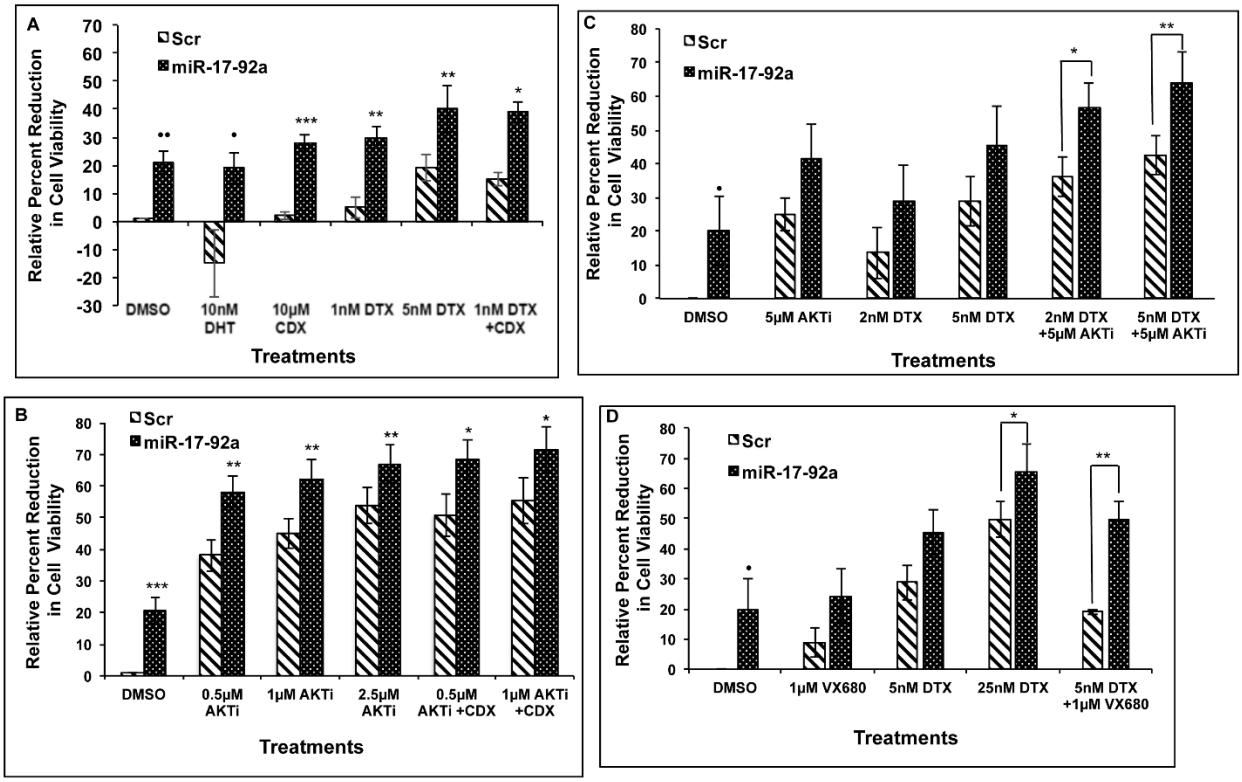

Figure 34: Expression of miR-17-92a cluster miRNAs increased drug sensitivity of prostate cancer cells.

Prostate cancer cells were transfected and treated with Casodex (CDX), docetaxel (DTX), pan-AKT inhibitor MK-2206 2HCl (AKTi), or Aurora kinase inhibitor VX-680. Sensitivity to individual or combinational treatments was measured through MTS assays. DMSO was used as the vehicle control. A and B. Androgen sensitive LNCaP104-S cells were transiently transfected and treated for 48 hours A. Percent reduction in viability of LNCaP cells expressing miR-17-92a miRNAs following treatment with 10 μM DHT, 10 μM CDX, 1 nM DTX, 5 nM DTX, and combination of 1 nM DTX + 10 μM CDX compared to cells expressing Scr RNAs. Data represent mean±SD of 4 independent experiments. •p=0.00003; ••p=0.0008; *p=0.00001; **p=0.002; ***p=0.00003; ****p=0.00001. B. Percent reduction in viability of LNCaP104-S cells expressing miR-17-92a miRNAs following treatment with 0.5 μM, 1 μM, and 2.5 μM AKTi alone or in combination with 10 μM CDX compared to cells expressing Scr RNAs. Data represent mean±SD of 4 independent experiments. *p=0.01; **p=0.004; ***p=0.008; •p=0.002; ••p=0.0006; •••p=0.0003. C and D. Androgen independent PC-3 cells were transiently transfected and treated for 72 hours. C. Percent reduction in viability of PC-3 cells expressing miR-17-92a miRNAs following treatment with 5 μM AKTi and 2 nM DTX or 5 nM DTX alone and in combination. Results show a significant reduction in viability of PC-3 cells only during combination treatments. Data show mean±SD of 3 independent experiments. *p=0.04; **p=0.03. D. Percent reduction in viability of PC-3 cells expressing miR-17-92a miRNAs following treatment with 1 μM VX680, 5nM DTX and 25 nM DTX alone or in combination. Data show a significant reduction in viability of transfected PC-3 cells upon 25 nM DTX alone and during combination treatment. Data represent mean±SD of 3 separate experiments. *p=0.01; **p=0.02.

4.5 miRNA Expressions Deregulated in Human Prostate Tumors

4.5.1 Genome-Wide miRNA Expression Profiling in Clinical Specimens

Prostate cancer is the most frequently diagnosed cancer in American men, yet the most commonly used biomarker for prostate cancer, PSA, is an unreliable prognostic tool. There is a need to better differentiate indolent from aggressive prostate cancer in order to properly treat this disease. The CAPRA-S scoring system was created to provide predictive rates of recurrence following radical prostatectomy and is a more accurate predictor of disease free regression compared to PSA values alone; however, an equally accurate predictive tool to identify preoperative high risk from low risk patients is still in need. To address this, we started investigating a possible correlation of CAPRA-S scores with miRNA expressions.

We requested chart reviews for patients with prostate tissues available from the Cooperative Human Tissue Network at UAB. CAPRA-S scores were calculated for each patient and tissues were macro-dissected. We obtained samples for treatment naïve patients stratified by risk grouping based on CAPRA-S score (low-risk 0-2, medium-risk 3-5, or high-risk ≥6). We used genome-wide miRNA array profiling approach to identify miRNA expression profiles for each patient's tumor and associated adjacent uninvolved prostate tissue. Normalized relative expression values were generated using the qBase+

software from Biogazelle.

Hierarchical clustering of the normalized and log2 transformed expression data (Additional File 9) showed 4 distinct clusters of miRNAs (Figure 35 and Additional File 10). Clusters 1 and 3 identified miRNAs distinctly expressed between malignant and uninvolved tissues (Figure 36A). The Log2 transformed relative expression values was extracted from each cluster and the average expression of each miRNA was calculated for both uninvolved tissue samples and tumor tissue samples. The average relative expression for individual miRNAs(unidentified) in both uninvolved and tumor groups was graphed (Figure 36B and C) for clusters 1 and 3 respectively. The dot plots display distribution of average miRNA expression values for both groups including the average of all miRNAs in the cluster (black bars) +/- 1 SD. In cluster 1 (Figure 36B) we identified 24 miRNAs (average values) that displayed down-regulation in tumor tissues compared to uninvolved tissues. Examination of this cluster distinguished 6 miRNAs with on average greater than 2 fold down-regulation in expression in malignant tissues. All 6 miRNAs (miR-133a/b, -143, -204, -221, -222) have published tumor suppressive functions in prostate cancer and have been found to be down-regulated in PCa [139-143]. Furthermore, miRs -143, -204, and -221/-222 are linked with CRPC or androgen receptor function. Alternatively, the trend of average miRNA expression presented in cluster 3 identified 17 miRNAs with increased expression in tumor tissues compared to uninvolved tissues (Figure 36C). Cluster 3 also contained a subset of 6 miRNAs that displayed on average a change in expression greater than 2 fold. However, these 6

miRNAs (miR-375, -183, -93, -96, -127-5p, and -380) are expressed at higher levels in malignant tissues compared to uninvolved tissue samples. All 6 miRNAs have been found to be aberrantly expressed in cancer, while 5 of which (miRs -93/-375, -96, -183, -380) have published oncogenic functions [144, 145],[146, 147]. The expressions of miRNAs -93 and -375 are commonly overexpressed with miR-106b, another member of cluster 3, and are believed to function in a regulatory axis promoting prostate cancer progression [145].

Initial analysis of Cluster 2 and 4, identified from genome-wide expression analysis (Figure 35), did not show the visibly unique expression patterns, between tumor and uninvolved prostate tissues, previously identified in clusters 1 and 3. The cluster 2 heat map (Figure 37A) depicts similar levels of expressions for all miRNAs (miR-103, -107, -29a/b/c, -199a/b-3p, and let-7a/b/d/e/g/i) within individual patient tissue; while, miRNAs display heterogeneous expression across samples. Further interrogation of the cluster revealed correlation of miRNA expression profiles with the patient's CAPRA-S score. Fifty percent (9/18) of tumor tissues from low and medium risk patients (CAPRA-S score 0-6) expressed cluster specific miRNA averages below the average observed in all benign samples. However, 83% (5/6) of tumor tissues from high risk patients (CAPRA-S score ≥ 7) expressed cluster specific miRNA averages below the average observed in all benign samples. Dissecting the cluster into individual miRNAs, there was 2-fold change in expression (+/- 0.2) for 9 of 13 miRNAs in cluster 2 while there was no significant reduction observed in low and medium risk patient tumors (Figure 37C).

These finding are in accordance with previous publications demonstrating tumor suppressive functions for all cluster 2 miRNAs in prostate cancer [148-151]. In cluster 4, the trend of increasing miRNA expression correlates positively with increasing risk of disease recurrence, as predicted by CAPRA-S score groups: low risk (CAPRA-S 0-2), medium risk (CAPRA-S 3-5) and high risk (CAPRA-S ≥6) (Figure 37B and D). Within cluster 4, three miRNAs (miR-129-5p, -138, -519e) have been associated with resistance to a Hsp90 inhibitor, Tanespimycin [152]. Hsp90 is known to promote AR activity [153], and co-targeting of HSP90 in addition to androgen blockade is a proposed adjuvant therapy [154]. Inhibiting Hsp90 when combined with AR antagonist, CDX, has shown to suppress PCa growth and inhibit induction of AR-V7 a spice variant of AR known to be involved in resistance to ADT [155]. Further investigation of this cluster of miRNAs may provide a miRNA profile that could be used to identify the efficacy this combinational therapy could provide on a patient specific basis.

The analysis of genome-wide miRNA expressions stratified by CAPRA-S score, identified patterns of miRNA expression profiles consistent with our hypothesis and previous reports. Emboldened by these results, we sought to identify miRNA expression profiles differentially expressed in malignant prostate tissues of African American men, specifically. The disparity in the rate of prostate cancer occurrence and mortality in African American men, necessitates the identification of biomarkers specific for race and ethnicity. From the data generated in our genome-wide profiling study, we compared the relative expression of miRNAs in prostate tumor tissues from African American (AA) men

against that of Caucasian American (CA) men. From this comparison we identified miRNAs that, on average, exhibited ≥2-fold difference in expression (increase and decrease), in African Americans compared to Caucasian Americans (Figure 38). The miRNAs highlighted in Figure 38 (miR-541, miR-34c-5p, miR-135b, miR-299-3p, miR-491-5p, and miR-30e) displayed reduced expression in the tumors of African American men. The miRNAs also have been shown to negatively regulate the expression of AR in prostate cancer cells [49]. Our data showing reduced expression of AR targeting miRNAs in AA men indicate a possible up-regulation of expression of AR and, correlates with previous studies showing increased expression of AR in the prostate tumors of AA men relative to CA men [156, 157]. To better understand how these miRNAs are regulated we examined the fold-change in expression of these miRNAs in patient specific tumor tissues compared with matched benign prostate tissue. The patients were grouped by race and subdivided by CAPRA-S score (0-3 or ≥4) (Figure 39). This analysis highlighted the consistent pattern of down-regulation of these 6 miRNAs in AA men. In comparison, CA patients displayed a much broader distribution in expression.

The genome-wide miRNA profiling has not been fully completed for all patients. However, from the completed profiling, we have compared the fold change in expression of miRNAs stratified by CAPRA-S risk groups and have identified the top 100 miRNAs with the greatest FC in expression (50 up-, and 50 down-regulated) (Table 18 and Table 19)

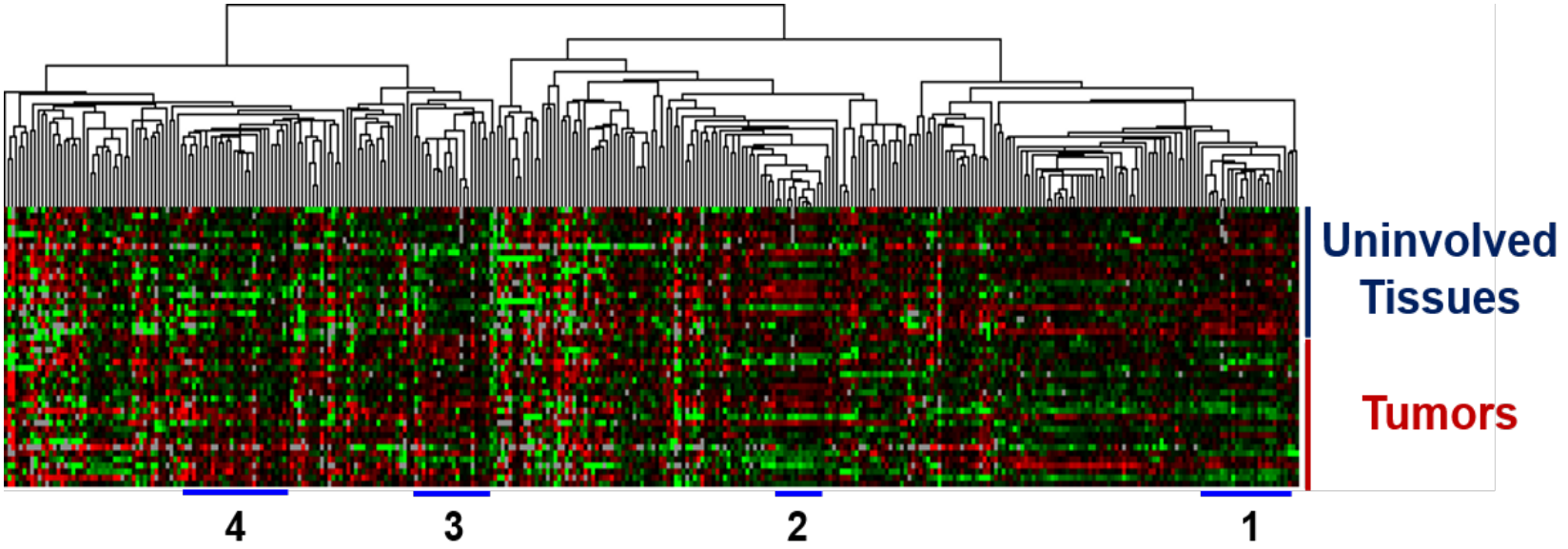

Figure 35: Clustering of genome-wide miRNA expressions in tumor tissues and uninvolved prostate tissues

Hierarchal clustering of Log2 transformed relative expression values of miRNAs in uninvolved prostate and tumor tissues. Four clusters were selected for further analysis.

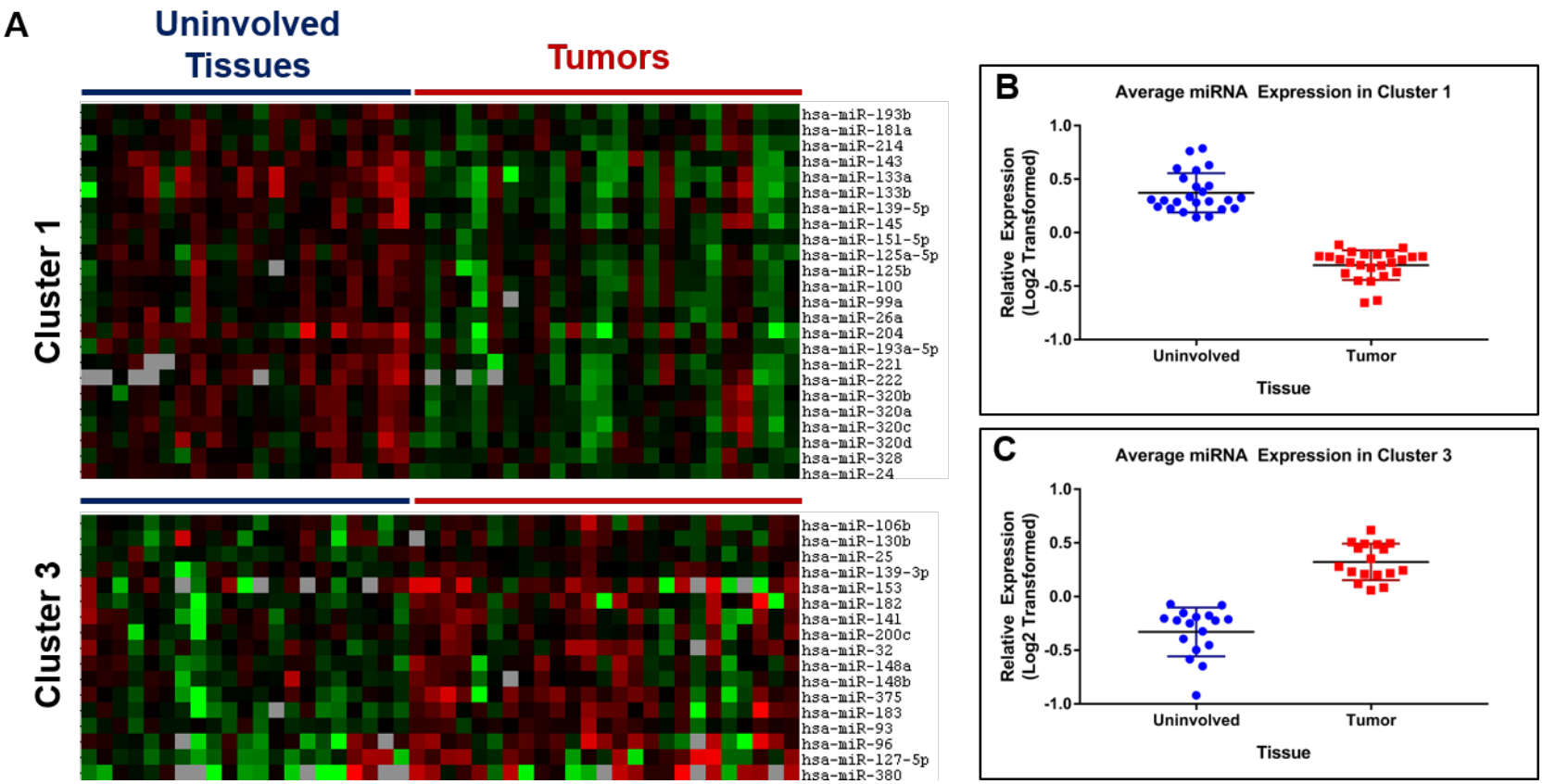

Figure 36: Analysis of clusters 1 and 3 identified from genome-wide miRNA profiling of prostate tissues

Hierarchal clustering of Log2 transformed relative expression values of miRNAs in uninvolved and malignant prostate tissues. A) Heat maps of expression data for miRNAs in cluster 1 and 3; uninvolved tissue samples grouped under blue line (left side) and tumor samples grouped under red line (right side). B and C) The average expression value of each miRNA was calculated for uninvolved tissue samples (blue circles) and tumor samples (red squares). These values were used to generate dot plots for Cluster 1 (B) and Cluster 2 (C).

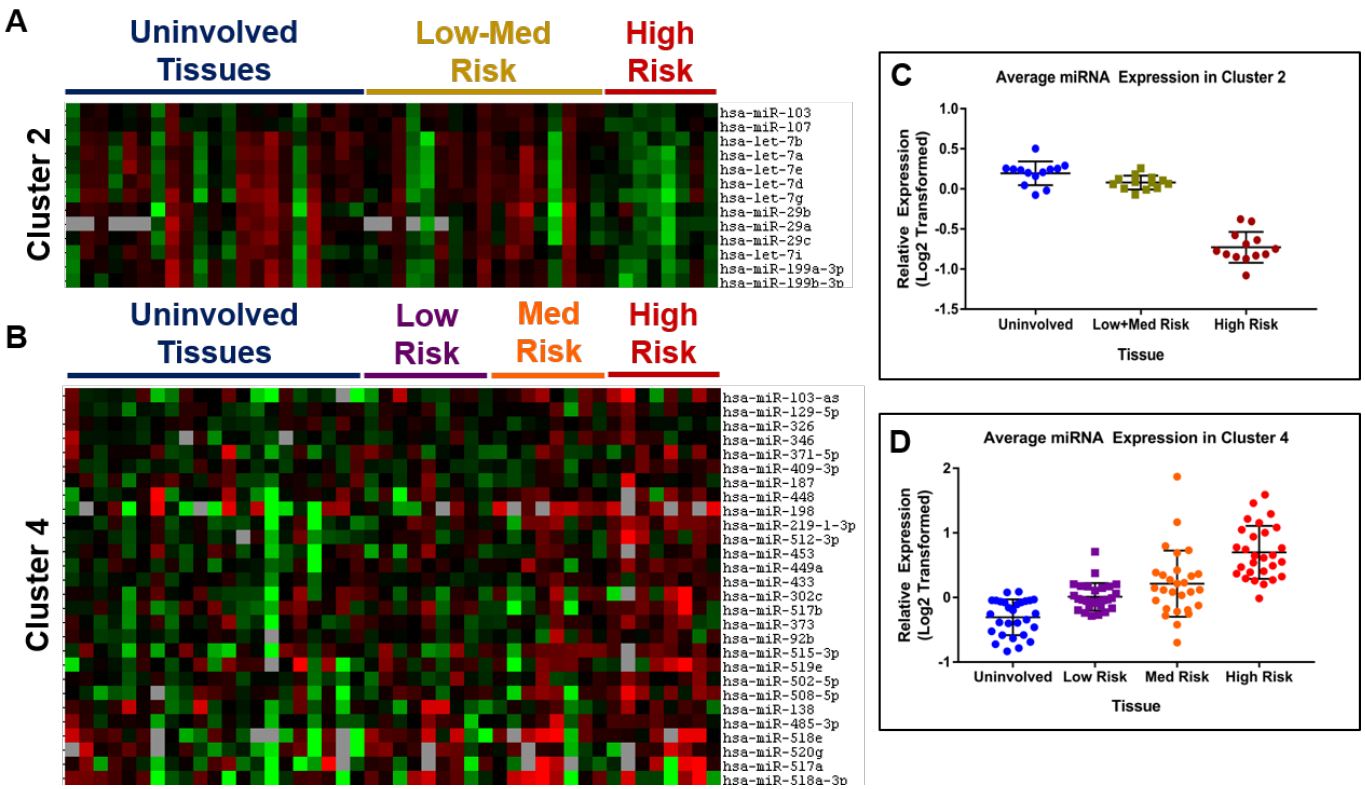

Figure 37: Analysis of clusters 2 and 4 identified from genome-wide miRNA profiling of prostate tissues

Hierarchal clustering of Log2 transformed relative expression values of miRNAs in uninvolved and malignant prostate tissues. Correlation of miRNA expressions with CAPRA-S risk group. A and B) Heat maps of expression data for miRNAs in cluster 2 (A) and 4 (B). A) Uninvolved tissue samples grouped under blue line, low and medium risk patient tumor samples grouped under gold line, and high risk patient tumor samples grouped under red line. B) Uninvolved tissue samples appear under blue line, low risk patient tumor samples grouped under purple line, and medium grouped under orange line and high risk patient tumor samples grouped under red line. C and D) Average expression value of each miRNA was calculated for uninvolved tissues and tumor tissues grouped by CAPRA-S risk. Values were used to generate dot plots for Cluster 2 (C) and Cluster 4 (D).

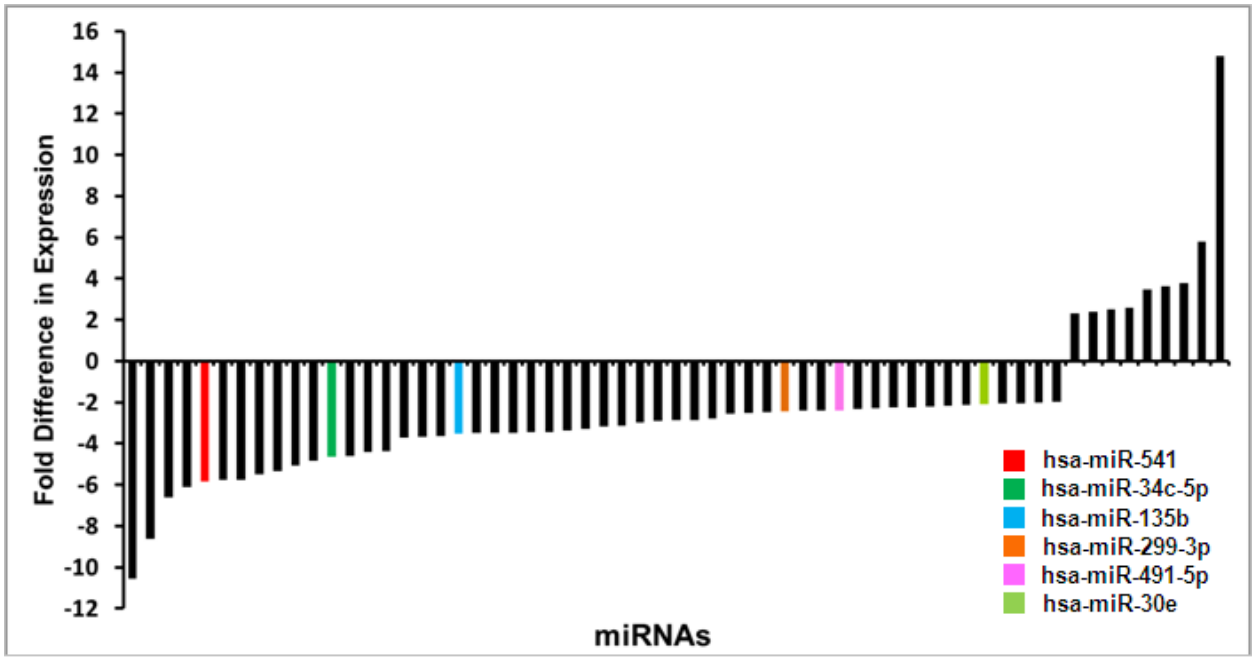

Figure 38: Top miRNAs with differential regulation between Caucasian and African Americans

The relative expression of miRNAs in prostate cancer of African Americans was compared against that of Caucasian American men. The values for induvial miRNAs that exhibited at least a 2-fold change were used to create the graph. A negative value represents decreased expression in AA patient samples compared to CA samples. The identified miRNAs have been shown to regulate the expression of AR.

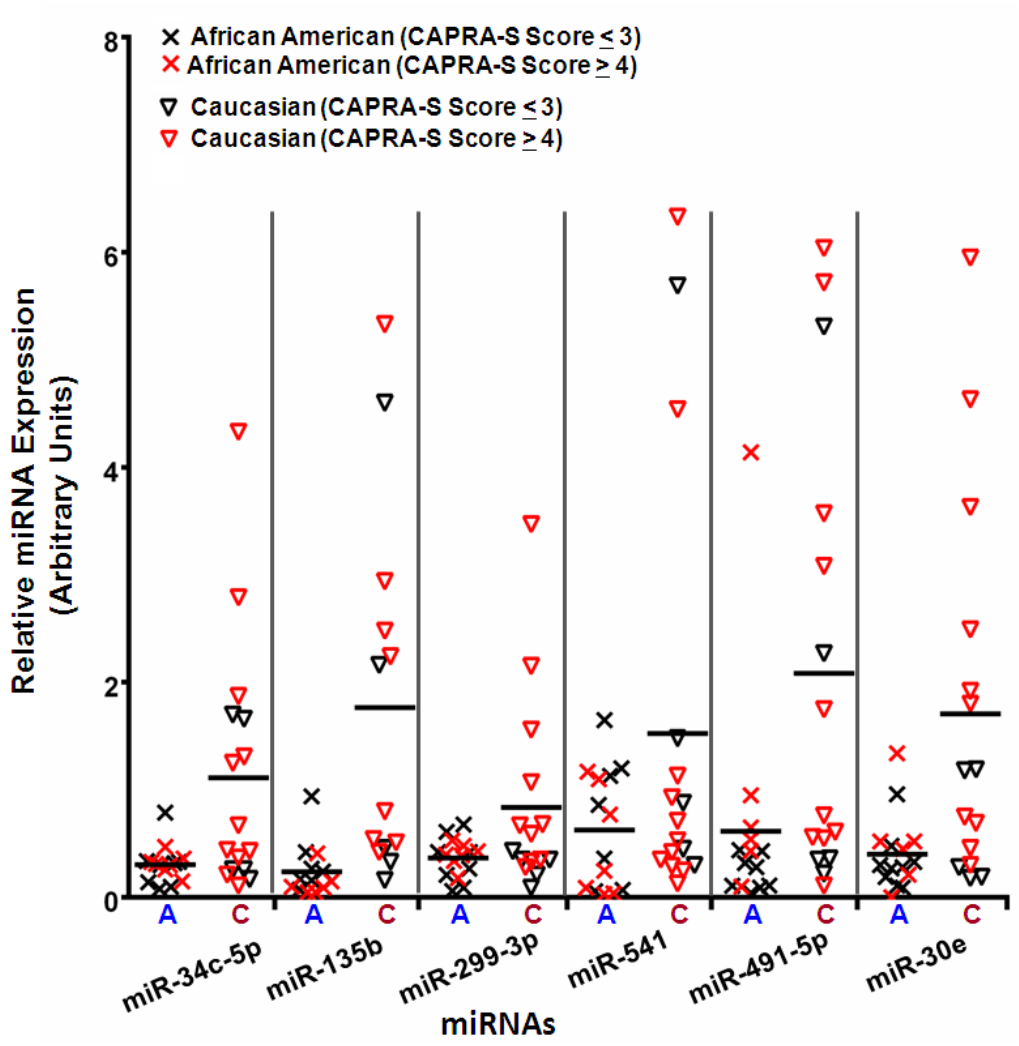

Figure 39: Comparing expression of AR regulated miRNAs in African Americans vs Caucasians

The fold change in expression of AR regulating miRNAs grouped by race, African American (**A**) or Caucasian American (**C**). Patients with CAPRA-S scores greater than 3 are identified by red symbols

Table 17: Top 50 Down-Regulated miRNAs Across CAPRA-S Grouping

miRNA	Low Risk Fc	Med Risk Fc	HighRisk Fc	Avg Fc
hsa-miR-204	-2.56	-1.83	-2.65	**-2.28**
hsa-miR-376c	-2.76	-2.04	-2.01	**-2.25**
hsa-miR-365	-2.05	-2.56	-2.05	**-2.21**
hsa-miR-221	-2.18	-2.07	-2.20	**-2.14**
hsa-miR-205	-1.21	-2.65	-4.26	**-2.06**
hsa-miR-133a	-2.52	-2.32	-1.36	**-1.98**
hsa-miR-143	-2.06	-1.97	-1.82	**-1.95**
hsa-miR-222	-1.90	-2.09	-1.63	**-1.87**
hsa-miR-218	-1.93	-2.19	-1.46	**-1.85**
hsa-miR-29a	-1.57	-1.93	-1.82	**-1.81**
hsa-miR-548b-5p	-1.27	-2.12	-2.22	**-1.76**
hsa-miR-452	-1.92	-1.87	-1.27	**-1.73**
hsa-miR-224	-1.16	-2.12	-2.69	**-1.72**
hsa-miR-29c	-1.42	-2.07	-1.64	**-1.67**
hsa-miR-125a-5p	-1.58	-1.82	-1.60	**-1.67**
hsa-miR-155	-1.68	-1.92	-1.39	**-1.66**
hsa-miR-24	-1.97	-1.41	-1.58	**-1.62**
hsa-let-7g	-1.54	-1.62	-1.74	**-1.62**
hsa-miR-424	-1.38	-2.20	-1.39	**-1.61**
hsa-miR-378	-2.24	-1.17	-1.82	**-1.60**
hsa-miR-517c	-2.38	1.02	-5.01	**-1.60**
hsa-miR-130a	-1.52	-1.82	-1.44	**-1.59**
hsa-miR-487b	-1.53	-1.54	-1.71	**-1.59**
hsa-miR-199a-3p	-1.65	-1.73	-1.37	**-1.58**
hsa-miR-211	-1.84	-1.73	-1.23	**-1.58**
hsa-let-7c	-1.51	-2.33	-1.22	**-1.57**
hsa-let-7a	-1.41	-1.61	-1.67	**-1.55**
hsa-miR-496	-1.09	-2.28	-1.59	**-1.52**
hsa-miR-99a	-1.42	-1.65	-1.50	**-1.52**
hsa-miR-196a	-2.09	-1.27	-1.39	**-1.52**
hsa-miR-125b	-1.61	-1.68	-1.26	**-1.51**
hsa-miR-100	-1.41	-1.66	-1.44	**-1.50**
hsa-miR-26a	-1.58	-1.67	-1.26	**-1.50**

miRNA	Low Risk Fc	Med Risk Fc	HighRisk Fc	Avg Fc
hsa-miR-199b-3p	-1.50	-1.76	-1.25	**-1.50**
hsa-let-7b	-1.22	-1.73	-1.57	**-1.47**
hsa-miR-374b	-1.49	-2.08	-1.08	**-1.46**
hsa-let-7d	-1.34	-1.66	-1.42	**-1.46**
hsa-miR-299-5p	-1.81	1.02	-2.29	**-1.46**
hsa-miR-381	-1.52	-1.10	-2.14	**-1.46**
hsa-miR-142-5p	-1.53	-3.29	1.97	**-1.45**
hsa-let-7e	-1.44	-1.41	-1.44	**-1.43**
hsa-miR-193a-5p	-1.46	-1.69	-1.14	**-1.42**
hsa-miR-28-5p	-1.72	-1.44	-1.10	**-1.40**
hsa-miR-145	-1.77	-1.73	1.10	**-1.38**
hsa-miR-22	-1.45	-1.74	-1.06	**-1.38**
hsa-miR-193b	-1.33	-1.91	-1.06	**-1.38**
hsa-miR-181a	-1.79	-1.67	1.10	**-1.38**
hsa-miR-9	-1.15	-1.76	-1.33	**-1.37**
hsa-miR-338-3p	-1.42	-1.22	-1.61	**-1.37**
hsa-miR-379	-1.66	-1.55	1.06	**-1.36**

Red Values > 2x fold change compared to adjacent uninvolved tissue.

Table 18: Top 50 Up-Regulated miRNAs Across CAPRA-S Grouping

miRNA	Low Risk Fc	Med Risk Fc	HighRisk Fc	Avg Fc
hsa-miR-524-3p	1.03	2.54	2.86	**2.08**
hsa-miR-519a	0.59	1.50	5.99	**2.30**
hsa-miR-508-5p	1.88	1.21	4.48	**2.32**
hsa-miR-127-5p	2.38	2.61	1.92	**2.35**
hsa-miR-517b	1.77	2.24	3.24	**2.36**
hsa-miR-515-5p	3.30	2.47	0.43	**2.39**
hsa-miR-515-3p	1.13	3.89	2.08	**2.40**
hsa-miR-522	1.56	1.14	6.31	**2.47**
hsa-miR-146b-3p	1.89	3.05	2.22	**2.49**
hsa-miR-198	0.39	5.04	2.31	**2.50**
hsa-miR-96	1.72	2.50	3.71	**2.51**
hsa-miR-219-1-3p	1.12	3.26	3.55	**2.54**
hsa-miR-520e	1.70	1.05	5.85	**2.59**
hsa-miR-521	1.84	3.97	2.09	**2.63**
hsa-miR-34c-5p	0.93	2.01	5.79	**2.65**
hsa-miR-302c	0.72	3.44	4.54	**2.72**
hsa-miR-300	0.78	4.92	2.50	**2.75**
hsa-miR-330-5p	0.82	2.72	5.26	**2.77**
hsa-miR-501-5p	0.63	2.21	6.20	**2.78**
hsa-miR-183	1.93	1.89	4.95	**2.81**
hsa-miR-520c-5p	2.96	1.41	5.97	**2.87**
hsa-miR-182	1.74	1.88	5.55	**2.88**
hsa-miR-516b	2.67	1.47	5.78	**2.88**
hsa-miR-519e	1.26	1.91	6.62	**2.89**
hsa-miR-511	1.20	0.97	10.07	**2.95**
hsa-miR-545	3.08	2.27	4.61	**3.02**
hsa-miR-448	0.81	6.11	1.77	**3.02**
hsa-miR-512-5p	2.36	2.42	4.94	**3.11**
hsa-miR-506	1.27	3.71	4.73	**3.12**
hsa-miR-520d-5p	1.67	2.77	6.15	**3.12**
hsa-miR-517a	0.94	5.17	4.21	**3.18**
hsa-miR-519d	2.89	1.39	5.33	**3.19**
hsa-miR-301b	1.10	5.20	4.25	**3.26**
hsa-miR-544	4.45	3.20	1.24	**3.30**
hsa-miR-488	1.84	0.58	11.88	**3.33**

miRNA	Low Risk Fc	Med Risk Fc	HighRisk Fc	Avg Fc
hsa-miR-513a-5p	1.34	2.24	7.72	**3.42**
hsa-miR-206	6.57	1.16	1.83	**3.51**
hsa-miR-514	2.03	5.26	3.59	**3.63**
hsa-miR-299-3p	1.16	5.81	4.11	**3.65**
hsa-miR-302d	1.99	1.35	8.97	**3.74**
hsa-miR-525-3p	1.38	4.26	6.91	**3.76**
hsa-miR-548d-3p	2.97	4.80	2.98	**3.77**
hsa-miR-518d-3p	2.88	2.28	7.14	**3.80**
hsa-miR-380	3.10	5.97	1.67	**3.86**
hsa-miR-527	1.37	5.03	5.48	**3.89**
hsa-miR-507	4.10	3.15	6.26	**3.99**
hsa-miR-302e	3.03	4.85	6.43	**4.23**
hsa-miR-412	4.20	2.32	8.61	**4.52**
hsa-miR-103-as	1.12	7.49	9.17	**5.57**
hsa-miR-371-3p	3.33	1.32	83.97	**28.35**

Red Values > 2x fold change compared to adjacent uninvolved tissue.

CHAPTER FIVE: DISCUSSION

5.1 miRNAs Involved in the Transition to Androgen Independence

Our studies on profiling and validation of miRNA expressions during transition of androgen-dependent LNCaP-104S cells to androgen-independent and CDX resistant cells revealed activation and inactivation of several signaling networks. We noted a difference in miRNA expressions between the androgen-independent subline LNCaP-104R1, and freshly generated CDX resistant LNCaP-104S cells, which includes some of the up-regulated (miR-146a) and down-regulated miRNAs (miR-15b-3p and miR-18b). Although we noted differential expression of miRNAs between CS-FBS and CDX treated LNCaP cells, we selected only miRNAs that showed either up-regulation or down-regulation in all treated samples for analysis of their putative targets. Despite similar expression profile of specific miRNAs in CS-FBS and CDX treated samples, some the targets such as DOK4 and VEGF showed differential expression in CSFBS and CDX treated cells. Presumably, this could be the effect of regulation of multiple targets by a given miRNA, which may indirectly affect the net expression of DOK4 and VEGF.

Over expression of miR-146a was noted in all treated cells contrary to the study showing loss of expression of miR-146a in CRPC [158]. Increased miR-146a expression was substantiated by down-regulation of its two bona fide targets TRAF6 and IRAK1 in both -104R1 and 3wks treated -104S cells. MiR-146a expression is induced by NF-κB [159] and acts in a negative feedback loop through degradation of TRAF6 and IRAK1 to

reduce NF-κB signaling and inflammatory response. An increase in transcription of miR-146a, as a result of elevated NF-κB activity is noted in thyroid cancer [160] and down-regulation of miR-146a is associated with hyperactivation of NF-kB [161]. Despite this association, an increase in NF-kB1 expression could be predicted in treated -104S cells, as NF-kB1 is a direct target of the down-regulated miRNA miR-9 [162]. Increased expression of the other subunit RelA, which heterodimerizes with NF-kB1 could also be predicted as it is a direct target of the down-regulated miR-7 [163]. It appears that the NF-kB signaling pathway is activated in the early stages of gaining resistance to CDX/androgen blockade and the increased expression of miR-146a is a secondary effect of the activation of the NFkB pathway. As a result, in the initial stages of anti-androgen drug resistance there is decreased inflammatory response but down regulation of tumor suppressor targets of miR-146a, BCORL1 [164] and RNASEL [165], which may not be detected in fully developed CRPC. Furthermore, over-expression of miR-146a has been identified in cells undergoing replicative senescence; which is a cellular fate induced by androgen deprivation therapy and contributes to ADT resistance [166-168]. A recent study has shown CDX treatment of LNCaP cells prevents AR from repressing expression of CCAAT/Enhancer Binding Protein β (C/EBPβ), a transcription factor involved in regulating proliferation and DNA damage response. Increased expression of C/EBPβ was detected in CRPC, compared to naïve patients, and over-expression of C/EBPβ sensitized LNCaP cells to cytotoxic chemotherapy following ADT [168]. Interestingly, C/EBPβ mRNA is a predicted target of miR-17, miR-20a, miR-106a, miR-374a, and miR-

374b; all of these miRNAs were found to be down-regulated (or undetectable) upon CDX treatment in our study. This suggests down-regulation of these miRNAs acts as a possible survival mechanism for PCa cells undergoing ADT. To further support this hypothesis, two studies published in May and June of this year (2016), linked down-regulation of a miR-374a/b with acquired cisplatin resistance in pancreatic cancer cells and nasopharyngeal carcinoma respectively [169, 170]. In nasopharyngeal carcinoma, miR-374a decreased expression of CyclinD1 leading to reduced PI3K/AKT activity. Additionally, miR-374a expression in nasopharyngeal carcinoma additionally reduced expression of c-MYC, E2F1, Snail, N-cadherin [170]. These findings further parallel the effect we observed in PCa cells over-expressing the miR-17-92a cluster.

The EGFR signaling pathway could also be activated in the early stages of androgen blockade and CDX treatment. The evidence of EGFR pathway activation in the treated LNCaP-104S cells is from our results showing an increased expression of EGFR, down regulation of miR-7 and up-regulation miR-222, which are the miRNA regulators of EGFR. Decreased expression of p27Kip1 and Cbl, as two other targets of the up-regulated miR-222, further aid activation of EGFR signaling. C-Cbl, an E3 ubiquitin ligase, inactivates ligand-bound EGFR through EGFR-Cbl complex formation leading to its degradation [171]. C-Cbl activation mediates the tumor suppressive effects of EPhB6 and inhibits cancer cell invasiveness [172]. C-Cbl is also targeted by the up regulated miRNA miR-136 in all treated cells. Down regulation of c-Cbl in treated -104S and untreated -104R1 cells possibly promotes antiandrogen resistance through EGFR stabilization. A

loss of expression of AR was noted in these cells, which supports the report showing an inverse relationship between expression of AR and EGFR in prostate cancer patients [28]. Up regulation of miR-136 in treated -104S cells was substantiated by the loss of expression of the miR-136 target ZFAND1, an uncharacterized AN1 type zinc finger domain 1 containing protein.

Activation of the PI3K/AKT signaling axis could also be predicted in treated -104S cells, as a result of down regulation of miR-7, which inhibits tumor growth and metastasis through inhibition of PI3K/AKT pathways [173]. Down-regulation of miR-7 in cancer cells including glioblastoma and its inhibitory effects on EMT and metastasis is well documented [174]. Activation of this pathway could be further aided by over expression of miR-22 in all treated cells, which exerts a proto-oncogenic effect through down-regulation of PTEN in androgen-independent prostate cancer cells [175]. Additionally, activation of VEGF and DOK4 could be predicted, as these proteins are over expressed in treated -104S cells possibly as a result of down-regulation of their regulatory miRNA, miR-205. Earlier studies showed an association between poor prognosis of localized prostate cancer and epigenetic repression of miR-205 [176], and thus confirms the relevance of the loss of miR-205 in development of CDX resistance. DOK4 is a newly identified substrate of ligand-bound insulin receptor (IRS-5), which, upon phosphorylation translocates to mitochondria and recruits c-Src kinase to the mitochondria. Up regulation of DOK4 is also noted in renal cell carcinoma [122]. VEGFA, also a target of miR-15b-5p, showed 2-10-fold reduction in expression in treated -104S cells and in chemotherapy-

resistant squamous cell carcinoma [177].

Other than modulation of specific signaling axes, altered expression of miRNA clusters is also evident in our study. Members of the miR-17-92a and its paralogous miR-106a-363 clusters, miR-17, miR-18a, miR-18b, miR-20a and miR-106a showed ~9-10-fold down regulation upon CDX treatment and androgen blockade. In support of our observation, loss of expression of miR-17 [178], miR-18a [139], miR-20a [179] and miR-106a [180] are reported in breast and other cancers. Loss of expression of miR-106a, miR-17 and miR-20a are further supported by an increased expression of their target protein FGD4 in these cells. Contrary to the published study [78], over-expression of miR-34b was noted in AI and CDXR cells, however, an inverse relationship between miR-34b expression and disease free survival of triple negative breast cancer has been reported [181], which suggests that miR-34b expression may be dependent on the status of hormone responsiveness. Among the other up-regulated miRNAs, over expression of let-7f-1 [182], miR-143 [183], miR-218 [184], miR-29a [185], miR-302a [186], miR-3144 [187], miR-493 [188] and miR-664 [189] in cancer cells has been reported earlier. Our study also identified a number of miRNAs with > 2-fold difference in expression such as miR-3138, miR-3192, miR-3199, and a subset of miR-548 series, which are not yet known to be involved in development of CRPC.

Additional miRNAs such as miR-518b, miR-205 and miR-596 showed a > 10-fold loss of expression upon CDX treatment or androgen withdrawal. In support of our

observation, loss of expression and tumor suppressor functions of mir-518b and miR-596 has been documented in other cancers [190]. MiR-1244 and miR-759 are two other miRNAs that are significantly down regulated in all treated cells. This is substantiated by an increased expression of their common target ABHD3 in these cells [112]. Among the other down regulated miRNAs, miR-9 and miR-422a are known to have tumor suppressor roles in various cancer cells [191, 192], whereas miRNAs -454, -3131 and -3185 are noted for the first time to be deregulated during progression of CRPC.

Functional contribution of some of the identified microRNAs in development of CRPC has been previously reported. Over expression of miR-222/221 in LAPC4 cells was shown to promote androgen independent cell growth, which was abrogated upon expression of anti-miR-222/221 inhibitors [58]. Down-regulation of miR-205 has been correlated with advanced prostate cancer and ectopic expression of miR-205 suppressed AR and MAPK signaling and inhibited cell growth [193]. Down-regulation of miR-17 in AI prostate cancer cells has also been demonstrated. Expression of pre-miR-17 in these cells prevented AR-induced gene transcription and inhibited cell proliferation [50].

Analysis of the altered cellular processes during progression towards CDX resistance and androgen independence showed a decreased percentage of miRNAs involved in cancer but an increased percentage in reproductive system, endocrine system, hepatic system and metabolic diseases. It can be speculated that up-regulated oncomiRs at earlier stages aid in transformation of cells through suppression of tumor

suppressors. Whereas, at later stages accumulation of abnormal cellular events triggers expression of additional sets of miRNA, which inhibit key regulatory proteins involved in metabolic process, hormone response and other cellular events. Our qRT-PCR FC data indicate differential expression of miRNAs between 1wk and 3wks treatment, which would have been undetected had the profiling been done only in CDX sensitive/AD and –resistant/AI cells. In silico analysis identified a number of targets that are potentially regulated by one or more altered miRNAs. This includes, two mitosis regulatory proteins CCNJ and CHAMP1 (ZNF828) [114, 115]; two oncogenic proteins PIK3CD [194] and MYB that are over expressed in CRPC [116]; a protein trafficking regulatory protein ,RAB9B; a ubiquitination promoting protein, SPOPL, involved in the Hedgehog/Gli signaling pathway [117]; and E2F1, transcription factor [121].

The overall evaluation of the changes in expression profiles of miRNAs during transition of CDX-sensitive and AD cells to the CDX-resistant and AI ones demonstrates that not any one or two miRNAs are responsible for development of drug-resistant prostate cancer. Instead, a complex network of activation and inactivation of specific signaling pathways, aided by degradation or accumulation of the target mRNAs as a result of differential expression of a significant number of miRNAs, plays the pivotal role. Also, there are transient changes in the expression of miRNAs as well as their target proteins during transition of cells towards ADT resistance, which may provide growth and survival advantage to a subset of cancer cells; and these changes in miRNA/mRNA signature may be missed in already developed castration resistant prostate cancer.

5.2 Functional Significance of miR-17-92a Expression in Prostate Cancer

In our analysis of miRNAs associated with androgen independence we identified the miR-17-92a cluster which displayed loss of expression as cells developed resistance to ADT and CDX. This suggests a possible tumor suppressive role of these miRNAs; however, this observation is contradictory to the published studies showing increased expression of miR-17-92a cluster miRNAs in lung cancer [195] and B-cell lymphomas [196]. The change in expression may either be driven by occasional amplification of the 13q31.3 locus and/or hyperactivation of *Myc* oncogene in these tumors, which is a potent transcriptional activator of *MIR17HG* gene, leading to increased synthesis of the primary transcripts of these miRNAs [197]. Alternatively, it may be due to increased stabilization of the mature miRNAs by endogenous regulatory RNAs or proteins that may lead to accumulation of these miRNAs. The expression pattern of miR-17-92a in prostate tumors also corroborated with the expression levels in prostate cancer cell lines, which further confirms the loss of expression of miR-17-92a cluster in prostate cancer. In support of our observations, down-regulation of miR-17-5p and miR-17-3p in prostate cancer cell lines and tissues have been documented earlier [50, 198].

Our studies on the functional consequence of the restored expression of miR-17-92a cluster miRNAs in PC-3 prostate cancer cells revealed down-regulation of Rho-GTPase signaling pathway proteins FGD4 and LIMK1, and cell cycle regulatory proteins cyclin D1 and SSH1, which have predicted binding sites of miRs-17 and -20a at the 3’

UTRs. Our study established FGD4 as a direct target of miR-17, and -20a, which is also overexpressed in prostate tumors with higher Gleason scores and in androgen independent tumors (unpublished observation in our laboratory). Importantly, the role of FGD4 in promotion of cancer cell migration has also been reported [124]. Although all six miRNAs were expressed from a single vector, the levels of expression of individual miRNAs varied with a maximum expression of miR-17 and -20a in both PC-3 and M12 cells (Figure 26). This result suggests that expression of the miR-17-92a cluster facilitates establishing an anti-oncogenic environment in prostate cancer cells, as overexpression and oncogenic/metastatic functions of LIMK1, cyclin D1 and SSH1 have been documented in prostate and other cancers [199-201]. The functional identity of miR-17-92a cluster in prostate cancer cells is further supported by our results showing reduced activation of ERK1/2 kinases and AKT in these cells. Reduced proliferation of these cells as noted by Ki67 staining and cell proliferation assays also aids in the overall interpretation of our results.

Results showing antitumorigenic and tumor growth inhibitory effects of miR-17-92a cluster further strengthen the inference that the miR-17-92a cluster exhibits tumor suppressor effects when expressed in highly aggressive tumorigenic prostate cancer cells. This effect could be mediated by differential regulation of cell cycle promoting cyclin D1 expression. The miR-17-92a cluster also inhibits expression of CDK inhibitor p21 gene [202], which inhibits G1/S transition, but inhibition of cyclin D1 expression by the miR-17-92a cluster could be more robust in these cells showing a net anti-proliferative effect of

these miRNAs. Furthermore, miR-17-92a cluster miRNAs also target E2F1 [203], which may be destabilized and further contribute to retardation of cell proliferation. Our study also demonstrates a migration inhibitory function of miR-17-92a cluster, which is substantiated by increased expression of e-cadherin and reduced expression of other mesenchymal markers. Migration inhibitory effects of miR-17-3p expression have been reported earlier in prostate cancer cells, which showed reduced vimentin expression upon of miR-17-3p overexpression [198].

Importantly, our studies further establish the potential of the miR-17-92a cluster as a therapeutic target, showing improved sensitivity of androgen-dependent and -independent prostate cancer cells to some of the drugs that are currently being used for the treatment of CRPC, such as anti-microtubule (DTX), AKTi, anti-androgen (CDX) (androgen dependent cells) and anti-Aurora kinases (androgen independent cells). It can be speculated that the enhanced sensitivity of the miR-17-92a cluster expressing LNCaP104-S (androgen sensitive) cell line to CDX is mediated through interfering androgen receptor function, as miR-17-5p has been noted to inhibit androgen receptor transcriptional activity through targeting p300/CBP [50]. The improved sensitivity of androgen independent PC-3 cells expressing miR-17-92a cluster to DTX and VX680 in combination is presumably mediated through the inhibition of LIMK1 expression and activity (Figure 27and Figure 28), as LIMK1 destabilizes microtubules [204] and interferes with DTX induced microtubule stability, and active LIMK1 is needed for Aurora kinase A functional activation [205]. The enhanced sensitivity to AKTi, singly and in combination

with CDX (LNCaP104-S) or DTX (PC-3) of both cell types expressing the miR-17-92a cluster, is also through miR-17-92a expression-associated inhibition of AKT activation (Figure 28).

Anti-proliferative, adhesive and anti-migratory properties of miR-17 upon overexpression in non-tumor cells and overall growth retardation and smaller organs in transgenic mice has been reported earlier [206] but our results show the maintenance of similar distinctive functions of the expressed miR-17 in the presence of expression of the other miRNAs of the cluster in prostate cancer cells. It is possible that both miR-17 and -20a, which share the exact seed sequence but slightly different central region, are maximally expressed in the transfected cells and in tumors and may functionally synergize. It is now becoming increasingly clear that altered expression of specific targets decides the fate of a cell and the functional designation of a miRNA. Because of the intricacies of the complex regulatory network and fine-tuning of gene expression by miRNAs and competing endogenous regulatory RNAs (ceRNAs), caution should be exercised to understand the function of miRNAs within the cellular context. Taken together, our results strongly support the designation of miR-17-92a cluster miRNAs as tumor suppressors for prostate cancer and that replenishment of expression of miR-17-92a miRNAs as a cluster could be used for combination therapy with other frontline chemotherapeutic agents for treating tumors with a potential for biochemical failure. Nonetheless, the reason for loss of expression of miR-17-92a cluster miRNAs in prostate tumor is not clear, which could be a result of transcription silencing through hyper-

methylation of the CPG Islands or enhanced destabilization of mature miRNAs. In depth studies are required to understand the mechanistic roles of miR-17-92a cluster in modulation of particular pathways that lead to inhibition of cell proliferation and increased drug sensitivity.

5.3 MicroRNAs as Potential Biomarkers in Prostate Cancer

Looking beyond the miR-17-92a cluster, we examined the miRNA landscape in prostate tumors from patients with varying CAPRA-S scores in an effort to identify distinguishing features. Our analysis identified groups of miRNAs that exhibited similar patterns of expression that differentiated tumor from benign tissues or varied with respect to CAPRA-S risk group. Furthermore, many of the miRNAs we identified as differentially expressed in prostate cancer are supported by similar findings published by other investigators. Our initial findings are promising and identify miRNAs with novel association with known oncomiRs or tumor suppressive miRNAs. More patient tissues need to be screened for validation of expression before we can firmly identify miRNA profiles that are predictive of a patient's risk of disease recurrence or resistance to certain chemotherapeutic strategies.

APPENDIX: DESCRIPTION OF ADDITIONAL FILES

Additional File 1: List of normalized and log-transformed values of the miRNA expression.

Additional File 2: List of the p-values, expression patterns and IDs of significant miRNAs identified in t-tests.

Additional File 3: List of the log-transformed fold change values of the up regulated and down regulated miRNAs identified in miRNA profiling.

Additional File 4: List of miRNAs in specific clusters identified in K-median cluster analysis.

Additional File 5: List of the p-values, expression profile and IDs of significant miRNAs from the list of validated miRNAs identified in two samples t-tests.

Additional File 6: List of the log-transformed values of the fold change in expression of the validated miRNAs.

Additional File 7: List of the up and down regulated subset of the validated miRNAs in specific clusters identified in K-median cluster analysis.

Additional File 8: Expression of total- and phospo- AKT1, ERK1/2, and PRAS40 in PC-3 cells expressing Scr RNA or miR-17-92a

Additional File 9: List of normalized expression values of miRNAs, in prostate tumor tissue samples and adjacent uninvolved prostate tissue samples, used for hierarchal clustering analysis.

Additional File 10: List of log-transformed relative expression values and averages of miRNAs identified in clusters 1, 2, 3, and 4.

Source of Additional Files 1-7:

Ottman, R., C. Nguyen, R. Lorch & R. Chakrabarti (2014) MicroRNA expressions associated with progression of prostate cancer cells to antiandrogen therapy resistance. *Mol Cancer,* 13**,** 1.

REFERENCES

1. Smith C, V.J., *Alternative pre-mRNA splicing: the logic of combinatorial control.* 2000.

2. MacNicol, M.C., et al., *Functional Integration of mRNA Translational Control Programs.* Biomolecules, 2015. **5**(3): p. 1580-99.

3. Wang, Y.C., S.E. Peterson, and J.F. Loring, *Protein post-translational modifications and regulation of pluripotency in human stem cells.* Cell Res, 2014. **24**(2): p. 143-60.

4. Baylin, S.B., et al., *Aberrant patterns of DNA methylation, chromatin formation and gene expression in cancer.* Hum Mol Genet, 2001. **10**(7): p. 687-92.

5. Yang, J.X., R.H. Rastetter, and D. Wilhelm, *Non-coding RNAs: An Introduction.* Adv Exp Med Biol, 2016. **886**: p. 13-32.

6. Liz, J. and M. Esteller, *lncRNAs and microRNAs with a role in cancer development.* Biochim Biophys Acta, 2016. **1859**(1): p. 169-76.

7. Yang, G., X. Lu, and L. Yuan, *LncRNA: a link between RNA and cancer.* Biochim Biophys Acta, 2014. **1839**(11): p. 1097-109.

8. Kaikkonen, M.U., M.T. Lam, and C.K. Glass, *Non-coding RNAs as regulators of gene expression and epigenetics.* Cardiovasc Res, 2011. **90**(3): p. 430-40.

9. Bartel, D.P., *MicroRNAs: target recognition and regulatory functions.* Cell, 2009. **136**(2): p. 215-33.

10. Lee, Y., et al.

11. Borchert, G.M., W. Lanier, and B.L. Davidson, *RNA polymerase III transcribes human microRNAs.* Nat Struct Mol Biol, 2006. **13**(12): p. 1097-1101.

12. Romero-Cordoba, S.L., et al., *miRNA biogenesis: Biological impact in the development of cancer.* http://dx.doi.org/10.4161/15384047.2014.955442, 2014.

13. Berezikov, E., et al., *Mammalian mirtron genes.* Mol Cell, 2007. **28**(2): p. 328-36.

14. Khvorova, A., A. Reynolds, and S.D. Jayasena, *Functional siRNAs and miRNAs exhibit strand bias.* Cell, 2003. **115**(2): p. 209-16.

15. Kusenda, B., et al., *MicroRNA biogenesis, functionality and cancer relevance.* Biomed Pap Med Fac Univ Palacky Olomouc Czech Repub, 2006. **150**(2): p. 205-15.

16. Eulalio, A., E. Huntzinger, and E. Izaurralde, *Getting to the root of miRNA-mediated gene silencing.* Cell, 2008. **132**(1): p. 9-14.

17. Liu, J., et al., *MicroRNA-dependent localization of targeted mRNAs to mammalian P-bodies.* Nat Cell Biol, 2005. **7**(7): p. 719-23.

18. Diederichs, S. and D.A. Haber, *Dual role for argonautes in microRNA processing and posttranscriptional regulation of microRNA expression.* Cell, 2007. **131**(6): p. 1097-108.

19. Pillai, R.S., C.G. Artus, and W. Filipowicz, *Tethering of human Ago proteins to mRNA mimics the miRNA-mediated repression of protein synthesis.* Rna, 2004. **10**(10): p. 1518-25.

20. Valencia-Sanchez, M.A., et al., *Control of translation and mRNA degradation by miRNAs and siRNAs.* 2006.

21. Doench, J.G. and P.A. Sharp, *Specificity of microRNA target selection in translational repression.* Genes Dev, 2004. **18**(5): p. 504-11.

22. Lim, L.P., et al., *Microarray analysis shows that some microRNAs downregulate large numbers of target mRNAs.* Nature, 2005. **433**(7027): p. 769-73.

23. Patel, A.R. and E.A. Klein, *Risk factors for prostate cancer.* Nat Clin Pract Urol, 2009. **6**(2): p. 87-95.

24. Cheng, I., et al., *Socioeconomic status and prostate cancer incidence and mortality rates among the diverse population of California*, in *Cancer Causes Control*. 2009. p. 1431-40.

25. Alcaraz, A., et al., *Is there evidence of a relationship between benign prostatic hyperplasia and prostate cancer? Findings of a literature review.* Eur Urol, 2009. **55**(4): p. 864-73.

26. HA, G. and G. HA, *Benign prostatic hyperplasia and prostate cancer.* Epidemiologic Reviews, 2016. **23**(1).

27. Roehrborn, C.G., *Pathology of benign prostatic hyperplasia.* Int J Impot Res, 2008. **20**(S3): p. S11-S18.

28. Baek, K.H., et al., *Correlation of AR, EGFR, and HER2 Expression Levels in Prostate Cancer: Immunohistochemical Analysis and Chromogenic In Situ Hybridization.* Cancer Res Treat, 2012. **44**(1): p. 50-6.

29. Lubik, A.A., et al., *IGF2 increases de novo steroidogenesis in prostate cancer cells.* Endocr Relat Cancer, 2013. **20**(2): p. 173-86.

30. Kokontis, J.M., et al., *Androgen suppresses the proliferation of androgen receptor-positive castration-resistant prostate cancer cells via inhibition of Cdk2, CyclinA, and Skp2.* PLoS One, 2014. **9**(10): p. e109170.

31. Robinson, J.L., et al., *Elevated levels of FOXA1 facilitate androgen receptor chromatin binding resulting in a CRPC-like phenotype.* Oncogene, 2014. **33**(50): p. 5666-74.

32. Ferraldeschi, R., et al., *PTEN protein loss and clinical outcome from castration-resistant prostate cancer treated with abiraterone acetate.* Eur Urol, 2015. **67**(4): p. 795-802.

33. Lin, H.P., et al., *Caffeic acid phenethyl ester induced cell cycle arrest and growth inhibition in androgen-independent prostate cancer cells via regulation of Skp2, p53, p21Cip1 and p27Kip1.* Oncotarget, 2015. **6**(9): p. 6684-707.

34. Cui, Y., et al., *Upregulation of glucose metabolism by NF-kappaB2/p52 mediates enzalutamide resistance in castration-resistant prostate cancer cells.* Endocr Relat Cancer, 2014. **21**(3): p. 435-42.

35. Braadland, P.R., et al., *Low beta(2)-adrenergic receptor level may promote development of castration resistant prostate cancer and altered steroid metabolism.* Oncotarget, 2016. **7**(2): p. 1878-94.

36. Chang, K.H., et al., *Dihydrotestosterone synthesis bypasses testosterone to drive castration-resistant prostate cancer.* Proc Natl Acad Sci U S A, 2011. **108**(33): p. 13728-33.

37. Sakai, M., et al., *De novo steroid biosynthesis in human prostate cell lines and biopsies.* Prostate, 2016. **76**(6): p. 575-87.

38. Bennett, N.C., et al., *Evidence for steroidogenic potential in human prostate cell lines and tissues.* Am J Pathol, 2012. **181**(3): p. 1078-87.

39. H, S., *Alterations of Epigenetics and MicroRNAs in Cancer and Cancer Stem Cell.* Frontiers in Genetics, 2014. **4**.

40. Melo, S.A. and M. Esteller, *Dysregulation of microRNAs in cancer: playing with fire.* FEBS letters, 2011. **585**(13): p. 2087-99.

41. Allantaz, F., et al., *Expression profiling of human immune cell subsets identifies miRNA-mRNA regulatory relationships correlated with cell type specific expression.* PLoS One, 2012. **7**(1): p. e29979.

42. Xu, J., et al., *The mRNA related ceRNA-ceRNA landscape and significance across 20 major cancer types.* Nucleic Acids Res, 2015. **43**(17): p. 8169-82.

43. Yu, Y., Y. Zhang, and S. Zhang, *MicroRNA-92 regulates cervical tumorigenesis and its expression is upregulated by human papillomavirus-16 E6 in cervical cancer cells.* Oncol Lett, 2013. **6**(2): p. 468-474.

44. Gibbons, D.L., et al., *Contextual extracellular cues promote tumor cell EMT and metastasis by regulating miR-200 family expression.* Genes Dev, 2009. **23**(18): p. 2140-51.

45. Sun, X., et al., *The insights of Let-7 miRNAs in oncogenesis and stem cell potency.* J Cell Mol Med, 2016.

46. Wang, Y.L., et al., *Role of MicroRNAs in Prostate Cancer Pathogenesis.* Clin Genitourin Cancer, 2015. **13**(4): p. 261-70.

47. ChunJiao, S., et al., *Uncovering the roles of miRNAs and their relationship with androgen receptor in prostate cancer.* IUBMB Life, 2014. **66**(6): p. 379-86.

48. Mo, W., et al., *Identification of novel AR-targeted microRNAs mediating androgen signalling through critical pathways to regulate cell viability in prostate cancer.* PLoS ONE, 2013. **8**(2): p. e56592.

49. Ostling, P., et al., *Systematic analysis of microRNAs targeting the androgen receptor in prostate cancer cells.* Cancer Res, 2011. **71**(5): p. 1956-67.

50. Gong, A.Y., et al., *miR-17-5p targets the p300/CBP-associated factor and modulates androgen receptor transcriptional activity in cultured prostate cancer cells.* BMC Cancer, 2012. **12**: p. 492.

51. Imamura, Y., et al., *FOXA1 promotes tumor progression in prostate cancer via the insulin-like growth factor binding protein 3 pathway.* PLoS ONE, 2012. **7**(8): p. e42456.

52. Javidan, J., et al., *The androgen receptor and mechanisms for androgen*

independence in prostate cancer. Cancer Invest, 2005. **23**(6): p. 520-8.

53. Culig, Z., et al., *Switch from antagonist to agonist of the androgen receptor bicalutamide is associated with prostate tumour progression in a new model system.* Br J Cancer, 1999. **81**(2): p. 242-51.

54. Seruga, B., A. Ocana, and I.F. Tannock, *Drug resistance in metastatic castration-resistant prostate cancer.* Nat Rev Clin Oncol, 2011. **8**(1): p. 12-23.

55. Scher, H.I., et al., *Targeting the androgen receptor: improving outcomes for castration-resistant prostate cancer.* Endocr Relat Cancer, 2004. **11**(3): p. 459-76.

56. Cooperberg, M.R., J.F. Hilton, and P.R. Carroll, *The CAPRA-S score: A straightforward tool for improved prediction of outcomes after radical prostatectomy.* Cancer, 2011. **117**(22): p. 5039-46.

57. Ribas, J., et al., *miR-21: an androgen receptor-regulated microRNA that promotes hormone-dependent and hormone-independent prostate cancer growth.* Cancer Res, 2009. **69**(18): p. 7165-9.

58. Sun, T., et al., *The role of microRNA-221 and microRNA-222 in androgen-independent prostate cancer cell lines.* Cancer Res, 2009. **69**(8): p. 3356-63.

59. Shi, X.B., et al., *An androgen-regulated miRNA suppresses Bak1 expression and induces androgen-independent growth of prostate cancer cells.* Proc Natl Acad Sci U S A, 2007. **104**(50): p. 19983-8.

60. Jalava, S.E., et al., *Androgen-regulated miR-32 targets BTG2 and is overexpressed in castration-resistant prostate cancer.* Oncogene, 2012. **31**(41): p. 4460-71.

61. Kokontis, J.M., et al., *Role of androgen receptor in the progression of human prostate tumor cells to androgen independence and insensitivity.* Prostate, 2005. **65**(4): p. 287-98.

62. Wright, M.E., M.J. Tsai, and R. Aebersold, *Androgen receptor represses the neuroendocrine transdifferentiation process in prostate cancer cells.* Mol Endocrinol, 2003. **17**(9): p. 1726-37.

63. Wang, Z., et al., *miR-106a Is frequently upregulated in gastric cancer and inhibits the extrinsic apoptotic pathway by targeting FAS.* Molecular carcinogenesis, 2012.

64. Satzger, I., et al., *MicroRNA-15b represents an independent prognostic parameter*

and is correlated with tumor cell proliferation and apoptosis in malignant melanoma. International journal of cancer. Journal international du cancer, 2010. **126**(11): p. 2553-62.

65. Chen, L., et al., *miR-17-5p as a novel prognostic marker for hepatocellular carcinoma.* Journal of investigative surgery : the official journal of the Academy of Surgical Research, 2012. **25**(3): p. 156-61.

66. Wu, C.W., et al., *MicroRNA-18a attenuates DNA damage repair through suppressing the expression of ataxia telangiectasia mutated in colorectal cancer.* PLoS ONE, 2013. **8**(2): p. e57036.

67. Xie, H., et al., *miR-205 expression promotes cell proliferation and migration of human cervical cancer cells.* PLoS ONE, 2012. **7**(10): p. e46990.

68. Kang, H.W., et al., *miR-20a promotes migration and invasion by regulating TNKS2 in human cervical cancer cells.* FEBS letters, 2012. **586**(6): p. 897-904.

69. Chou, Y.T., et al., *EGFR promotes lung tumorigenesis by activating miR-7 through a Ras/ERK/Myc pathway that targets the Ets2 transcriptional repressor ERF.* Cancer research, 2010. **70**(21): p. 8822-31.

70. Shibahara, Y., et al., *Aromatase inhibitor treatment of breast cancer cells increases the expression of let-7f, a microRNA targeting CYP19A1.* The Journal of pathology, 2012. **227**(3): p. 357-66.

71. Yang, Y., et al., *MiR-136 promotes apoptosis of glioma cells by targeting AEG-1 and Bcl-2.* FEBS letters, 2012. **586**(20): p. 3608-12.

72. Lin, T., et al., *MicroRNA-143 as a tumor suppressor for bladder cancer.* J Urol, 2009. **181**(3): p. 1372-80.

73. Li, Y., et al., *miR-146a suppresses invasion of pancreatic cancer cells.* Cancer research, 2010. **70**(4): p. 1486-95.

74. Venkataraman, S., et al., *MicroRNA 218 acts as a tumor suppressor by targeting multiple cancer phenotype-associated genes in medulloblastoma.* The Journal of biological chemistry, 2013. **288**(3): p. 1918-28.

75. Li, B., et al., *miRNA-22 suppresses colon cancer cell migration and invasion by inhibiting the expression of T-cell lymphoma invasion and metastasis 1 and matrix metalloproteinases 2 and 9.* Oncology reports, 2013. **29**(5): p. 1932-8.

76. Fuse, M., et al., *Tumor suppressive microRNAs (miR-222 and miR-31) regulate molecular pathways based on microRNA expression signature in prostate cancer.* Journal of human genetics, 2012. **57**(11): p. 691-9.

77. Wang, F., et al., *miR-29a and miR-142-3p downregulation and diagnostic implication in human acute myeloid leukemia.* Molecular biology reports, 2012. **39**(3): p. 2713-22.

78. Majid, S., et al., *miRNA-34b inhibits prostate cancer through demethylation, active chromatin modifications, and AKT pathways.* Clin Cancer Res, 2013. **19**(1): p. 73-84.

79. Ueno, K., et al., *Tumor suppressor microRNA-493 decreases cell motility and migration ability in human bladder cancer cells by downregulating RhoC and FZD4.* Molecular cancer therapeutics, 2012. **11**(1): p. 244-53.

80. Gallagher, D.J., et al., *Germline BRCA mutations denote a clinicopathologic subset of prostate cancer.* Clin Cancer Res, 2010. **16**(7): p. 2115-21.

81. Martin, P., et al., *Prostate epithelial Pten/TP53 loss leads to transformation of multipotential progenitors and epithelial to mesenchymal transition.* Am J Pathol, 2011. **179**(1): p. 422-35.

82. Matsuda, M., et al., *Mutations in the RAD54 recombination gene in primary cancers.* Oncogene, 1999. **18**(22): p. 3427-30.

83. Bi, X., et al., *Loss of interferon regulatory factor 5 (IRF5) expression in human ductal carcinoma correlates with disease stage and contributes to metastasis.* Breast Cancer Res, 2011. **13**(6): p. R111.

84. Lin, S.C., et al., *Suppression of dual-specificity phosphatase-2 by hypoxia increases chemoresistance and malignancy in human cancer cells.* J Clin Invest, 2011. **121**(5): p. 1905-16.

85. Liu, B., et al., *IKKalpha is required to maintain skin homeostasis and prevent skin cancer.* Cancer Cell, 2008. **14**(3): p. 212-25.

86. Gao, Q., et al., *Deletion of the de novo DNA methyltransferase Dnmt3a promotes lung tumor progression.* Proc Natl Acad Sci U S A, 2011. **108**(44): p. 18061-6.

87. Jang, M.S., et al., *Phosphorylation by polo-like kinase 1 induces the tumor-suppressing activity of FADD.* Oncogene, 2011. **30**(4): p. 471-81.

88. Choucair, K., et al., *PTEN genomic deletion predicts prostate cancer recurrence and is associated with low AR expression and transcriptional activity.* BMC Cancer, 2012. **12**: p. 543.

89. Qi, W., et al., *Tumor suppressor FOXO3 mediates signals from the EGF receptor to regulate proliferation of colonic cells.* Am J Physiol Gastrointest Liver Physiol, 2011. **300**(2): p. G264-72.

90. Takata, A., et al., *A miRNA machinery component DDX20 controls NF-kappaB via microRNA-140 function.* Biochem Biophys Res Commun, 2012. **420**(3): p. 564-9.

91. Zhang, Y., et al., *EBP1, an ErbB3-binding protein, is decreased in prostate cancer and implicated in hormone resistance.* Mol Cancer Ther, 2008. **7**(10): p. 3176-86.

92. Hakariya, T., et al., *EGFR signaling pathway negatively regulates PSA expression and secretion via the PI3K-Akt pathway in LNCaP prostate cancer cells.* Biochem Biophys Res Commun, 2006. **342**(1): p. 92-100.

93. Cao, Y., et al., *VEGF exerts an angiogenesis-independent function in cancer cells to promote their malignant progression.* Cancer Res, 2012. **72**(16): p. 3912-8.

94. Aggarwal, H., A. Aggarwal, and D.K. Agrawal, *Epidermal growth factor increases LRF/Pokemon expression in human prostate cancer cells.* Exp Mol Pathol, 2011. **91**(2): p. 496-501.

95. Bhatt, D.K. and G. Nagda, *Modulation of acid phosphatase and lactic dehydrogenase in hexachlorocyclohexane-induced hepatocarcinogenesis in mice.* J Biochem Mol Toxicol, 2012. **26**(11): p. 439-44.

96. Domingo-Domenech, J., et al., *Activation of nuclear factor-kappaB in human prostate carcinogenesis and association to biochemical relapse.* Br J Cancer, 2005. **93**(11): p. 1285-94.

97. Bonci, D., et al., *The miR-15a-miR-16-1 cluster controls prostate cancer by targeting multiple oncogenic activities.* Nat Med, 2008. **14**(11): p. 1271-7.

98. Berger, E., et al., *Gene network analysis leads to functional validation of pathways linked to cancer cell growth and survival.* Biotechnol J, 2012. **7**(11): p. 1395-404.

99. Derdak, Z., et al., *The mitochondrial uncoupling protein-2 promotes chemoresistance in cancer cells.* Cancer Res, 2008. **68**(8): p. 2813-9.

100. Liu, P., et al., *Sex-determining region Y box 4 is a transforming oncogene in human*

prostate cancer cells. Cancer Res, 2006. **66**(8): p. 4011-9.

101. Jin, F., et al., *ERK and AKT signaling pathways promote MED1 overexpression in prostate cancer cells in association with elevated proliferation and tumorigenicity.* Mol Cancer Res, 2013.

102. Wei, J., et al., *The ubiquitin ligase TRAF6 negatively regulates the JAK-STAT signaling pathway by binding to STAT3 and mediating its ubiquitination.* PLoS One, 2012. **7**(11): p. e49567.

103. Tiacci, E., et al., *The corepressors BCOR and BCORL1: two novel players in acute myeloid leukemia.* Haematologica, 2012. **97**(1): p. 3-5.

104. Chen, H.Y., et al., *Inhibition of redox/Fyn/c-Cbl pathway function by Cdc42 controls tumour initiation capacity and tamoxifen sensitivity in basal-like breast cancer cells.* EMBO Mol Med, 2013. **5**(5): p. 723-36.

105. Iourov, I.Y., et al., *Increased chromosome instability dramatically disrupts neural genome integrity and mediates cerebellar degeneration in the ataxia-telangiectasia brain.* Hum Mol Genet, 2009. **18**(14): p. 2656-69.

106. Park, S.J., et al., *Epigenetic alteration of CCDC67 and its tumor suppressor function in gastric cancer.* Carcinogenesis, 2012. **33**(8): p. 1494-501.

107. Srougi, M.C. and K. Burridge, *The nuclear guanine nucleotide exchange factors Ect2 and Net1 regulate RhoB-mediated cell death after DNA damage.* PLoS One, 2011. **6**(2): p. e17108.

108. Maity, B., et al., *Regulator of G Protein Signaling 6 (RGS6) is a novel suppressor of breast tumor initiation and progression.* Carcinogenesis, 2013.

109. Sharma, P., D. Patel, and J. Chaudhary, *Id1 and Id3 expression is associated with increasing grade of prostate cancer: Id3 preferentially regulates CDKN1B.* Cancer Med, 2012. **1**(2): p. 187-97.

110. Ha, S., et al., *Phosphorylation of the androgen receptor by PIM1 in hormone refractory prostate cancer.* Oncogene, 2012.

111. Bisbal, C. and R.H. Silverman, *Diverse functions of RNase L and implications in pathology.* Biochimie, 2007. **89**(6-7): p. 789-98.

112. Long, J.Z., et al., *Metabolomics annotates ABHD3 as a physiologic regulator of medium-chain phospholipids.* Nat Chem Biol, 2011. **7**(11): p. 763-5.

113. Hayashi, A., et al., *p63RhoGEF-mediated formation of a single polarized lamellipodium is required for chemotactic migration in breast carcinoma cells.* FEBS Lett, 2013. **587**(6): p. 698-705.

114. Ting, H.J., et al., *Identification of microRNA-98 as a therapeutic target inhibiting prostate cancer growth and a biomarker induced by vitamin D.* J Biol Chem, 2013. **288**(1): p. 1-9.

115. Itoh, G., et al., *CAMP (C13orf8, ZNF828) is a novel regulator of kinetochore-microtubule attachment.* EMBO J, 2011. **30**(1): p. 130-44.

116. Srivastava, S.K., et al., *Myb overexpression overrides androgen depletion-induced cell cycle arrest and apoptosis in prostate cancer cells, and confers aggressive malignant traits: potential role in castration resistance.* Carcinogenesis, 2012. **33**(6): p. 1149-57.

117. Errington, W.J., et al., *Adaptor protein self-assembly drives the control of a cullin-RING ubiquitin ligase.* Structure, 2012. **20**(7): p. 1141-53.

118. Yang, P., et al., *Histone methyltransferase NSD2/MMSET mediates constitutive NF-kappaB signaling for cancer cell proliferation, survival, and tumor growth via a feed-forward loop.* Mol Cell Biol, 2012. **32**(15): p. 3121-31.

119. Yoon, S. and G. De Micheli, *Prediction and Analysis of Human microRNA Regulatory Modules.* Conf Proc IEEE Eng Med Biol Soc, 2005. **5**: p. 4799-802.

120. Cai, C., et al., *Androgen receptor expression in prostate cancer cells is suppressed by activation of epidermal growth factor receptor and ErbB2.* Cancer Res, 2009. **69**(12): p. 5202-9.

121. Gandellini, P., et al., *miR-205 Exerts tumor-suppressive functions in human prostate through down-regulation of protein kinase Cepsilon.* Cancer Res, 2009. **69**(6): p. 2287-95.

122. Al-Sarraf, N., et al., *DOK4/IRS-5 expression is altered in clear cell renal cell carcinoma.* Int J Cancer, 2007. **121**(5): p. 992-8.

123. Ottman, R., et al., *MicroRNA expressions associated with progression of prostate cancer cells to antiandrogen therapy resistance.* Mol Cancer, 2014. **13**: p. 1.

124. Liu, H.P., et al., *Epstein-Barr virus-encoded LMP1 interacts with FGD4 to activate Cdc42 and thereby promote migration of nasopharyngeal carcinoma cells.* PLoS Pathog, 2012. **8**(5): p. e1002690.

125. Davila, M., et al., *LIM kinase 1 is essential for the invasive growth of prostate epithelial cells: implications in prostate cancer.* J Biol Chem, 2003. **278**(38): p. 36868-75.

126. Tapia, T., R. Ottman, and R. Chakrabarti, *LIM kinase1 modulates function of membrane type matrix metalloproteinase 1: implication in invasion of prostate cancer cells.* Mol Cancer, 2011. **10**: p. 6.

127. Kaji, N., et al., *Cell cycle-associated changes in Slingshot phosphatase activity and roles in cytokinesis in animal cells.* J Biol Chem, 2003. **278**(35): p. 33450-5.

128. Drobnjak, M., et al., *Overexpression of cyclin D1 is associated with metastatic prostate cancer to bone.* Clin Cancer Res, 2000. **6**(5): p. 1891-5.

129. Ridley, A.J., et al., *Cell migration: integrating signals from front to back.* Science, 2003. **302**(5651): p. 1704-9.

130. Scholzen, T. and J. Gerdes, *The Ki-67 protein: from the known and the unknown.* J Cell Physiol, 2000. **182**(3): p. 311-22.

131. Kokkinos, M.I., et al., *Vimentin and epithelial-mesenchymal transition in human breast cancer--observations in vitro and in vivo.* Cells Tissues Organs, 2007. **185**(1-3): p. 191-203.

132. Yang, J., et al., *Twist, a master regulator of morphogenesis, plays an essential role in tumor metastasis.* Cell, 2004. **117**(7): p. 927-39.

133. Medici, D., E.D. Hay, and B.R. Olsen, *Snail and Slug promote epithelial-mesenchymal transition through beta-catenin-T-cell factor-4-dependent expression of transforming growth factor-beta3.* Mol Biol Cell, 2008. **19**(11): p. 4875-87.

134. Liu, Y., et al., *Zeb1 links epithelial-mesenchymal transition and cellular senescence.* Development, 2008. **135**(3): p. 579-88.

135. Gumbiner, B.M., *Regulation of cadherin-mediated adhesion in morphogenesis.* Nat Rev Mol Cell Biol, 2005. **6**(8): p. 622-34.

136. Cavallaro, U. and G. Christofori, *Cell adhesion and signalling by cadherins and Ig-CAMs in cancer.* Nat Rev Cancer, 2004. **4**(2): p. 118-32.

137. Friedberg, J.W., et al., *Phase II study of alisertib, a selective Aurora A kinase inhibitor, in relapsed and refractory aggressive B- and T-cell non-Hodgkin*

lymphomas. J Clin Oncol, 2014. **32**(1): p. 44-50.

138. Schwartz, G.K., et al., *Phase I study of barasertib (AZD1152), a selective inhibitor of Aurora B kinase, in patients with advanced solid tumors.* Invest New Drugs, 2013. **31**(2): p. 370-80.

139. Tao, J., et al., *microRNA-18a, a member of the oncogenic miR-17-92 cluster, targets Dicer and suppresses cell proliferation in bladder cancer T24 cells.* Molecular medicine reports, 2012. **5**(1): p. 167-72.

140. Tao, J., et al., *microRNA-133 inhibits cell proliferation, migration and invasion in prostate cancer cells by targeting the epidermal growth factor receptor.* Oncology Reports, 2016. **27**(6): p. 1967-1975.

141. Chu, H., et al., *A functional variant in miR-143 promoter contributes to prostate cancer risk.* Arch Toxicol, 2016. **90**(2): p. 403-14.

142. Ding, M., et al., *A dual yet opposite growth-regulating function of miR-204 and its target XRN1 in prostate adenocarcinoma cells and neuroendocrine-like prostate cancer cells.* Oncotarget, 2015. **6**(10): p. 7686-700.

143. Goto, Y., et al., *MicroRNA expression signature of castration-resistant prostate cancer: the microRNA-221/222 cluster functions as a tumour suppressor and disease progression marker.* Br J Cancer, 2015.

144. Yu, J.J., et al., *miR-96 promotes cell proliferation and clonogenicity by down-regulating of FOXO1 in prostate cancer cells.* Med Oncol, 2014. **31**(4): p. 910.

145. Choi, N., et al., *miR-93/miR-106b/miR-375-CIC-CRABP1: a novel regulatory axis in prostate cancer progression.* Oncotarget, 2015. **6**(27): p. 23533-47.

146. Sarver, A.L., L. Li, and S. Subramanian, *MicroRNA miR-183 functions as an oncogene by targeting the transcription factor EGR1 and promoting tumor cell migration.* Cancer research, 2010. **70**(23): p. 9570-80.

147. Swarbrick, A., et al., *miR-380-5p represses p53 to control cellular survival and is associated with poor outcome in MYCN-amplified neuroblastoma.* Nature medicine, 2010. **16**(10): p. 1134-40.

148. Fu, X., et al., *MicroRNA-103 suppresses tumor cell proliferation by targeting PDCD10 in prostate cancer.* Prostate, 2016. **76**(6): p. 543-51.

149. Sun, F., et al., *Androgen receptor splice variant AR3 promotes prostate cancer via*

modulating expression of autocrine/paracrine factors. J Biol Chem, 2014. **289**(3): p. 1529-39.

150. Qu, Y., et al., *miR-199a-3p inhibits aurora kinase A and attenuates prostate cancer growth: new avenue for prostate cancer treatment.* Am J Pathol, 2014. **184**(5): p. 1541-9.

151. Wagner, S., et al., *Role of miRNA let-7 and its major targets in prostate cancer.* Biomed Res Int, 2014. **2014**: p. 376326.

152. Yang, D.S., *Novel prediction of anticancer drug chemosensitivity in cancer cell lines: evidence of moderation by microRNA expressions.* Conf Proc IEEE Eng Med Biol Soc, 2014. **2014**: p. 4780-6.

153. Solit, D.B., H.I. Scher, and N. Rosen, *Hsp90 as a therapeutic target in prostate cancer.* Semin Oncol, 2003. **30**(5): p. 709-16.

154. Gillis, J.L., et al., *Constitutively-active androgen receptor variants function independently of the HSP90 chaperone but do not confer resistance to HSP90 inhibitors.* Oncotarget, 2013. **4**(5): p. 691-704.

155. Centenera, M.M., et al., *Co-targeting AR and HSP90 suppresses prostate cancer cell growth and prevents resistance mechanisms.* Endocr Relat Cancer, 2015. **22**(5): p. 805-18.

156. Kim, H.S., et al., *Prostate biopsies from black men express higher levels of aggressive disease biomarkers than prostate biopsies from white men.* Prostate Cancer Prostatic Dis, 2011. **14**(3): p. 262-5.

157. Koochekpour, S., et al., *Androgen Receptor Mutations and Polymorphisms in African American Prostate Cancer.* Int J Biol Sci, 2014. **10**(6): p. 643-51.

158. Lin, S.L., et al., *Loss of mir-146a function in hormone-refractory prostate cancer.* RNA, 2008. **14**(3): p. 417-24.

159. Taganov, K.D., et al., *NF-kappaB-dependent induction of microRNA miR-146, an inhibitor targeted to signaling proteins of innate immune responses.* Proc Natl Acad Sci U S A, 2006. **103**(33): p. 12481-6.

160. Pacifico, F., et al., *Nuclear factor-{kappa}B contributes to anaplastic thyroid carcinomas through up-regulation of miR-146a.* The Journal of clinical endocrinology and metabolism, 2010. **95**(3): p. 1421-30.

161. Boldin, M.P., et al., *miR-146a is a significant brake on autoimmunity, myeloproliferation, and cancer in mice.* J Exp Med, 2011. **208**(6): p. 1189-201.

162. Bazzoni, F., et al., *Induction and regulatory function of miR-9 in human monocytes and neutrophils exposed to proinflammatory signals.* Proc Natl Acad Sci U S A, 2009. **106**(13): p. 5282-7.

163. Shahab, S.W., et al., *The effects of MicroRNA transfections on global patterns of gene expression in ovarian cancer cells are functionally coordinated.* BMC Med Genomics, 2012. **5**: p. 33.

164. Li, M., et al., *Somatic mutations in the transcriptional corepressor gene BCORL1 in adult acute myelogenous leukemia.* Blood, 2011. **118**(22): p. 5914-7.

165. Al-Ahmadi, W., et al., *RNase L downmodulation of the RNA-binding protein, HuR, and cellular growth.* Oncogene, 2009. **28**(15): p. 1782-91.

166. Bhaumik, D., et al., *MicroRNAs miR-146a/b negatively modulate the senescence-associated inflammatory mediators IL-6 and IL-8.* Aging (Albany NY), 2010. **1**(4): p. 402-11.

167. Ewald, J.A., et al., *Androgen Deprivation Induces Senescence Characteristics in Prostate Cancer Cells In vitro and In vivo.* Prostate, 2013. **73**(4): p. 337-45.

168. Barakat, D.J., et al., *CCAAT/Enhancer Binding Protein β Controls Androgen Deprivation-Induced Senescence in Prostate Cancer Cells.* Oncogene, 2015. **34**(48): p. 5912-22.

169. Schreiber, R., et al., *Evidence for the role of microRNA 374b in acquired cisplatin resistance in pancreatic cancer cells.* Cancer Gene Ther, 2016.

170. Zhen, Y., et al., *miR-374a-CCND1-pPI3K/AKT-c-JUN feedback loop modulated by PDCD4 suppresses cell growth, metastasis, and sensitizes nasopharyngeal carcinoma to cisplatin.* Oncogene, 2016.

171. Ravid, T., et al., *c-Cbl-mediated ubiquitinylation is required for epidermal growth factor receptor exit from the early endosomes.* J Biol Chem, 2004. **279**(35): p. 37153-62.

172. Truitt, L., et al., *The EphB6 receptor cooperates with c-Cbl to regulate the behavior of breast cancer cells.* Cancer Res, 2010. **70**(3): p. 1141-53.

173. Zhao, X., et al., *MicroRNA-7 functions as an anti-metastatic microRNA in gastric*

cancer by targeting insulin-like growth factor-1 receptor. Oncogene, 2013. **32**(11): p. 1363-72.

174. Kong, X., et al., *MicroRNA-7 inhibits epithelial-to-mesenchymal transition and metastasis of breast cancer cells via targeting FAK expression.* PLoS ONE, 2012. **7**(8): p. e41523.

175. Poliseno, L., et al., *Identification of the miR-106b~25 microRNA cluster as a proto-oncogenic PTEN-targeting intron that cooperates with its host gene MCM7 in transformation.* Sci Signal, 2010. **3**(117): p. ra29.

176. Hulf, T., et al., *Epigenetic-induced repression of microRNA-205 is associated with MED1 activation and a poorer prognosis in localized prostate cancer.* Oncogene, 2012.

177. Sun, L., et al., *MiR-200b and miR-15b regulate chemotherapy-induced epithelial-mesenchymal transition in human tongue cancer cells by targeting BMI1.* Oncogene, 2012. **31**(4): p. 432-45.

178. Hossain, A., M.T. Kuo, and G.F. Saunders, *Mir-17-5p regulates breast cancer cell proliferation by inhibiting translation of AIB1 mRNA.* Mol Cell Biol, 2006. **26**(21): p. 8191-201.

179. Chang, C.C., et al., *MicroRNA-17/20a functions to inhibit cell migration and can be used a prognostic marker in oral squamous cell carcinoma.* Oral oncology, 2013.

180. Hummel, R., et al., *MiRNAs and their association with locoregional staging and survival following surgery for esophageal carcinoma.* Annals of surgical oncology, 2011. **18**(1): p. 253-60.

181. Svoboda, M., et al., *MiR-34b is associated with clinical outcome in triple-negative breast cancer patients.* Diagn Pathol, 2012. **7**: p. 31.

182. Gottardo, F., et al., *Micro-RNA profiling in kidney and bladder cancers.* Urol Oncol, 2007. **25**(5): p. 387-92.

183. Fan, X., et al., *Up-regulated microRNA-143 in cancer stem cells differentiation promotes prostate cancer cells metastasis by modulating FNDC3B expression.* BMC Cancer, 2013. **13**: p. 61.

184. Leite, K.R., et al., *Change in expression of miR-let7c, miR-100, and miR-218 from high grade localized prostate cancer to metastasis.* Urol Oncol, 2011. **29**(3): p. 265-9.

185. Han, Y.C., et al., *microRNA-29a induces aberrant self-renewal capacity in hematopoietic progenitors, biased myeloid development, and acute myeloid leukemia.* The Journal of experimental medicine, 2010. **207**(3): p. 475-89.

186. Watson, J.A., et al., *miRNA profiles as a predictor of chemoresponsiveness in Wilms' tumor blastema.* PLoS ONE, 2013. **8**(1): p. e53417.

187. Hamfjord, J., et al., *Differential expression of miRNAs in colorectal cancer: comparison of paired tumor tissue and adjacent normal mucosa using high-throughput sequencing.* PLoS ONE, 2012. **7**(4): p. e34150.

188. Lehmann, U., et al., *Identification of differentially expressed microRNAs in human male breast cancer.* BMC Cancer, 2010. **10**: p. 109.

189. Yang, H., et al., *MicroRNAs regulate methionine adenosyltransferase 1A expression in hepatocellular carcinoma.* The Journal of clinical investigation, 2013. **123**(1): p. 285-98.

190. Zhang, M., et al., *miR-518b is down-regulated, and involved in cell proliferation and invasion by targeting Rap1b in esophageal squamous cell carcinoma.* FEBS letters, 2012. **586**(19): p. 3508-21.

191. Faltejskova, P., et al., *Identification and functional screening of microRNAs highly deregulated in colorectal cancer.* Journal of cellular and molecular medicine, 2012. **16**(11): p. 2655-66.

192. Guo, L.M., et al., *MicroRNA-9 inhibits ovarian cancer cell growth through regulation of NF-kappaB1.* FEBS J, 2009. **276**(19): p. 5537-46.

193. Boll, K., et al., *MiR-130a, miR-203 and miR-205 jointly repress key oncogenic pathways and are downregulated in prostate carcinoma.* Oncogene, 2013. **32**(3): p. 277-85.

194. Fang, Y., et al., *MicroRNA-7 inhibits tumor growth and metastasis by targeting the phosphoinositide 3-kinase/Akt pathway in hepatocellular carcinoma.* Hepatology, 2012. **55**(6): p. 1852-62.

195. Hayashita, Y., et al., *A polycistronic microRNA cluster, miR-17-92, is overexpressed in human lung cancers and enhances cell proliferation.* Cancer Res, 2005. **65**(21): p. 9628-32.

196. Thapa, D.R., et al., *Overexpression of microRNAs from the miR-17-92 paralog clusters in AIDS-related non-Hodgkin's lymphomas.* PLoS One, 2011. **6**(6): p.

e20781.

197. Rinaldi, A., et al., *Concomitant MYC and microRNA cluster miR-17-92 (C13orf25) amplification in human mantle cell lymphoma.* Leuk Lymphoma, 2007. **48**(2): p. 410-2.

198. Zhang, X., et al., *MicroRNA-17-3p is a prostate tumor suppressor in vitro and in vivo, and is decreased in high grade prostate tumors analyzed by laser capture microdissection.* Clin Exp Metastasis, 2009. **26**(8): p. 965-79.

199. Davila, M., et al., *Expression of LIM kinase 1 is associated with reversible G1/S phase arrest, chromosomal instability and prostate cancer.* Mol Cancer, 2007. **6**: p. 40.

200. Pereira, R.A., et al., *Cyclin D1 expression in prostate carcinoma.* Braz J Med Biol Res, 2014. **47**(6): p. 515-21.

201. Wang, Y., et al., *Cofilin-phosphatase slingshot-1L (SSH1L) is over-expressed in pancreatic cancer (PC) and contributes to tumor cell migration.* Cancer Lett, 2015. **360**(2): p. 171-6.

202. Fontana, L., et al., *Antagomir-17-5p abolishes the growth of therapy-resistant neuroblastoma through p21 and BIM.* PLoS One, 2008. **3**(5): p. e2236.

203. O'Donnell, K.A., et al., *c-Myc-regulated microRNAs modulate E2F1 expression.* Nature, 2005. **435**(7043): p. 839-43.

204. Gorovoy, M., et al., *LIM kinase 1 coordinates microtubule stability and actin polymerization in human endothelial cells.* J Biol Chem, 2005. **280**(28): p. 26533-42.

205. Ritchey, L., et al., *A functional cooperativity between Aurora A kinase and LIM kinase1: implication in the mitotic process.* Cell Cycle, 2012. **11**(2): p. 296-309.

206. Shan, S.W., et al., *MicroRNA MiR-17 retards tissue growth and represses fibronectin expression.* Nat Cell Biol, 2009. **11**(8): p. 1031-8.